UNCLASSIFIED

AD NUMBER
AD102442
LIMITATION CHANGES
TO: **Approved for public release; distribution is unlimited.**
FROM: **Distribution authorized to U.S. Gov't. agencies and their contractors; Administrative/Operational Use; MAY 1955. Other requests shall be referred to Wrignt Air Development Center, Wright-Patterson AFB, OH 45433.**
AUTHORITY
AFAL ltr, 27 Dec 1979

THIS PAGE IS UNCLASSIFIED

UNCLASSIFIED

102442

rmed Services Technical Information Agency

Reproduced by

DOCUMENT SERVICE CENTER

KNOTT BUILDING, DAYTON, 2, OHIO

This document is the property of the United States Government. It is furnished for the duration of the contract and shall be returned when no longer required, or upon recall by ASTIA to the following address: Armed Services Technical Information Agency, Document Service Center, Knott Building, Dayton 2, Ohio.

OTICE: WHEN GOVERNMENT OR OTHER DRAWINGS, SPECIFICATIONS OR OTHER DATA RE USED FOR ANY PURPOSE OTHER THAN IN CONNECTION WITH A DEFINITELY RELATED OVERNMENT PROCUREMENT OPERATION, THE U. S. GOVERNMENT THEREBY INCURS O RESPONSIBILITY, NOR ANY OBLIGATION WHATSOEVER; AND THE FACT THAT THE OVERNMENT MAY HAVE FORMULATED, FURNISHED, OR IN ANY WAY SUPPLIED THE AID DRAWINGS, SPECIFICATIONS, OR OTHER DATA IS NOT TO BE REGARDED BY IPLICATION OR OTHERWISE AS IN ANY MANNER LICENSING THE HOLDER OR ANY OTHER ERSON OR CORPORATION, OR CONVEYING ANY RIGHTS OR PERMISSION TO MANUFACTURE, E OR SELL ANY PATENTED INVENTION THAT MAY IN ANY WAY BE RELATED THERETO.

UNCLASSIFIED

AD No. 102442
ASTIA FILE COPY

WADC TECHNICAL REPORT 54-267

FC

STUDY OF SYSTEMS FOR TRUE ANGLE OF ATTACK MEASUREMENT

F. M. EMERSON
F. H. GARDNER
G. D. GRUENWALD
R. OLSHAUSEN
L. V. SLOMA

NORTH AMERICAN AVIATION, INC.

MAY 1955

WRIGHT AIR DEVELOPMENT CENTER

WADC TECHNICAL REPORT 54-267

STUDY OF SYSTEMS FOR TRUE ANGLE OF ATTACK MEASUREMENT

F. M. EMERSON

F. H. GARDNER

G. D. GRUENWALD

R. OLSHAUSEN

L. V. SLOMA

NORTH AMERICAN AVIATION, INC.

MAY 1955

FLIGHT CONTROL LABORATORY

CONTRACT No. AF 33(616)-2348

PROJECT No. 1373

TASK No. 13681

WRIGHT AIR DEVELOPMENT CENTER

AIR RESEARCH AND DEVELOPMENT COMMAND

UNITED STATES AIR FORCE

WRIGHT-PATTERSON AIR FORCE BASE, OHIO

Carpenter Litho & Prtg. Co., Springfield, O.
100 - June 1956

FOREWORD

This report describes studies on angle of attack measurements made by North American Aviation, Inc., under Contract No. AF 33(616)-2348, Project No. 1373, "Two Angles of Attack System (Sixth Pickup)," Task No. 13681. Mr. John Kearns served as project engineer for the Flight Control Laboratory.

The following personnel of North American Aviation, Inc., contributed to the investigation and study:

G. M. Andrews	G. D. Gruenwald	R. B. Oliver
M. Beilock	D. B. Harrington	R. Olshausen
F. M. Emerson	I. A. Kohn	L. V. Sloma
F. H. Gardner	C. H. Lauritsen	

ABSTRACT

Recommendations resulting from the study of true angle of attack and yaw measurement are presented. The desired accuracy is 0.10 degree under normal flight conditions at Mach numbers up to 3.0 and altitudes up to 100,000 ft. Sensor location on the airframe, the actual sensing device, and the associated computing mechanism are deemed to be the problems of prime importance.

A wide variety of methods for determining angle of attack were analyzed with emphasis on sensor sensitivity, computer complexity, and system reliability. Studies were carried through the stage of devising mechanization for systems showing any promise.

In general, pressure sensing and lift mechanization methods appear to offer the most promise for satisfying the operating conditions set forth in this contract.

PUBLICATION REVIEW

This report has been reviewed and is approved

FOR THE COMMANDER:

Benjamin H. Beerwald
for J. L. MARTIN, Jr.,
Colonel, USAF
Flight Control Laboratory
Directorate of Laboratories

CONTENTS

Introduction 1
Basic Considerations 5
Detailed Discussion of Systems 17
Sensor Locations 83
Components 89
Extension to Flight Data Computers 112
Accuracy Requirements. 116
Summary and Conclusions 121
Nomenclature. 125
References 131

TABLES

1. Hot-wire sensor parameters for four points in flight envelope 69
2. Comparison of systems investigated 120

ILLUSTRATIONS

Figure		Page
1.	Aircraft reference system	2
2.	Modified flight envelope	4
3.	Altitude vs. Mach number for various dynamic pressures	8
4.	Compressibility factor vs. Mach number	8
5.	Static pressure vs. compressible dynamic pressure for various Mach numbers	10
6.	Total temperature vs. Mach number for selected altitude ranges	10
7.	Typical zero lift characteristics for present-day aircraft	12
8.	Proper wave drag coefficient at Mach 3 of a parabolic body of revolution vs. fineness ratio	14
9.	Pressure distribution across 10-degree wedge vs. Mach number	18
10.	Mechanization of wedge angle of attack indicator	19
11.	Pressure ratio vs. angle of attack for wing sensor	21
12.	Pressure ratio vs. angle of attack for cone sensor	21
13.	Mechanization of Spencer angle of attack indicator	22
14.	Mechanization of yaw-pitch pitot tube angle of attack indicator	26
15.	Mechanization of yaw-pitch pitot tube angle of attack and angle of yaw indicator	28
16.	Dual cone angle of attack sensor	29
17.	Dual cone angle of attack and angle of yaw sensor and its mechanization	32
18.	Yaw-pitch pitot tube with dual differential ports	33
19.	Block diagram of null-seeking angle of attack sensor	36
20.	Possible internal mechanism for null-seeking angle of attack and angle of yaw sensor	36
21.	Possible external configuration of null-seeking angle of attack sensor	38
22.	Specialties, Inc., air stream direction detector	40
23.	Lift coefficient vs. attack angle for a selected Mach number	44
24.	Square-law approximation to trim lift coefficient, F-86D aircraft	48

Figure		Page

25. Mechanization of attack and skid angles 58
26. Typical curve of lift force vs. angle of attack for given N, q, and h 62
27. Dual vane sensor showing reference angles 62
28. Mechanization of hot-wire angle of attack indicator . . . 74
29. Smoke particle system with fixed detector 76
30. Smoke particle system with movable detector 76
31. Smoke particle system with movable source 76
32. Single-receiver sonic system 78
33. Dual-receiver sonic system 78
34. Sonic angle of attack indicator. 81
35. Vector resolution of airspeed 81
36. Comparison of possible external sensor locations 84
37. Closed-cycle pressure transducer 90
38. Methods of measuring force 92
39. A sensitive force-measuring system 92
40. Stagnation temperature probe 96
41. Flush-mounted temperature probe 96
42. Compound lever quotient computer 100
43. Force-balance divider 100
44. Dual sensor system using force-balance divider 102
45. Vector-resolution divider 102
46. Function generator as divider 104
47. Multiplier used as divider 106
48. Servo multiplier with servo not in feedback 106
49. Servo multiplier with servo in feedback 106
50. Servo-balanced bridge circuit 107
51. Logarithmic divider. 107
52. Variable feedback high-gain amplifier 107
53. Mechanization of correction computer 110
54. Integrated flight data computer block diagram 114
55. Variation of total system rms error with rms error in accurate element 117

INTRODUCTION

As authorized by contract AF 33(616)-2348, North American Aviation, Inc., initiated a design study for a system capable of measuring true angles of attack and yaw of an aircraft. The capabilities and merits of all pertinent systems were to be evaluated in the light of the contractual requirements.

CONTRACTUAL REQUIREMENTS

The requirements specified in the contract are:

"The Contractor shall undertake to devise a method of measuring angle of attack of an aircraft. The method shall utilize sensing element(s) a compensating distribution amplifier, and indicator. The sensing element shall have a minimum protuberance beyond the skin of the aircraft and shall not utilize or consist of any externally moving parts. The compensating distribution amplifier shall include a computing mechanism to introduce the necessary data (from other sensing elements, if necessary) to compensate for any errors in the basic system and thereby provide for an output of true angle of attack. The amplifier shall provide two isolated synchro type outputs.

"The method shall be suitable for measuring angle of yaw through reorientation of the sensing element and necessary mechanization modifications.

"The goal for accuracy is set at an error of less than 0.1 degree of true angle of attack during normal flight conditions.

"Minimum aerodynamic drag and interference.

"No moving parts external to the aircraft or exposed to environmental conditions.

"Best accuracy attainable under all compatible flight conditions. This accuracy should be maintained:

Throughout the speed range of 90 knots to Mach 3.
Throughout all altitudes up to 100,000 feet.
For all configurations of aircraft such as all wheel, flaps, and bomb bay door positions.

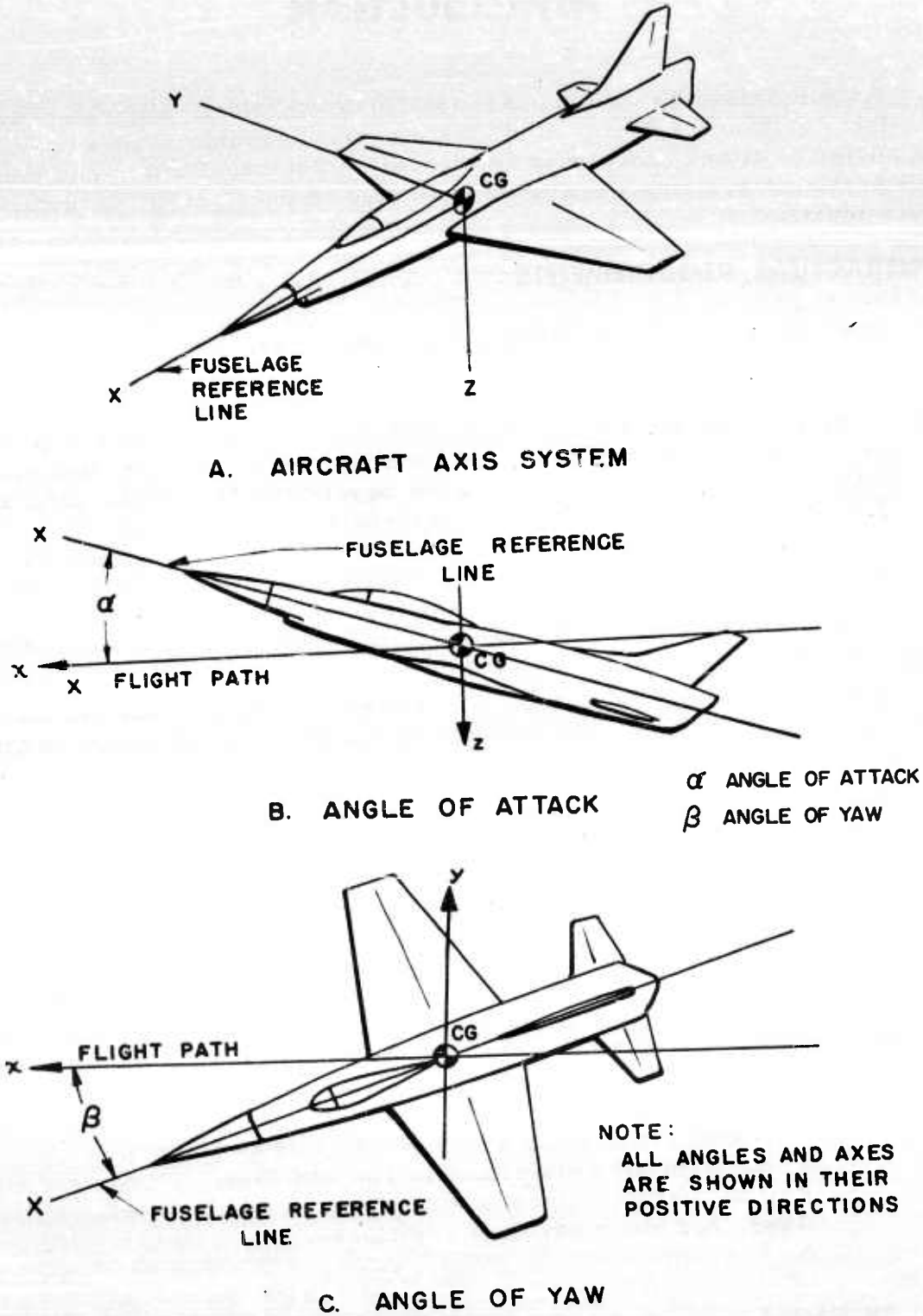

Fig. 1. Aircraft reference system

"Minimum space and weight requirements.

"Maximum reliability and resistance to environmental conditions.

"Practical from standpoint of ease of installation by aircraft contractor.

"Ease of operation.

"Minimum maintenance to keep in operating condition.

"Generally suitable for all types of aircraft with necessary mechanization modifications. For study purposes, arbitrary airplane characteristics will be assumed."

DEFINITIONS

The standard notation for the aircraft reference axis system is shown in Fig. 1, along with the geometrical representation of the angles of attack and yaw. All angles and axes are shown in their positive directions.

The angle of attack of an aircraft (Fig. 1) is that angle between the fuselage reference line and the aircraft flight path within the aircraft vertical plane of symmetry (XZ-plane). It is a pitching angle about the Y-axis with the aircraft nose-up attitude being considered as a positive angle of attack.

The angle of yaw (Fig. 1) is that angle between the fuselage reference line and the aircraft flight path in the aircraft horizontal plane (XY-plane) normal to the aircraft vertical plane of symmetry. When the aircraft nose is to the left of the flight path, as seen along the positive direction of flight path, the angle of yaw is considered positive. "Yaw angle" is frequently labeled "side slip" or "skid angle" by other agencies.

FLIGHT ENVELOPE

The contractual requirements call for the measurement of angle of attack for aircraft operating within the following boundaries:

V = 90 knots to Mach 3.0
h = sea level to 100,000 ft

The envelope defined by these limits is shown in Fig. 2. A modification of this envelope, which encompasses a smaller range of flight parameters, is shown in the same figure. This modification represents the flight envelope recommended by considerations which limit flight. The reasons for modifying the envelope are discussed under the "Flight Parameters" heading of the second chapter.

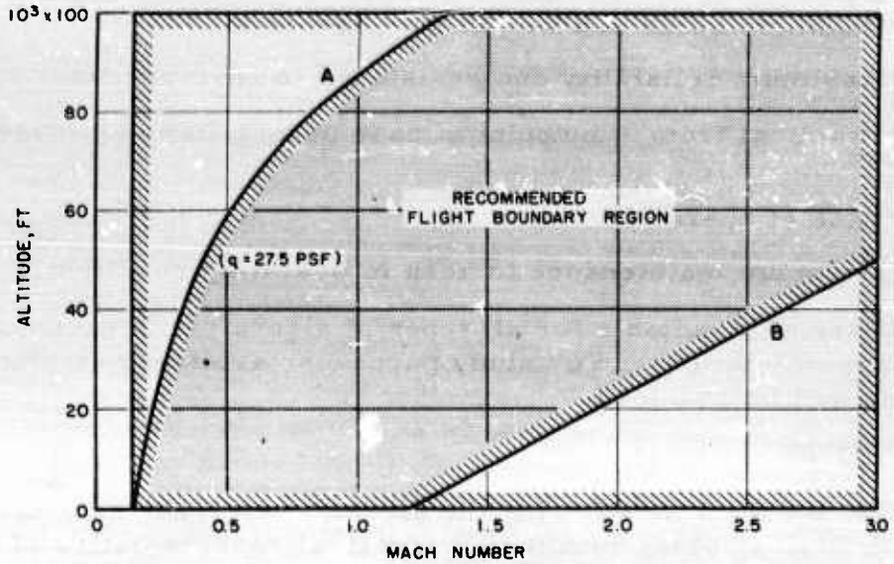

Fig. 2. Modified flight envelope

EXPECTED USES

The true angle of attack indicator has the following applications:

1. Fire control computers
2. Bombing systems
3. Stall warning
4. Cruise control
5. Flight instrument compensation
6. Gust alleviation
7. Fire control autopilots (when used to measure yaw angle)
8. Pilot relief autopilots (when used to measure yaw angle)

Because it is difficult to design and maintain a system providing true angle of attack with an accuracy of 0.1 degree for the entire specified Mach number range of 0.14 to 3.0, the above applications were examined to determine whether regions in the flight envelope exist where this stringent tolerance might be relaxed. Present requirements indicate that the 0.10-degree accuracy is needed only for the fire control and bombing systems, which usually place emphasis on maintaining accuracy at the upper portion of the aircraft speed range. Considering the capabilities of near-future aircraft, it seems reasonable that most importance should be attached to the supersonic portion of the flight envelope.

BASIC CONSIDERATIONS

SENSING METHODS THEORETICALLY AVAILABLE

Before discussing in detail the various angle of attack systems investigated, it is worth while to review the basic principles that can be useful for sensing the air stream direction. Some of these principles can be discarded immediately; others will require more detailed study and comparison.

As stated before, angle of attack is the angle between some reference line in the airplane and the free-stream velocity vector. The free-stream velocity is defined by motion with respect to air molecules. Obviously, then, the sensor must be sensitive to the direction of relative flow of air molecules. The methods available for sensing can be classified according to the angle of attack function measured.

PRESSURE-SENSITIVE DEVICES

As the air flows around any body it creates a certain pressure pattern over the surface of the body for each set of conditions, which are usually velocity, density, and Mach number. If the angle of the air flow over the body changes, the pressure distribution over the body changes. This change in pressure distribution has been widely considered for sensing angle of attack. Pressures are usually sensed at two ports on the surface of the body, located to give as linear an indication of flow angle as possible. Pressure ports may be installed in spheres, cones, or wedges, usually mounted on a boom, as well as in the leading edge of the wing or in the fuselage nose.

These devices usually require information on Mach number, dynamic pressure, and angle of yaw to compute angle of attack. Also, for large ranges of angle of attack, corrections are required for nonlinearities in the relation between pressure readings and angle of attack. Angular rate information may be required for dynamic accuracy.

FORCE-SENSITIVE DEVICES

The above-mentioned pressure distribution over a body results in a net force being produced on the body. The direction and magnitude of this force vary with angle of attack and with the other parameters mentioned. One way of utilizing this principle is to measure the lift force on

the airplane itself. Another possibility is to measure the lift force on a small surface and to use this as an indication of angle of attack. This method also requires corrections for Mach number, dynamic pressure, nonlinearities, and, possibly, yaw.

THERMODYNAMIC DEVICES

As the air encounters a body moving through it, some portion of the velocity energy is converted into thermal energy. A temperature rise at the body surface results. If the body is an ogive or cone, the nose temperature increases most, while that of other portions increases less and depends upon body shape, the flow angle, and general fluid flow parameters.

One possibility is to measure the variation of temperature over a surface with angle of attack. However, the stagnation temperature does not vary as much with change in flow direction (over the body) as does pressure, and is also more difficult to measure accurately (on a surface), because of thermal lag effects. No work has been done on this method.

Another possibility is to measure the rate of heat conduction away from a body due to the air flow over the body. An example of this is the hot-wire anemometer. By using one or two small wires at known fixed angles, one can reduce the thermal lag effects. This also requires information on the flow conditions and wire temperature, from which angle of attack is computed. This system was investigated.

AIR PARTICLE IDENTIFICATION

Under this classification fall all devices which measure the direction of motion of selected particles in air with respect to the airframe. The principal problem is to identify the selected particles.

One example is the sonic transit time method. Basically, it entails exciting the air molecules by a sound pulse and noting the differential transit time to two receivers appropriately located downstream.

Another application ionizes a small volume of air to provide the particles for identification downstream. Some possible configurations have been speculated upon, but none have been investigated thoroughly. A third possibility, to inject some easily identifiable particles such as smoke, has been speculated upon, but not investigated thoroughly.

A fourth is to use the Doppler effect of electromagnetic radiation reflected from selected air masses to obtain true airspeed in two directions.

From these two airspeeds true angle of attack may be obtained. Only a brief study of the basic equations was made for this case.

All the above devices may be used as sensors in some sort of null-seeking device. In general, this means that some device is positioned until the sensor indicates a null signal. The null position of the device is the local angle of attack. The force required to position the device can come from the sensor itself or from an actuator controlled by the sensor. An illustration of the first case is a vane which is free to take up a position dictated by the forces acting on it. An illustration of the second case is a null-seeking differential pressure sensor.

The advantage of a null-seeking device is that it is not necessary to know specifically how the angle of attack sensitive quantity, such as pressure or force, varies with angle of attack and with the various flight conditions. However, the necessity of having external moving parts introduces mechanical difficulties in making the device rugged. A few null-seeking devices are discussed because they are used on present aircraft and require simple mechanisms to obtain local angle of attack.

FLIGHT PARAMETERS

To assist with the analysis of angle of attack measuring systems and the selection of sensors, charts have been prepared which provide the values of important variables over the ranges considered in this study.

The contract requires that the angle of attack be measured throughout the speed range of 90 knots to Mach 3 and throughout all altitudes up to 100,000 ft. This implies possible flight at 90 knots at 100,000 ft and also at Mach 3 at sea level. Since no known present or near-future aircraft flies at these extremes, NAA has recommended the speed-altitude envelope given in Fig. 2. Curves A and B constitute the boundaries which deviate from the boundaries of the contract. Both curves are theoretical and not based on any actual airframe, but there is sufficient supporting evidence in analyses of existing and near-future airframes to substantiate the curves.

Curve A is based on the assumption that the minimum dynamic pressure for flight is the same at all altitudes. If 90 knots at sea level is assumed as the practical condition, the remaining points on curve A are determined by the corresponding dynamic pressure (27.5 psf).

Curve B is based on the limits of maximum dynamic pressure loading for current structural design, the maximum temperatures of aerodynamic heating for current structural materials, and the maximum

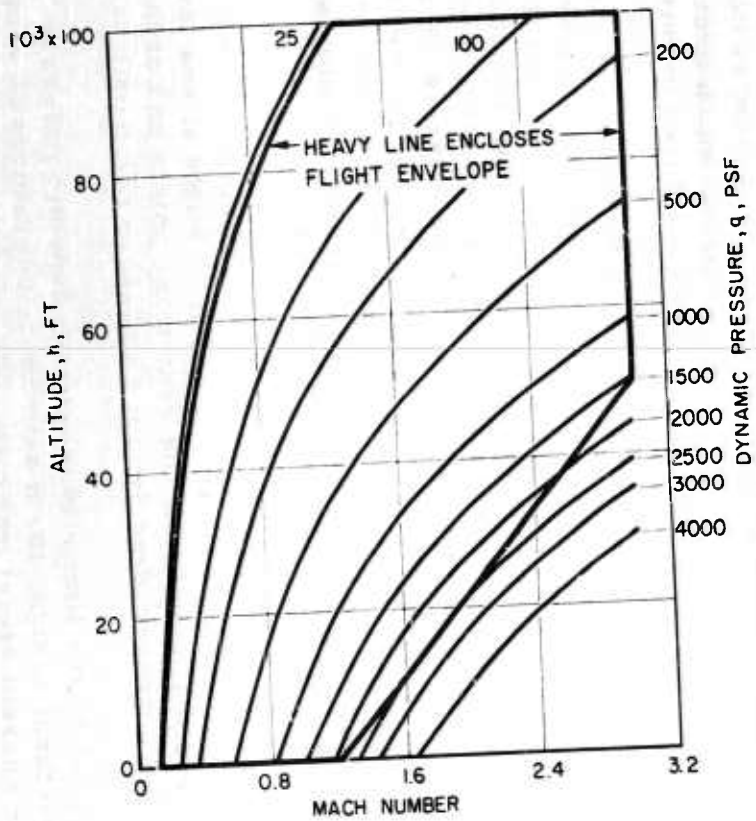

Fig. 3. Altitude vs Mach number for various dynamic pressures

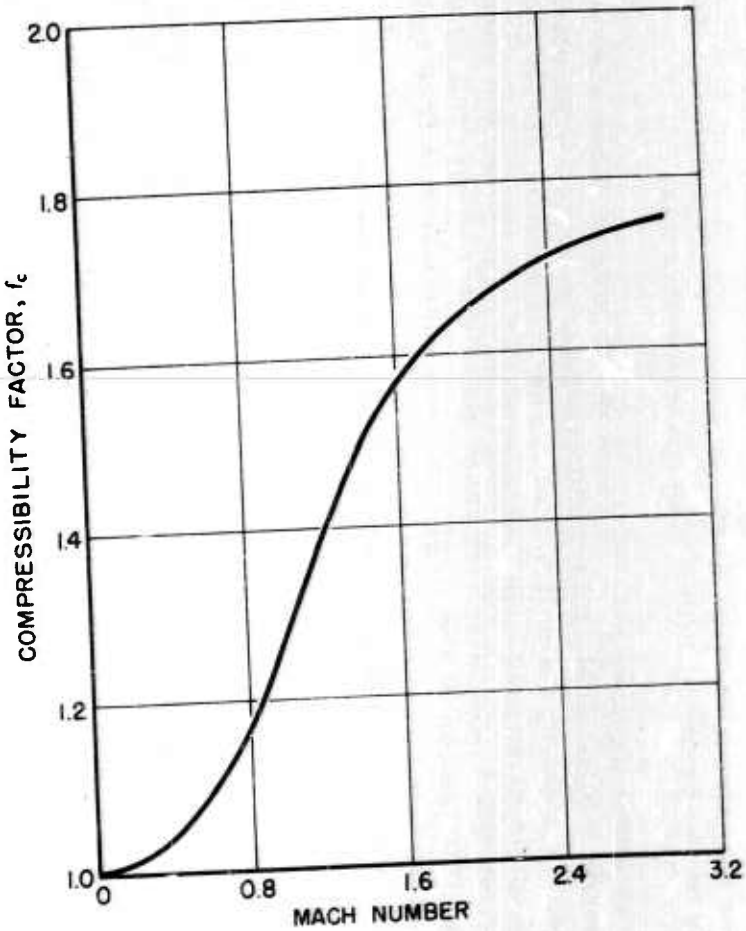

Fig. 4. Compressibility factor vs Mach number

temperatures of high-speed flight for current turbojet engines. Although flight in the region below curve B is possible with new materials, new engines, and heavier structures, the boundaries chosen typify a select group of present-day aircraft.

Figure 3 gives the Mach-number-altitude relationship with constant dynamic pressure lines added. The dynamic pressure is the incompressible dynamic pressure, q, defined by

$$q = \frac{\rho}{2} V^2 \tag{1}$$

where

ρ is air density
V is aircraft velocity

Figure 4 provides the compressibility factor-Mach number information. The compressibility factor, f_c, is defined as the ratio of the compressible to the incompressible dynamic pressure:

$$f_c = \frac{q_i}{q} \tag{2}$$

where

q_i is $P_T - P_S$ and is the indicated, or compressible, dynamic pressure
P_T is total pressure (Supersonically, P_T is the total pressure behind the shock wave.)
P_S is free-stream static pressure

Figure 5 is the plot of free-stream static pressure vs compressible dynamic pressure for pertinent Mach numbers. Figure 6 gives total temperature as a function of Mach number and altitude.

Total temperature is defined by

$$T_T = T \left(1 + \frac{\gamma - 1}{2} M^2\right) \tag{3}$$

where

M is Mach number
T_T is total temperature in degrees absolute
T is ambient temperature in degrees absolute
γ is 1.4 for air

Numerical values for all these aerodynamic parameters are based on the NACA standard atmosphere. (NACA report No. 538)

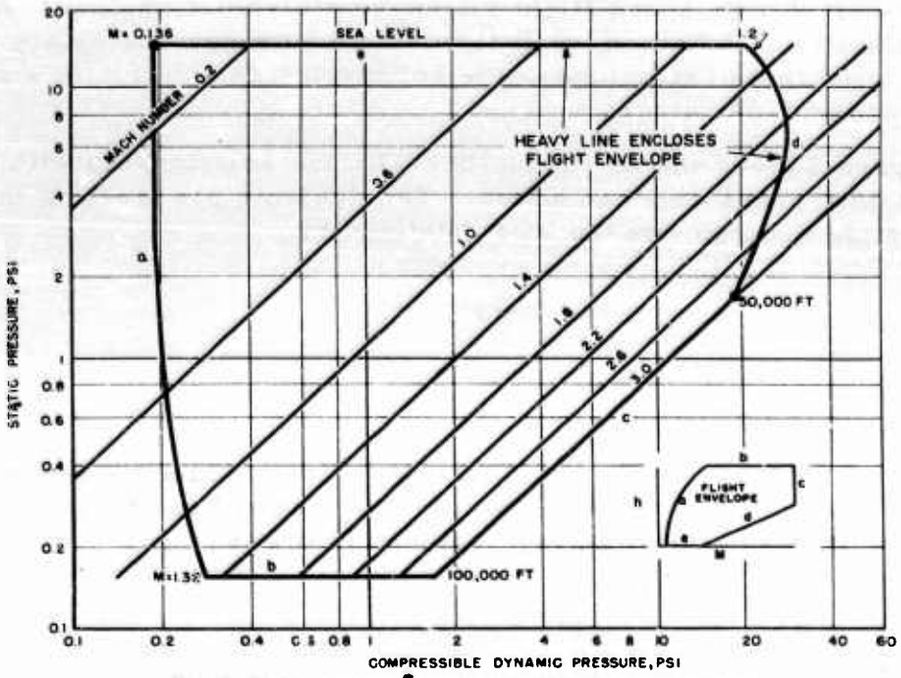

Fig. 5. Static pressure vs compressible dynamic pressure for various Mach numbers

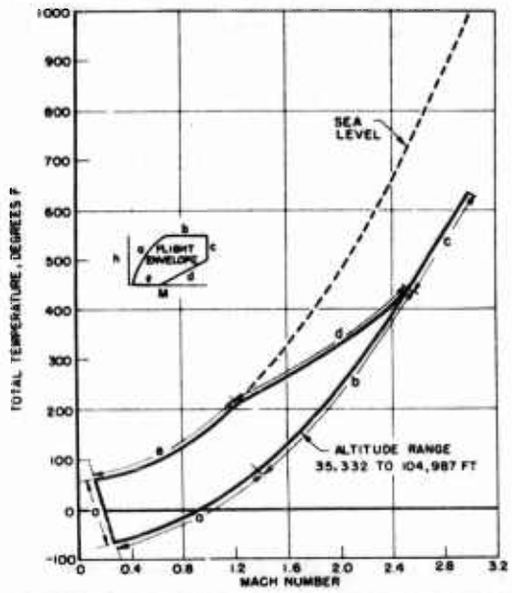

Fig. 6. Total temperature vs Mach number for selected altitude ranges

AERODYNAMIC FLOW CONSIDERATIONS

An aircraft in flight is a body moving through a homogenous mass of air molecules or, better, a flow field. This flow field, disturbed by the body, is the region in which measurements must be made. Any small protuberances such as astrodomes, antennas, external stores, and ripples in the aircraft skin affect the flow direction. At subsonic velocities, pressure is propagated in all directions from the disturbance, and the flow is distorted forward of the body or protuberance, the distance being dependent upon the velocity and upon body or protuberance shape. At supersonic velocities, pressure cannot be propagated forward of the disturbance, as the disturbance is traveling at a velocity faster than the speed of pressure propagation: i.e., than the speed of sound. These effects are of importance in considerations of angle of attack sensor location.

Position Error

Because of the distorted flow field induced by the body, the flow over the body is not in the same direction as the free stream velocity vector (relative wind). The difference between the local flow angle and the free stream direction is defined as position error. Generally speaking, position error is experienced at all points on the body throughout the Mach number, altitude, and flight attitude ranges. Whenever possible, fuselage or wing-mounted flight data sensing devices are mounted at a point where the position error is small and does not vary too much throughout the flight envelope.

Position error can be predicted analytically or determined empirically with good accuracy for a particular aircraft, but the results may not be valid for other aircraft of the same configuration. Manufacturing tolerances and structural deformation, including skin panel ripples, influence the flow direction. Furthermore, any dents or surface roughening experienced in the general vicinity of the sensing element during the service life of the aircraft affect the position error.

In addition, the local flow field is occasionally distorted by protuberances such as retractable components, external stores (not used on every mission and probably dropped prior to combat), and even gun and rocket blast. The latter are short-time effects and not considered important.

It is difficult to determine the position error of an individual aircraft so closely that a system accuracy of 0.10 degree may be obtained, as the error contribution of uncertainty of local flow conditions must then be reduced to a small portion of 0.10 degree. The problem becomes more

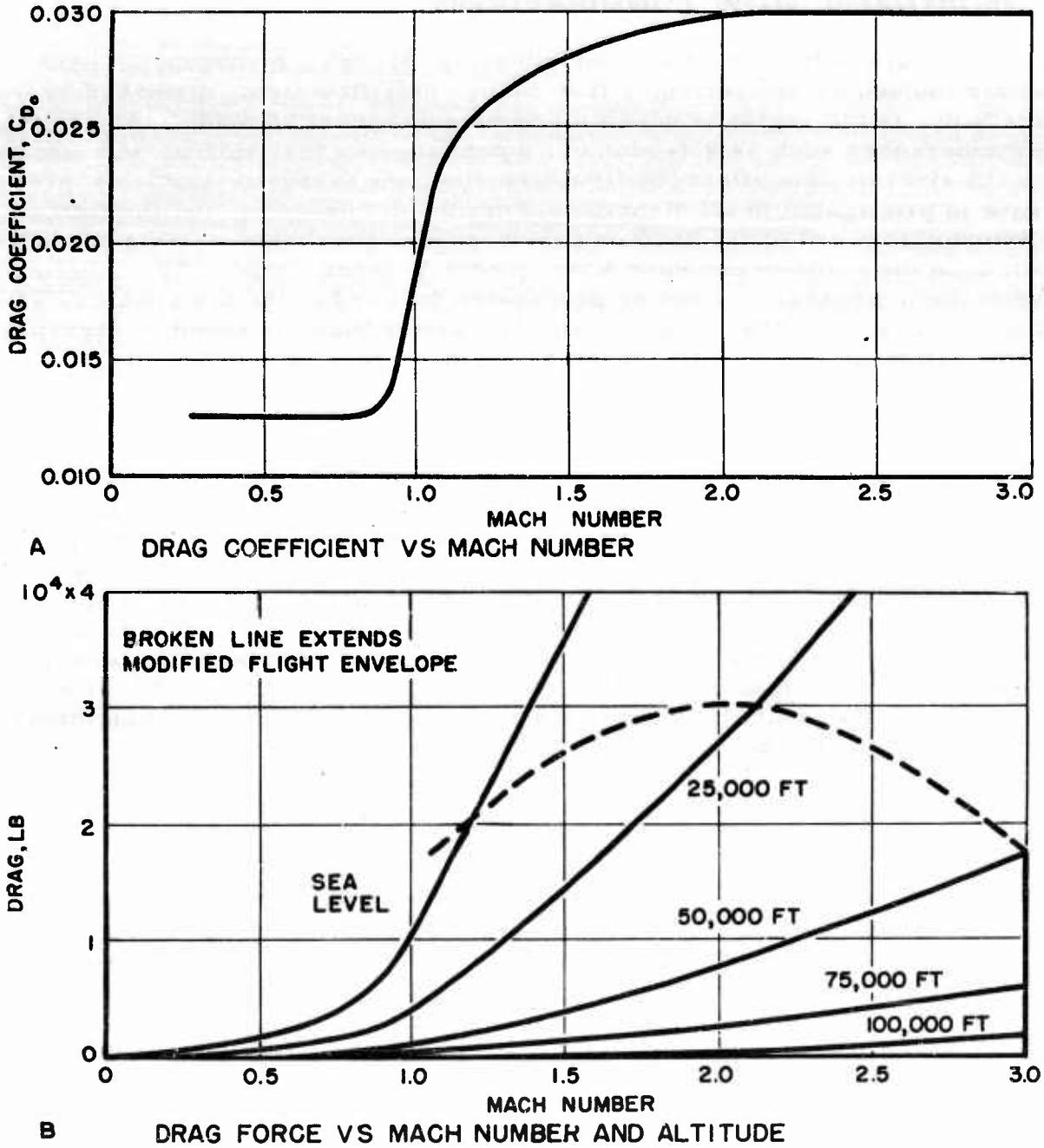

Fig. 7. Typical zero lift characteristics for present-day aircraft

acute for production aircraft because of variations among individual aircraft and because the installation is made, and the system maintained, by less skilled personnel than those available during flight test operations. The overall problem of determination of flow direction to such a small angular tolerance when a large number of variables are involved predicates an advancement in calibration technique, in maintenance procedures, or in both.

From position error considerations, the most suitable location for the external sensing device is forward of the aircraft, perhaps on a short boom mounted on the fuselage nose. Position error effects are experienced at subsonic velocities, but for most airframe configurations the position error here is more accurately predictable than for any other location.

In an aircraft with a nose radar installation, mounting a sensor boom forward of the radar may present problems. Under certain circumstances proper operation of the radar may forbid the use of a nose boom, but there are also conditions under which a boom is permissible. Supersonic radome configurations are such that use of a nose boom on future high-speed aircraft may be possible with no compromise on radar performance.

Probable Aircraft Configurations

Because present-day aircraft are reaching up into the highly supersonic and high-altitude regions of the flight envelope dictated by this contract, streamlining is a factor of prime importance. Drag, a function of the streamlining designed into the aircraft, must be kept to a minimum for efficient high performance.

Figure 7 represents the zero-lift drag characteristics of a typical present-day fighter aircraft. In Fig. 7, A the zero-lift drag coefficient is assumed to be independent of altitude, as the data are only typical. Actually, that portion of the zero-lift drag due to viscous skin friction (C_{D_f}) is a function of altitude as well as Mach number. The lower portion (Fig. 7, B) is the actual drag or resistive force in pounds as a function of Mach number for various altitudes. The area bounded by the curves for sea level and 100,000 ft, as well as the dashed line, is the recommended flight envelope already discussed.

Maximum Mach number and minimum fuel consumption require that none of the available engine thrust be wasted on needless drag. For a given aircraft-engine combination proper emphasis on streamlining is

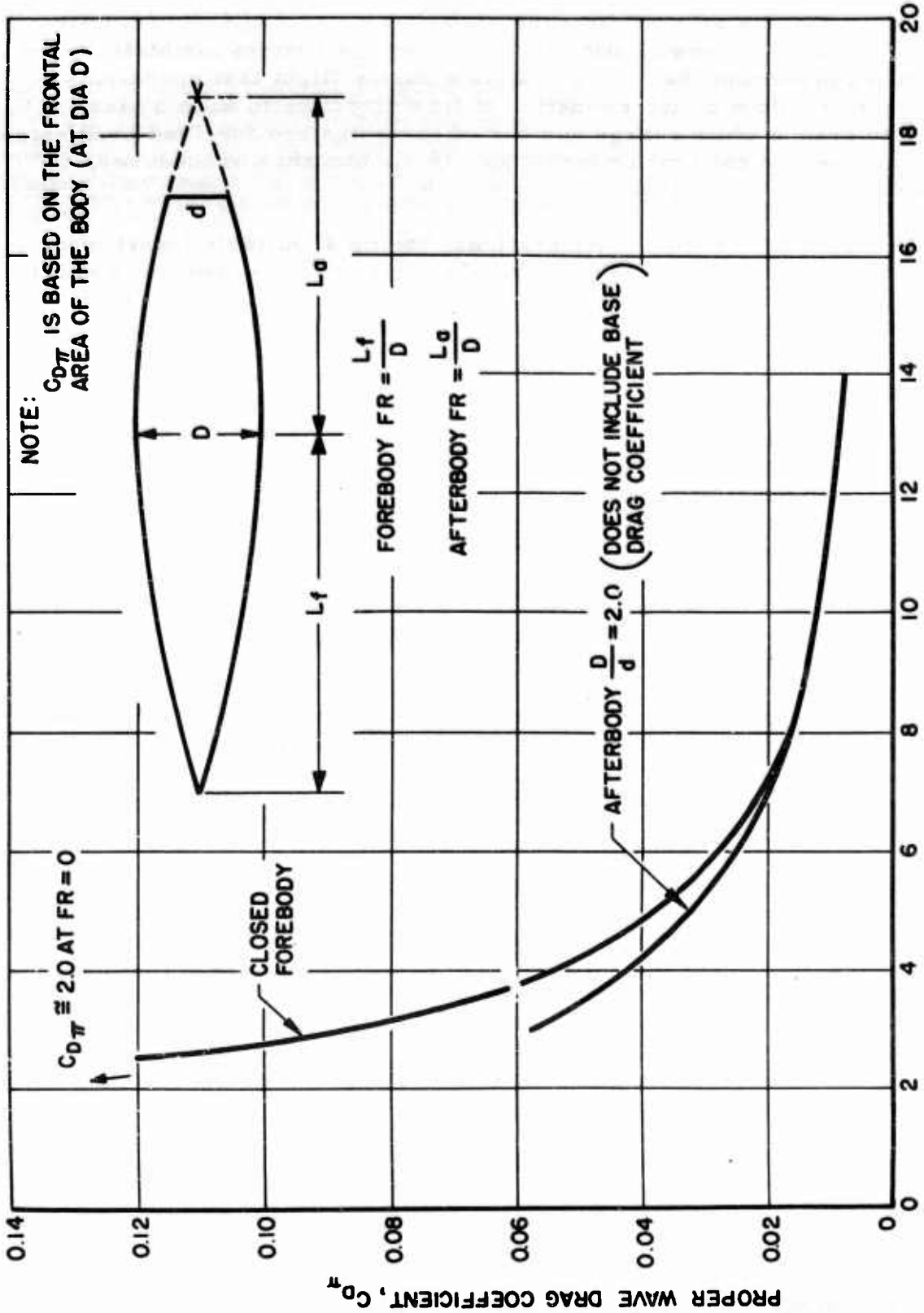

Fig. 8. Proper wave drag coefficient at Mach 3 of a parabolic body of revolution vs fineness ratio

necessary for optimum performance, and with current engines minimum drag is of utmost importance in achieving high supersonic velocities.

Because supersonic vehicles are primarily of interest, the following discussions will be limited to the analysis of the various forms of drag build-up in supersonic compressible flow. In addition, only the zero-lift drag characteristics will be considered. The types of drag which contribute to the zero-lift drag are wave drag and skin friction drag.

Wave Drag

Wave drag is the drag induced by pressures on a body. In Fig. 8 are presented the proper wave drag coefficients at Mach 3.0 for a closed parabolic forebody of revolution and for a blunt-base parabolic after-body of revolution, where the ratio of the maximum frontal area diameter to the base diameter is two. It can be seen that the drag coefficient increases very rapidly for fineness ratios lower than eight. Therefore it is reasonable to assume that for high-performance supersonic vehicles, the fineness ratios of the fore and afterbodies must be high (at least greater than eight). A slight rounding of the nose of the forebody is permissible without too large a drag penalty, as long as the ratio of the radius of the hemispherical nose section is small in comparison to the maximum frontal area body diameter.

Supersonically, wave drag of a wing is proportional to the square of the thickness ratio (section thickness to chord). For a biconvex section, the proper wave drag coefficient is

$$C_{D_\pi} = \frac{K\left(\frac{t}{C}\right)^2}{\mathcal{M}} \tag{4}$$

where

$\mathcal{M}$ is $\sqrt{M^2 - 1}$

$\frac{t}{C}$ is thickness ratio

K is a function of the planform aspect ratio, taper ratio, and sweep angle

Here, again, it can be seen that streamlining in the form of thin wings is important for drag reduction.

Skin Friction Drag

Skin friction drag is due to the shearing stresses within the boundary layer. The stresses within a laminar boundary layer produce a lower drag than those in a turbulent boundary layer. Therefore transition from a laminar to a turbulent boundary layer should occur as far back on the body as possible. This can be achieved by streamlining for wave drag reduction and by other means of boundary layer control such as cooling or creation of a vacuum below the surface to pull the boundary layer down on the body.

In conclusion, it is reasonable to assume that the aircraft configuration of the future will be characterized by high fineness ratio bodies of revolution and by thin, aerodynamically clean wings employing some means of boundary layer control.

DETAILED DISCUSSION OF SYSTEMS

PRESSURE-SENSITIVE DEVICES

Wedge

A wedge-shaped block with pressure ports or sensors in the upper and lower surfaces can be used as an angle of attack sensor. The difference in pressure between the upper and lower ports is used as an indication of the local angle of attack.

A study of the two-dimensional pressure distribution across a 10-degree wedge has been made, with the results presented in Fig. 9. It can be seen that there is some doubt as to the predictability of the pressure coefficient below Mach 1.2. Whether the real characteristic is unique and repeatable would have to be determined empirically. The sharp leading edge of the wedge causes separation of flow at large angles of attack. This separation might cause difficulty in getting repeatable readings and also might cause sudden changes in pressure.

A wedge with a larger angle would most likely increase the angle of attack before separation occurs. Another disadvantage would be that another wedge is required to get angle of yaw. By using cones or spheres as discussed later it is possible to measure angle of attack and angle of yaw from the same probe.

A practical difficulty with the wedge method is that the leading edge shape and surface condition must be maintained in spite of contact with objects in flight and in ground handling.

On the basis of present information, the differential pressure across the wedge can be expressed as

$$\Delta P_a = q_i f_1(M)\ f_4(\beta)\ [\alpha_L + f_2(M)\ f_3(\alpha_L)] \tag{5}$$

Here $f_1(M)$, $f_2(M)$, $f_3(\alpha_L)$, and $f_4(\beta)$ are arbitrary functions to be determined by experiment. Equation 5 may be rewritten as

$$\alpha_L = \frac{\Delta P_a}{q_i f_1(M)\ f_4(\beta)} - f_2(M)\ f_3(\alpha_L) \tag{6}$$

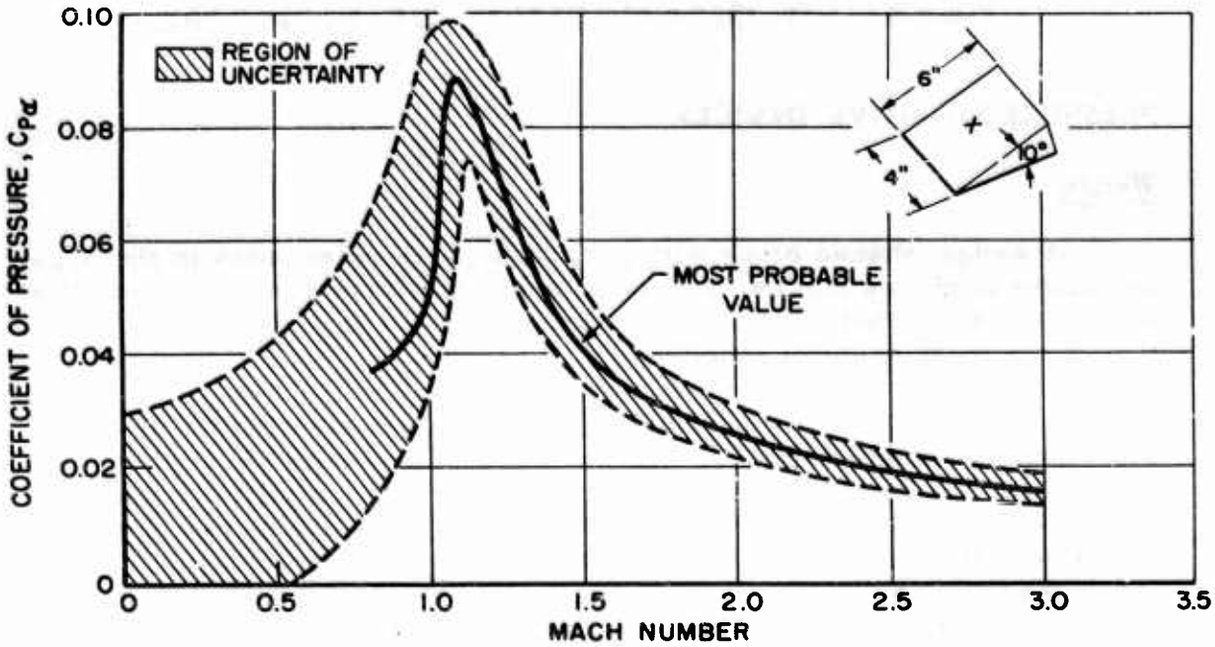

Fig. 9. Pressure distribution across 10-degree wedge vs Mach number

The mechanization of this equation is presented in Fig. 10. Here the quotient is computed in a mechanical divider which calculates the resultant angle of a vector addition. An operational amplifier, potentiometer function generators, and multipliers are used to compute

$$\frac{\Delta P_\alpha}{q_i f_1(M)\ f_4(\beta)} \text{ and } f_2(M)\ f_3(\alpha_L),$$

which are then summed in an operational amplifier to obtain α_L. This signal is fed to a servo which drives one of the function potentiometers and also provides an input to the correction computer, which computes the true angle of attack. This computer is discussed in pp. 108 ff. Another wedge at 90 degrees (about the X-axis) to the first is used to obtain β. As β is used only in a correction term, it does not have to be known as accurately as α and therefore the ratio $\frac{\Delta P_\beta}{q_i}$, as computed by variable feedback around an operational amplifier, is used instead of β.

Spencer System

This system utilizes two pressure orifices, one on the upper surface and one on the lower surface of a wing leading edge. Angle of attack is

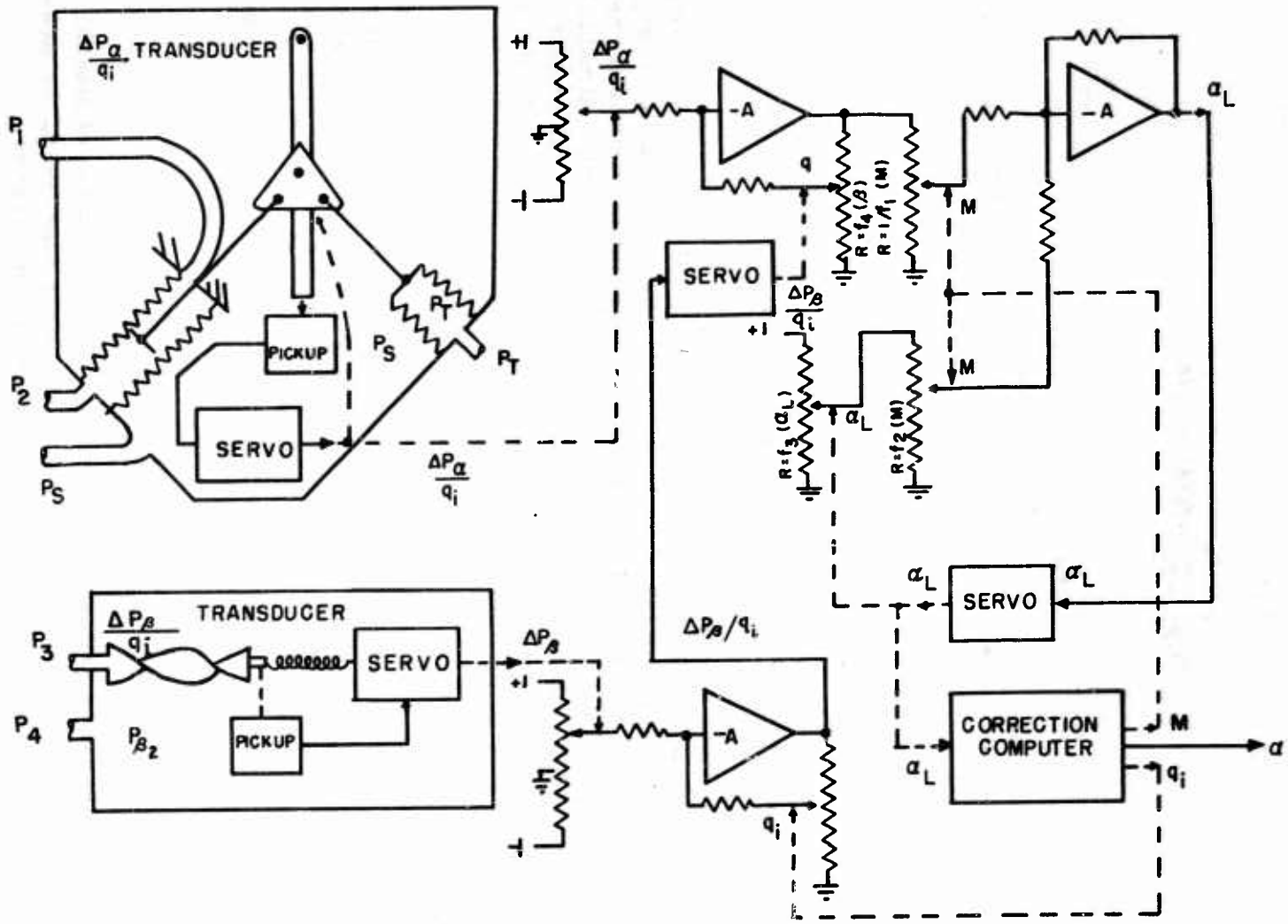

Fig. 10. Mechanization of wedge angle of attack indicator

given by the following formula, where the pressures are obtained from the locations shown below:

$$f_1 \frac{P_U - P_T}{P_L - P_T} \quad f_2(M) + f_3(M)$$

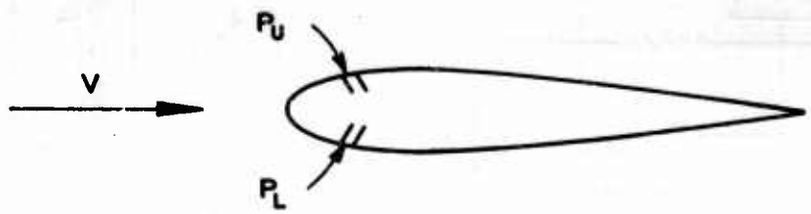

Here f_1, f_2, and f_3 are functions to be determined from flight test.

This angle of attack system is the result of several years of development. When originally conceived, it was proposed to use the position of the stagnation point on the wing leading edge as an indication of angle of attack. Later it was decided to measure the point of minimum pressure on the upper surface. After experimentation, a system similar to the present one but using static instead of total pressure was constructed and tested. The results of the test were not conclusive because the relatively large size of the model caused excessive distortion of the tunnel flow.

The Spencer system is basically a wing sensor in which the ratio of pressures at the upper and lower orifices, rather than their difference is used to compute the angle of attack. The principle of calculation of angle of attack from a pressure ratio rather than a pressure difference can be applied to the other pressure sensors discussed. Figures 11 and 12 present wind tunnel data on this subject. Figure 11 is based on data obtained from Ref. 98, which presents the results of NACA wind tunnel tests made to determine the chordwise pressure distributions on a wing. (These data are also used by Spencer in Ref. 85.) Figure 12 is based on data obtained by NAA on tests of a cone pressure sensor. These figures present the pressure ratios $\frac{P_U - P_T}{P_L - P_T}$ and $\frac{P_L - P_U}{q_t}$ vs. angle of attack. The curves show that the angle of attack is a nonlinear function of the pressure ratio but is a linear function of the pressure difference.

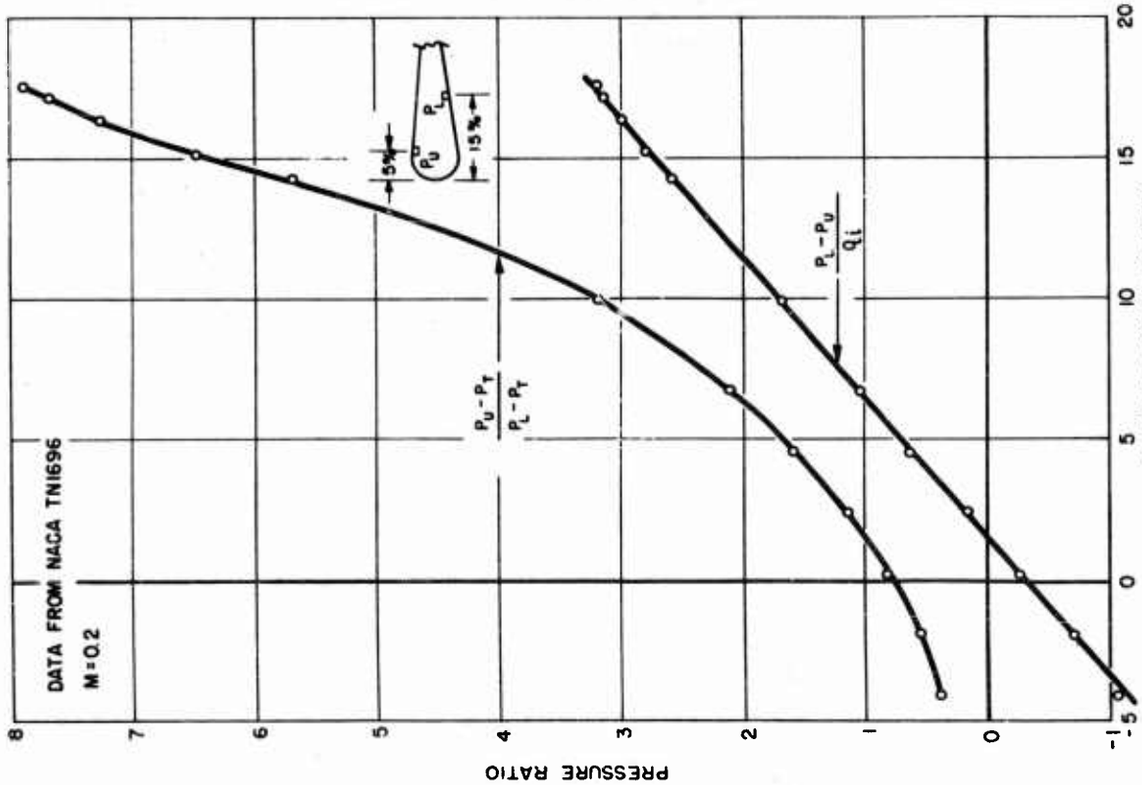

Fig. 11. Pressure ratio vs angle of attack for wing sensor

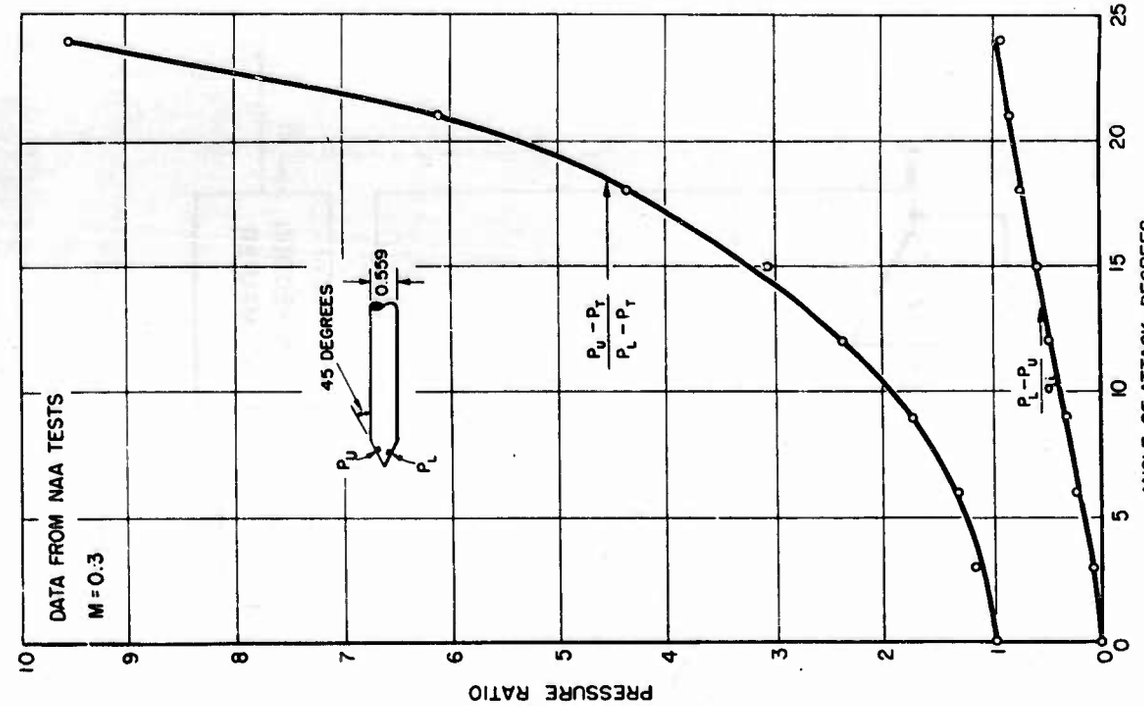

Fig. 12. Pressure ratio vs angle of attack for cone sensor

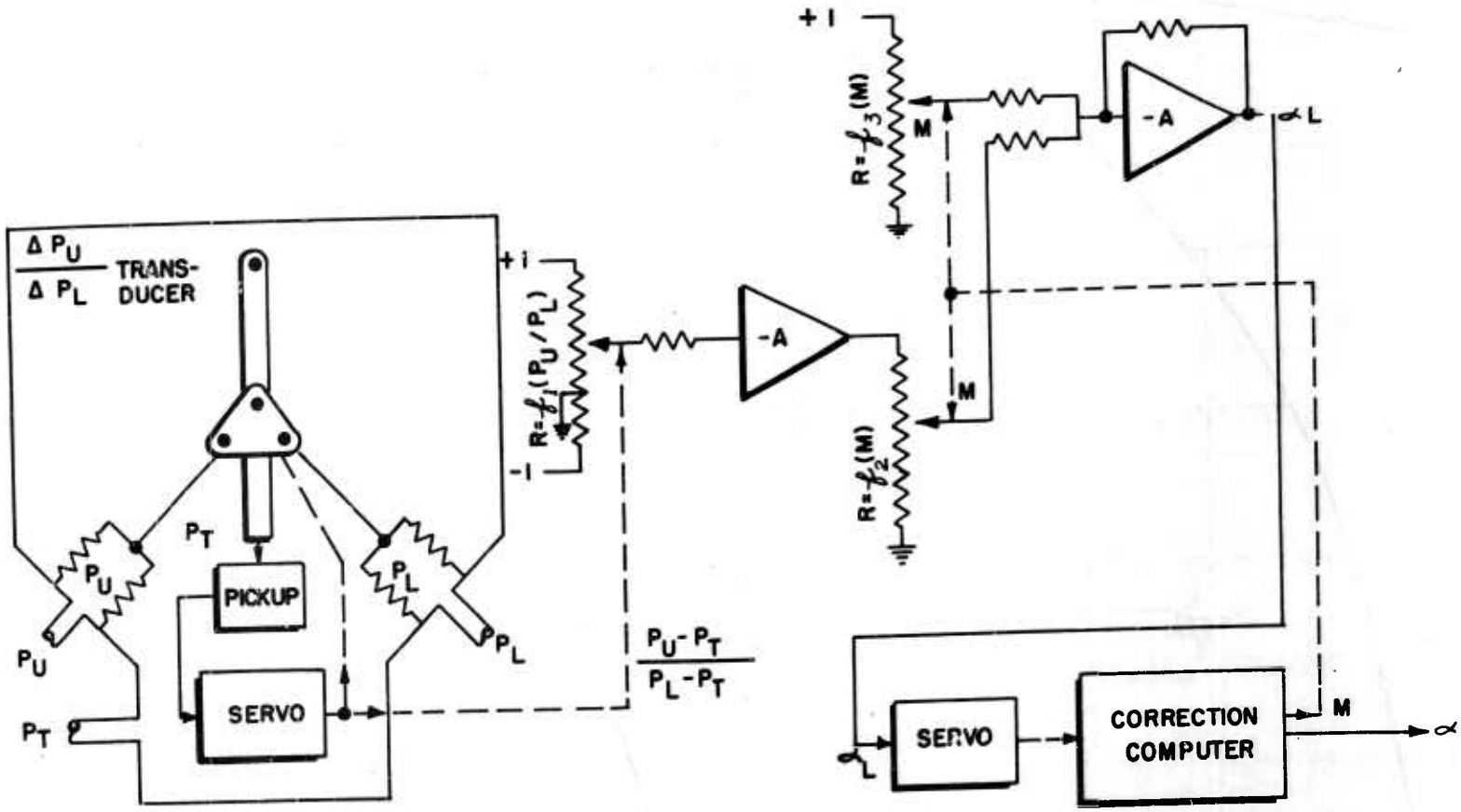

Fig. 13. Mechanization of Spencer angle of attack indicator

A possible advantage of the Spencer system is that the final equation for obtaining angle of attack from the pressure information may be simpler. Since both wing pressure distribution and wing induced velocity are caused by the wing traveling through the air, it is not necessary to correct for local flow due to the wing. However, it is necessary to correct for local flow due to the presence of the fuselage. Because of the lack of information over a wider speed range, it is not possible to tell whether there is any simplification. An advantage (Ref. 85) of using a wing section is that it is not necessary to mount the sensor on a boom. However, the advantage of eliminating a boom for mounting a sensor is not realized because a boom is still needed for P_T and P_S information to compute Mach number for the Mach number corrections.

A Cornell Aeronautical Laboratory study (Ref. 27) mentions using the wing leading edge for a differential pressure source. It indicates that a greater differential pressure can be obtained by this approach. It also mentions the disadvantage that if the wing surface in the area of the sensor is dented, the calibration will change. The pressure ports on the wing also suffer from yaw effects, which must be corrected by a computer.

For use on present and future supersonic fighters this system has disadvantages. Location on the wing means that the pressure measurements are subject to discontinuities due to shock waves from parts of the plane ahead of the swept wings. Also, whenever wing flaps, slots, or boundary layer control are used, the equation for computing angle of attack must be changed. In general, if part of the plane is to be used as a differential pressure sensor, some section that has less interference, such as the nose section, is desirable.

The mechanization of the Spencer system is presented in Fig. 13. Here the quotient $\frac{P_U - P_T}{P_L - P_T}$ is computed in a mechanical divider, which is discussed in the section on computers. Function potentiometers and an operational amplifier are used to compute the local angle of attack, which is then fed to the correction computer to provide true angle of attack. This correction computer is more complex than that discussed on p. 108 because it must compensate for shock waves crossing the wing. It should be pointed out that the computer requires major change in mechanization for application to each different type of airplane.

Nose Location of Pressure Ports

The nose location of pressure ports offers some advantage for supersonic aircraft. For present and future supersonic or transonic planes

radar is definitely needed to assist the pilot in or to take over completely the task of sighting and tracking the enemy. Even noncombat planes are beginning to use radar for location of obstacles in the flight path.

A nose location of radar is common in most planes. A pointed nose is also necessary for the reasons discussed on p. 15. Also discussed in this section is the fact that the nose on these planes is most free from local velocity disturbances subsonically, and supersonically the only local disturbances encountered are those due to the nose. In the event a sensor on a short nose boom is not feasible, pressure ports on the tip of the nose are a good possibility.

The tip of the nose is sufficiently small in cross section that little trouble is expected in making a surface of the required shape and uniformity on production planes. The tip of the nose could be a cone, hemisphere, or similar shape. The characteristics of such a nose sensor are similar to those of a yaw-pitch pitot tube, which is discussed next. The tubing to the ports in the nose would be of a material that would not affect the radar pattern.

Yaw-pitch Pitot Tube

This is a tube with a symmetrical head, such as a hemisphere or cone, with pressure ports on the surface to obtain total pressure and differential pressure information as functions of angle of attack. The ports are located as illustrated.

$$\alpha_L = \frac{\Delta P_\alpha}{q_i} f_1\left(\frac{\Delta P_\beta}{q_i}\right) f_2(M) \qquad P_1 - P_2 = \Delta P_\alpha \qquad (7)$$

$$P_3 - P_4 = \Delta P_\beta$$

$$\beta_L = \frac{\Delta P_\beta}{q_i} f_1\left(\frac{\Delta P_\alpha}{q_i}\right) f_2(M) \qquad P_T - P_S = q_i \qquad (8)$$

The functions f_1 and f_2 must be determined from accurate wind tunnel tests on a particular probe shape through the range of variables. Cornell Aeronautical Laboratory, Inc., has done considerable work on this tube and much of what is reported here is from its work (Ref. 28).

On the basis of present information some generalizations can be made for the functions f_1 and f_2. First, it is assumed that the surface is symmetrical and that the holes are located accurately and symmetrically and within such production tolerances that α may be consistently computed within 0.1 degree. The data given by Cornell presenting $\frac{\Delta P_\alpha}{q_i}$ and $\frac{\Delta P_\beta}{q_i}$ vs. α and β show no symmetry for positive and negative values of α and β. This indicates that some care is required in machining the probe and/or recording the pressure data. How accurate machining should be has not yet been determined. In order to avoid making a specific correction computer for a specific probe, it would be desirable to have all probes made perfectly symmetrical.

At a fixed Mach number and a zero angle of yaw it can be stated that $\alpha = K\frac{\Delta P_\alpha}{q_i}$ over some range of α, where K is a constant. From the information so far obtained for 0.1-degree accuracy, the range of α is from 0 to 10 or 15 degrees. The variation from nonlinearity is a second-order effect. As β is varied from zero with α constant, the value of $\frac{\Delta P_\alpha}{q_i}$ varies. This is a second-order effect for the range of yaw angle at which an airplane would fly, say, ±10 degrees. The Mach number effect is a first-order effect. The main result is to change the value of K which ranges from 11.1 at subsonic speeds to 28.6 at around $M = 2.0$.

Cornell made wind tunnel tests on cones of various cone angles (30, 40, and 50 degrees) and hemispheres with holes located at angles of 30 and 45 degrees to find out how linearity and sensitivity varied with the various configurations. They found that the hemispherical probe with holes at 45 degrees gave the best sensitivity. The linearity with α was about the same for all configurations. Cones required the least Mach number correction.

The yaw-pitch pitot tube and other differential pressure sensors require a pressure transducer having high sensitivity over a wide range of pressure. A study of pressure transducers that would work over such a range is reported in the chapter entitled "Components."

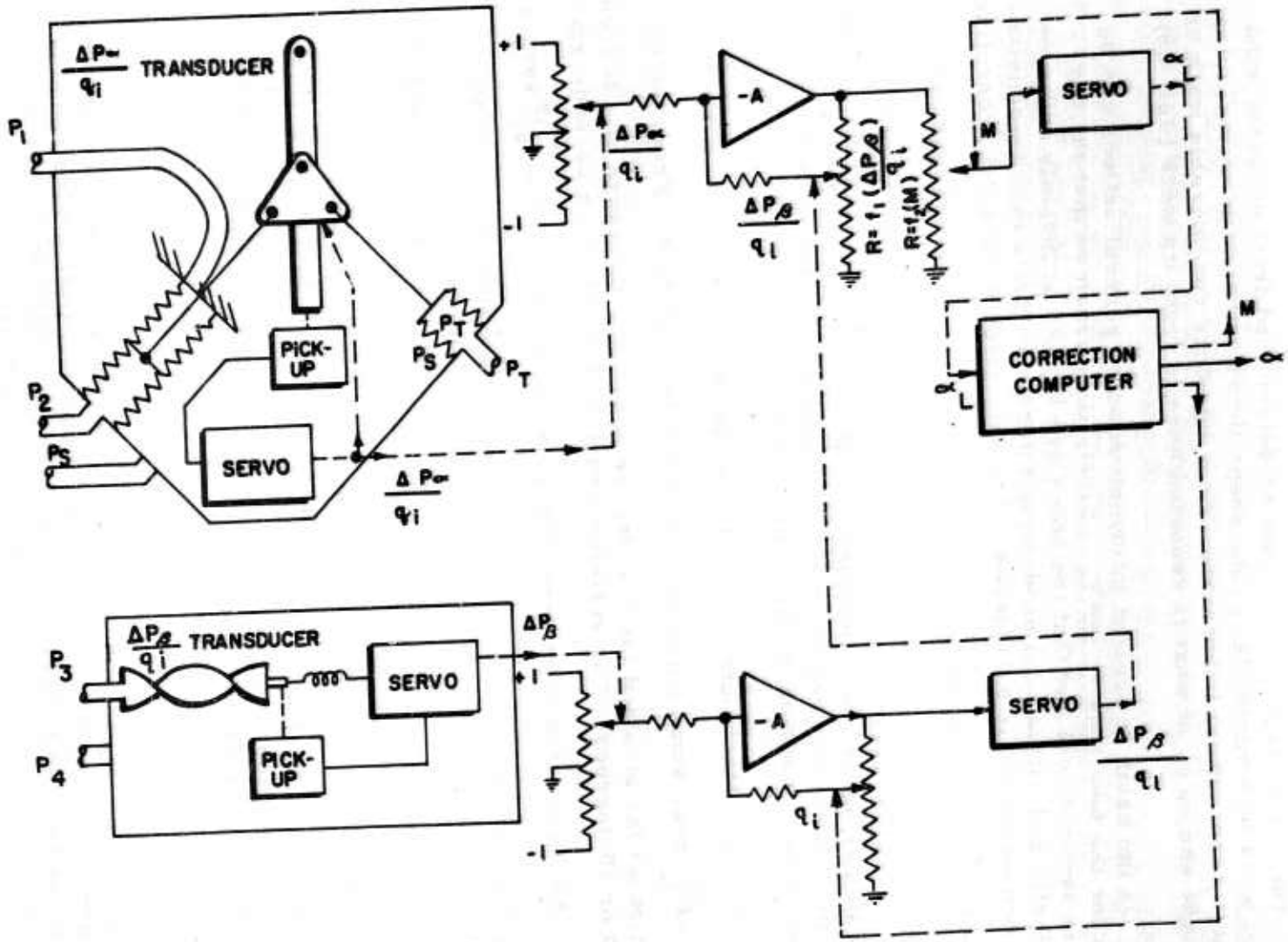

Fig. 14. Mechanization of yaw-pitch pitot tube angle of attack indicator

The mechanization of the equation for local angle of attack is presented in Fig. 14. Here the quotient $\frac{\Delta P_\alpha}{q_i}$ is computed in a mechanical divider. Since $\frac{\Delta P_\beta}{q_i}$ is used in a correction term, it can be computed with less accuracy, and this calculation is made by variable feedback around an operational amplifier. Function potentiometers and an operational amplifier are used to compute the local angle of attack, which is then fed into the correction computer to obtain the true angle of attack. The correction computer is discussed on p. 108.

By a slight modification of the mechanization (Fig. 15), the same pitot tube can be used to compute the angle of yaw. Here the same type of divider (Fig. 14) is used to calculate both $\frac{\Delta P_\alpha}{q_i}$ and $\frac{\Delta P_\beta}{q_i}$. The remainder of the calculation of the true angle of attack is also the same as in the mechanization of Fig. 14. The calculation of the true angle of yaw is done similarly, but no correction computer is required, as the relationship between the true angle of yaw and the local angle of yaw is quite simple and can easily be handled by the choice of scale factors. True angle of yaw is given by

$$\beta = K_1 \beta_L + K_2 \tag{9}$$

In general, the yaw-pitch pitot tube shows promise of being a successful device for measuring angle of attack. The sensor itself can be built to withstand extremes of environment during flight. During ground maintenance, however, precautions must be taken, as with present pitot-static tubes, to keep the tube from being bent or the hemispherical or conical surface from being disfigured.

This system does require an accurate computer to compute local and free-stream angle of attack from the pressure information. The part of the computer that measures pressures and divides $\frac{\Delta P}{q_i}$ is the most critical. As many computations for nonlinearities and α-β coupling can be made as necessary to achieve the desired accuracy, the limitation being that the computer becomes increasingly complex as more corrections are required. The computer and pressure transducers can be installed in a suitable environment in the plane. Present experience indicates that a computer could be built to give the desired accuracy.

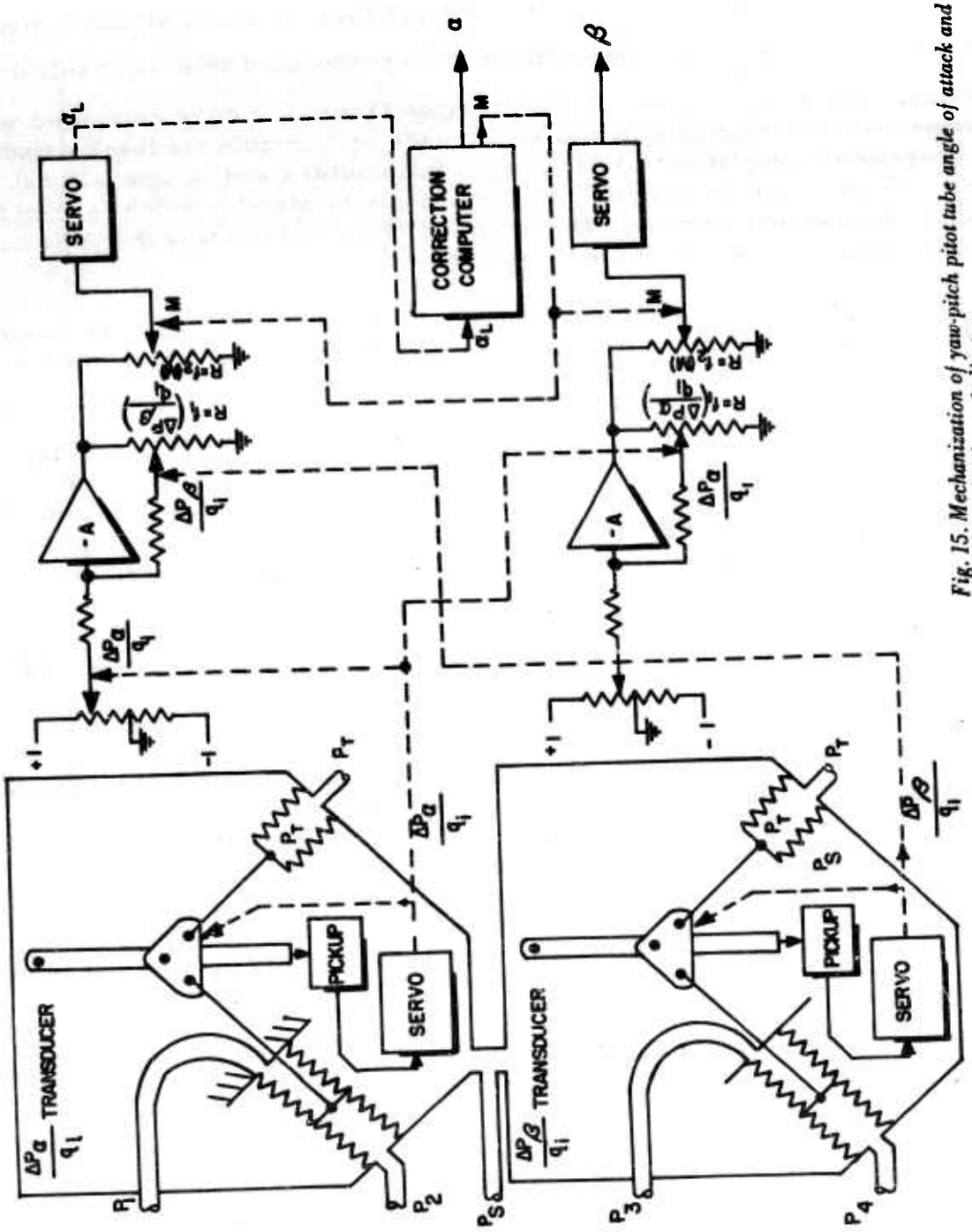

Fig. 15. Mechanization of yaw-pitch pitot tube angle of attack and angle of yaw indicator

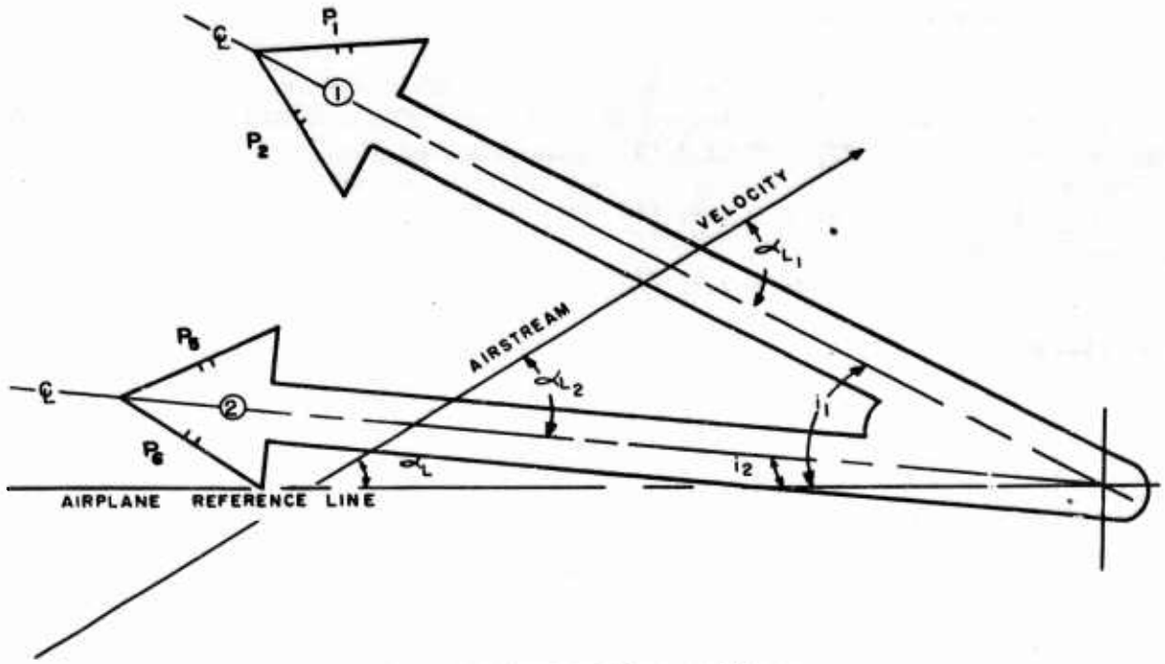

Fig. 16. Dual cone angle of attack sensor

Dual Sensors

The angle of attack detector utilizing dual pressure sensors is composed of two similar sensors: one mounted with its center line at an angle i_1 with the airplane reference line and the other mounted with its center line at an angle i_2 with the reference line. Figure 16 presents a dual cone system; however, the sensors may be wedges, cones, or pitot tubes as long as both sensors are identical. For any of these sensors the differential pressure between the upper and lower ports is given by an equation of the form

$$\Delta P = q_i \alpha_L f(M, \beta) \tag{10}$$

For sensors 1 and 2,

$$\alpha_{L_1} = \alpha_L + i_1$$

$$\alpha_{L_2} = \alpha_L + i_2$$

$$\Delta P_{1-2} = q_i \alpha_{L_1} f(M, \beta)$$

$$\Delta P_{5-6} = q_i \alpha_{L_2} f(M, \beta)$$

Therefore

$$\Delta P_{1-2} - \Delta P_{5-6} = (i_1 - i_2)\, q_i f(M, \beta) \tag{11}$$

and

$$\frac{\Delta P_{5-6}}{\Delta P_{1-2} - \Delta P_{5-6}} = \frac{\alpha_L + i_2}{i_1 - i_2} \tag{12}$$

Solving for α_L gives

$$\alpha_L = \frac{\Delta P_{5-6}}{\Delta P_{1-2} - \Delta P_{5-6}} (i_1 - i_2) - i_2 \tag{13}$$

If the sensors are rigged with $i_2 = 0$,

$$\alpha_L = i_1 \frac{\Delta P_{5-6}}{\Delta P_{1-2} - \Delta P_{5-6}} \tag{14}$$

This system is self-calibrating, since effects of dynamic pressure, Mach number, and yaw angle are cancelled.

One effect that may cause difficulties with this system is that subsonically the flow fields around the cones interfere with each other. In supersonic flow, shock waves are formed. As the shock wave from one cone passes over the other cone, a pressure discontinuity exists. So, if a cone or a hemisphere can be found that satisfies the equation $\alpha = K \frac{\Delta P}{q_i} f(M, \beta)$, where K is constant for a given q_i, M and β for all values of q_i, M and β in the flight envelope, then the advantage of the system is realized. The above must also remain true of one cone when

mounted near the other cone. NAA has made wind tunnel tests of two 45-degree cones mounted as shown in Fig. 17, A. When these cones were tested it was found that they were separated by the yaw angles shown in Fig. 17, A and in angle of attack by 45 minutes of arc.

These tests were made to demonstrate the above principle. The idea was to use $\Delta P_{3-4} - \Delta P_{7-8}$ as the reference differential pressure, as was done with $\Delta P_{1-2} - \Delta P_{5-6}$ in Eq. 14; knowing this, one can get α_L and β_L from the following equations:

$$\alpha_L = \frac{\Delta P_{1-2}}{\Delta P_R} 4^\circ 25' \tag{15}$$

$$\beta_L = \frac{\Delta P_{7-8}}{\Delta P_R} 2^\circ 55' \tag{16}$$

where

$$\Delta P_R = (\Delta P_{3-4} - \Delta P_{7-8})$$

In the tests it appeared that the induced flow of the airfoil-shaped supporting structure caused some changes in slope of the curves. It was also found that the reference differential pressure changed with the angles of attack and yaw. This could be due to the probes being misalined 45 minutes of arc in angle of attack in addition to angle of yaw, causing unwanted coupling effect. In general, it is important that both cones have the same characteristics within the 0.1-degree tolerance and be alined with one another within the 0.1-degree tolerance. Further tests will have to be made to determine the feasibility of this system. Care will have to be taken to maintain the physical dimensions of this probe in field use.

The mechanization of this system is presented in Fig. 17, B. Because of its self-calibrating feature, this mechanization is considerably simpler than that of other systems. It consists of a mechanical force-balance divider which computes the local angle of attack directly. The output of this divider is fed to the correction computer, which is discussed in pp. 108 ff.

Yaw-pitch Pitot Tube with Dual Differential Pressure Ports

Many advantages result from applying the principle of the dual pressure sensors to the head of a yaw-pitch pitot tube. Two pairs of pressure ports are located on the head of a yaw-pitch pitot tube as shown in Fig. 18, A.

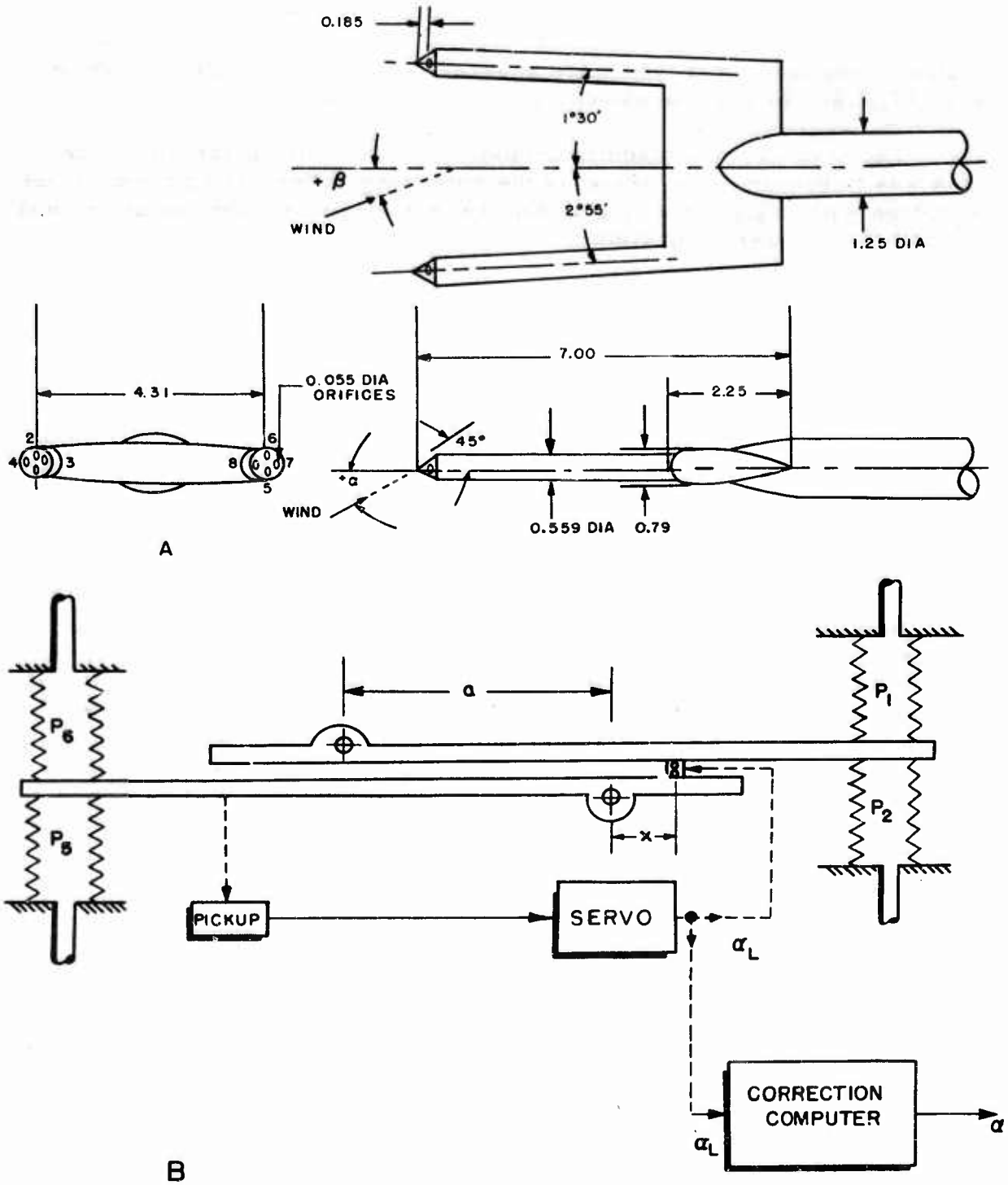

Fig. 17. Dual cone angle of attack and angle of yaw sensor and its mechanization

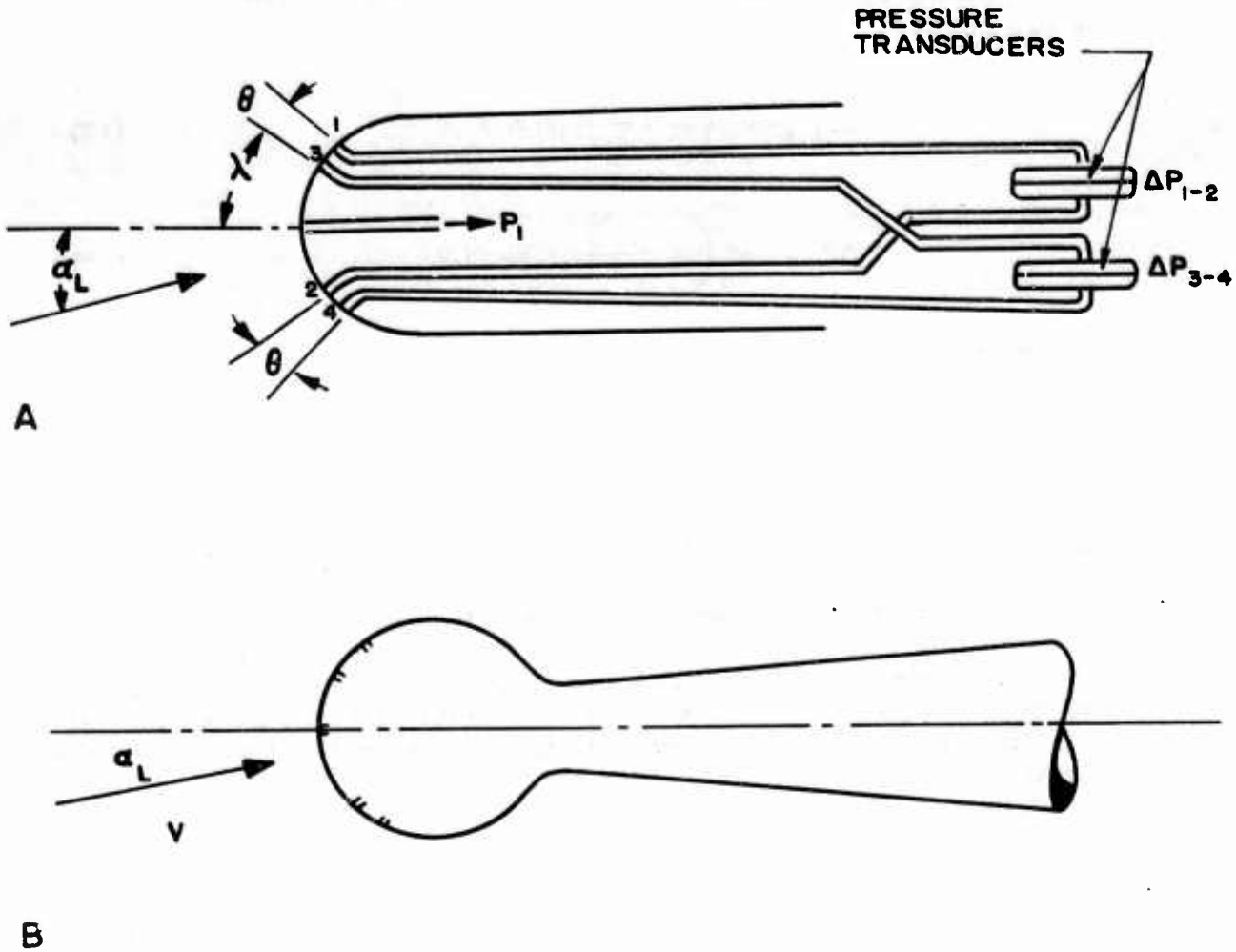

Fig. 18. Yaw-pitch pitot tube with dual differential ports

Similar equations can be developed for the pairs of pressure ports, as for the two cones:

$$\Delta P_{1-2} = \left(\alpha_L + \frac{\theta}{2}\right) q_i f(M)\ f(\beta) \tag{17}$$

$$\Delta P_{3-4} = \left(\alpha_L - \frac{\theta}{2}\right) q_i f(M)\ f(\beta) \tag{18}$$

Combining the equations to solve for α_L gives

$$\alpha_L = \frac{\Delta P_{3-4}}{\Delta P_{1-2} - \Delta P_{3-4}}\ \theta + \frac{\theta}{2} \tag{19}$$

In developing Eq. 19 several assumptions have been made:

1. The variation of ΔP with the angle between the velocity vector and the line bisecting the angle between a pair of differential pressure orifices 1 and 2 or 3 and 4 is the same whether α_L or the locations of the pair of orifices are varied relative to the pitot tube axis.
2. Item 1 holds true for angle of attack measurement when the tube is at small angles of yaw.
3. The relations in items 1 and 2 are linear under all flight conditions.
4. The holes do not interfere with the pressure distribution over the surface.

The validity of items 1 and 2 can be estimated by considering the hemisphere to be replaced by a perfect sphere. It can then be seen that they are true. In practice it is necessary to support the sphere by a boom attached to the rear of the sphere (Fig. 18, B). The presence of this boom slightly invalidates items 1 and 2, and the error becomes greater as the angle of attack relative to the axis of the boom is increased. The error also depends on the size of the boom relative to the sphere. The effect of the boom is reduced as the boom diameter is decreased. However, the minimum allowable diameter of the boom is dictated by the stress in the boom and by the space required for pressure lines.

The linear relation of item 3 is expected to be valid for an angle of attack of ±10 degrees about the boom center line. This statement is based on wind tunnel tests of Ref. 28 and 45. Reference 28 gives data for

a yaw-pitch pitot tube at Mach 0.35, 0.6, and 1.70. Reference 45 gives data at Mach 1.71 for a hemisphere attached to a tube one-third the diameter of the hemisphere. These data show $\frac{\Delta P}{q_i}$ to be a linear function of angle of attack within ± 0.1 degree.

Item 4 is valid if the holes are small relative to the diameter of the sphere. The limitation on the smallness of the holes is their susceptibility to getting clogged with dirt.

The above statements have been general. To evaluate these assumptions, wind tunnel tests on probes through the range of flight parameters, varying the ratio of sphere to boom diameter and also the angular locations (e.g., λ and θ in Fig. 18, A) and the sizes of the ports are required. For measuring yaw another two pairs of holes can be used. It also may be possible to use only one pair of holes for yaw and to use the denominator in Eq. 19 as the reference differential pressure for computing angle of yaw. This requires that the slope of the curve of ΔP vs. α_L remain the same when the sphere is in yaw. Present information in Ref. 28 indicates that this is not true. Therefore another set of dual pressure orifices will probably be needed for yaw.

The necking down of the tube in Fig. 18, B influences the pressure at static pressure orifices, if they are located on this tube. Because static pressure must be corrected anyway for supersonic flight, this should not be too serious a problem.

The mechanization for this system will be the same as that for the dual cone pressure sensors. One computer each (Fig. 17, B) is needed for α_L and β_L. This system, when used with a computer as shown, should prove to be simpler than the yaw-pitch pitot tube. It does not have the disadvantageous interference effects and large size of the dual cone sensors. But, in common with the yaw-pitch pitot tube, it requires accurate machining of the sphere and accurate location of the pressure orifices.

Null-seeking Differential Pressure Sensor

As the study of the differential pressure angle of attack sensor has progressed it has become apparent that the sensor used must accurately measure a wide range of pressures. It is also necessary to perform some computing operations to get the local angle of attack from the pressure information. A null-seeking differential pressure sensor eliminates the need for a computer to get local angle of attack and eliminates the need for a wide-range pressure transducer.

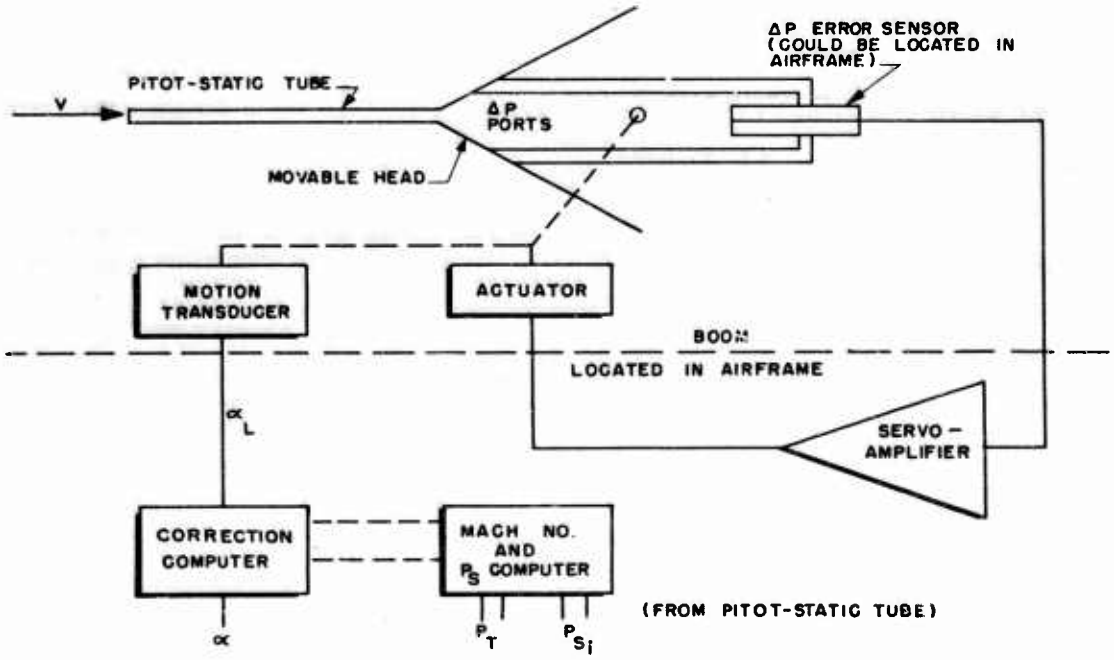

Fig. 19. Block diagram of null-seeking angle of attack sensor

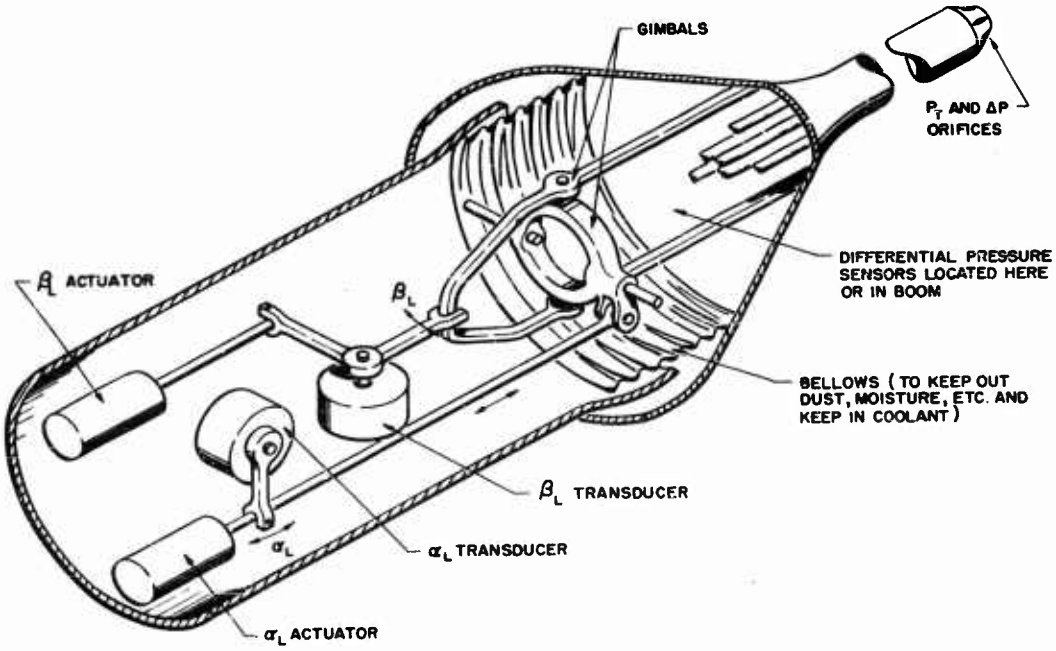

Fig. 20. Possible internal mechanism for null-seeking angle of attack and angle of yaw sensor

A null-seeking sensor has an external moving part, and for this reason does not meet the contractual requirements. However, the advantages of simplification offer the possibility of meeting other contractual requirements better than by "fixed" sensors. For this reason it was thought worth while to look into the possibility of making a null-seeking sensor with comparable external ruggedness.

A schematic of this system is shown in Fig. 19, and in Fig. 20 a drawing of a possible mechanism which could be mounted on the end of a short boom. This consists of a conical surface with two pressure ports near the apex to provide the differential pressure information. These ports are connected to a differential pressure sensor, which gives an error signal. This signal is amplified and used to operate an actuator, which rotates the cone in such a direction that pressures at the two ports are equal. Thus the cone is always alined to the local free stream. A motion transducer is connected to the cone to convert the angular rotation into an electrical output signal.

A discussion of the various components in this system indicates which are critical. The particular shape from which the pressure information is obtained is not critical. It is important that the angles of incidence of the free stream on the ports for zero differential pressure remain constant as angle of attack and flight parameters are changed relative to the airplane or boom. It is also important that the sensitivity, $\frac{d\left(\frac{\Delta P}{q_i}\right)}{d\alpha}$, be as large as possible. Some wind tunnel testing may be required to find such a surface; however, it does seem reasonable that if the movable pressure ports are far enough forward of the fixed boom, the differential pressure is not affected by the angular position of the moving head or pressure ports. The actual shape is not important since ΔP is not required to be linear with respect to the angle between the movable head and the velocity vector. One possible shape is shown in Fig. 21.

Wind tunnel tests were made by NAA on a probe made by soldering four tubes together and cutting the ends off at 45 degrees (Fig. 21). This device had a sensitivity greater than a hemispherical sensor. The ΔP ports are far enough forward that the boom interference is negligible. But there is a limit to how far forward the ΔP ports can be placed. As the weight and surface area ahead of the pivot point are increased, the loads on the servo are increased, as are the acceleration effects.

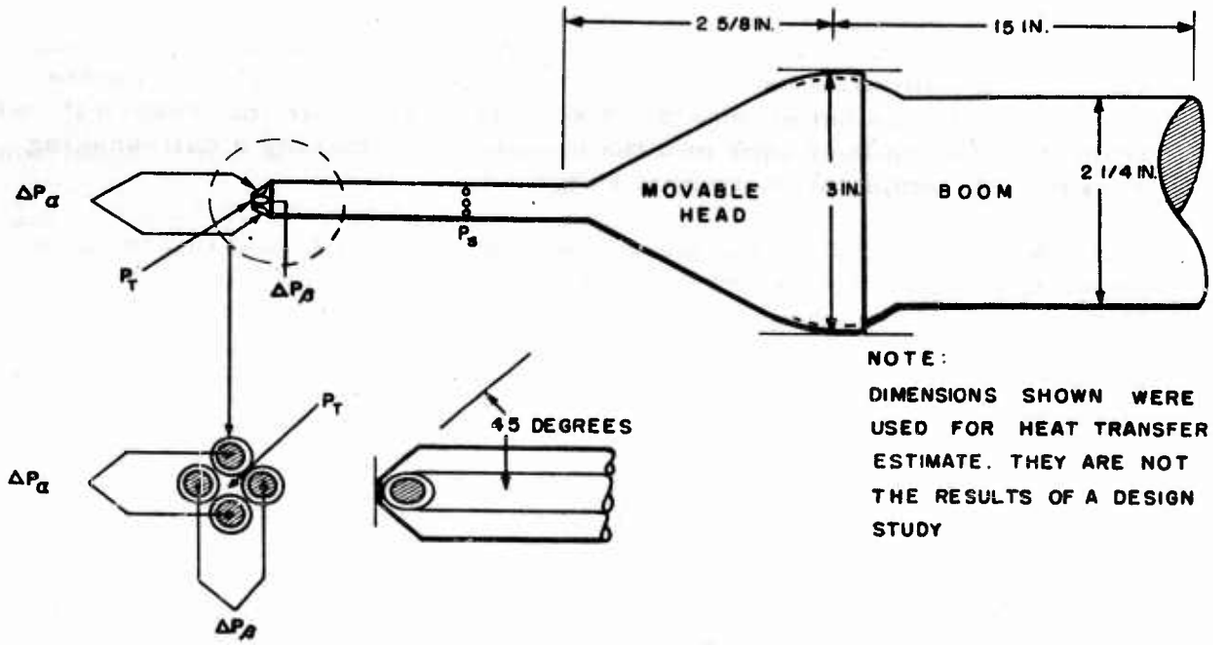

Fig. 21. Possible external configuration of null-seeking angle of attack sensor

The next problem is to determine the angle between the movable head and the velocity vector when ΔP is zero. Here the same problem is encountered as in the yaw-pitch pitot tube. All movable heads could be built symmetrical so that they would all have $\Delta P = 0$ at this same angle. Or, more desirably, they could be manufactured with little regard to dimensional equality, but calibrated with an air stream to find the angle for zero ΔP. This angle would remain constant with variations in flight parameters and could be set into each computer as a fixed adjustment.

The angular motion of the head must be translated accurately into an electrical signal. Figure 20 is shown to illustrate the relative complexity of the mechanism and is not necessarily an optimum design. The sketch shown is for measuring angles of attack and yaw. The connecting mechanism from the head to a motion transducer, such as a potentiometer, should give a constant relationship between the head angle and the

motion transducer angle, in spite of temperature variations. The relationship need not be linear; a potentiometer could be wound to take care of nonlinearities.

Whatever relationship is used, it must be similar for all production probes. The zero setting could be determined by one flight test on each instrument. This would take care of all the system zero errors, and the correction would be the same for all other flight conditions.

In Fig. 21 provision is made for a total pressure port on the movable head. The static pressure ports can be located on the total pressure tube (Fig. 21) if this tube is long enough to provide static pressure at the static pressure ports with sufficient accuracy. This would make both total and static pressures independent of angle of attack.

Work has been done by other investigators on null-seeking differential pressure angle of attack transducers. One of the earliest investigators was the Cornell Aeronautical Laboratory (Ref. 28) which used a movable cone on the end of a boom to sense differential pressure. It was found that as the angle of the air flow relative to the supporting boom was changed, the angle of zero differential pressure between the orifices changed. Thus the angular position of the cone was not the local air stream angle. This fact was thought to be due to the flow interference of the boom. By reducing the diameter of the boom behind the cone to 1/2 the base diameter of the cone, this effect was reduced. However, it then became difficult to design a mechanism for servoing the cone. For this reason further work on this system was abandoned by Cornell. As stated above, it is believed that this effect can be eliminated by mounting the ΔP ports sufficiently forward of the fixed boom.

The Flight Test Division of the Air Materiel Command (Ref. 12) built and tested a null pressure device using an ellipsoidal surface as the movable head. The data show some scattering of points, mainly because of worn gears in the drive mechanism. A good design should alleviate this problem.

Specialties, Inc., (Ref. 58) manufactures a null-seeking probe (Fig. 22) with a cylinder projecting from the side of the fuselage. This cylinder has two slots which sense the differential pressure. The pressure is used to rotate an enclosed vane, which, in turn, rotates the cylinder slots to a null position. This device senses local angle of attack to 0.2 degree at speeds between 200 and 300 knots and to a greater accuracy at higher speeds. Flight tests indicate that it works satisfactorily.

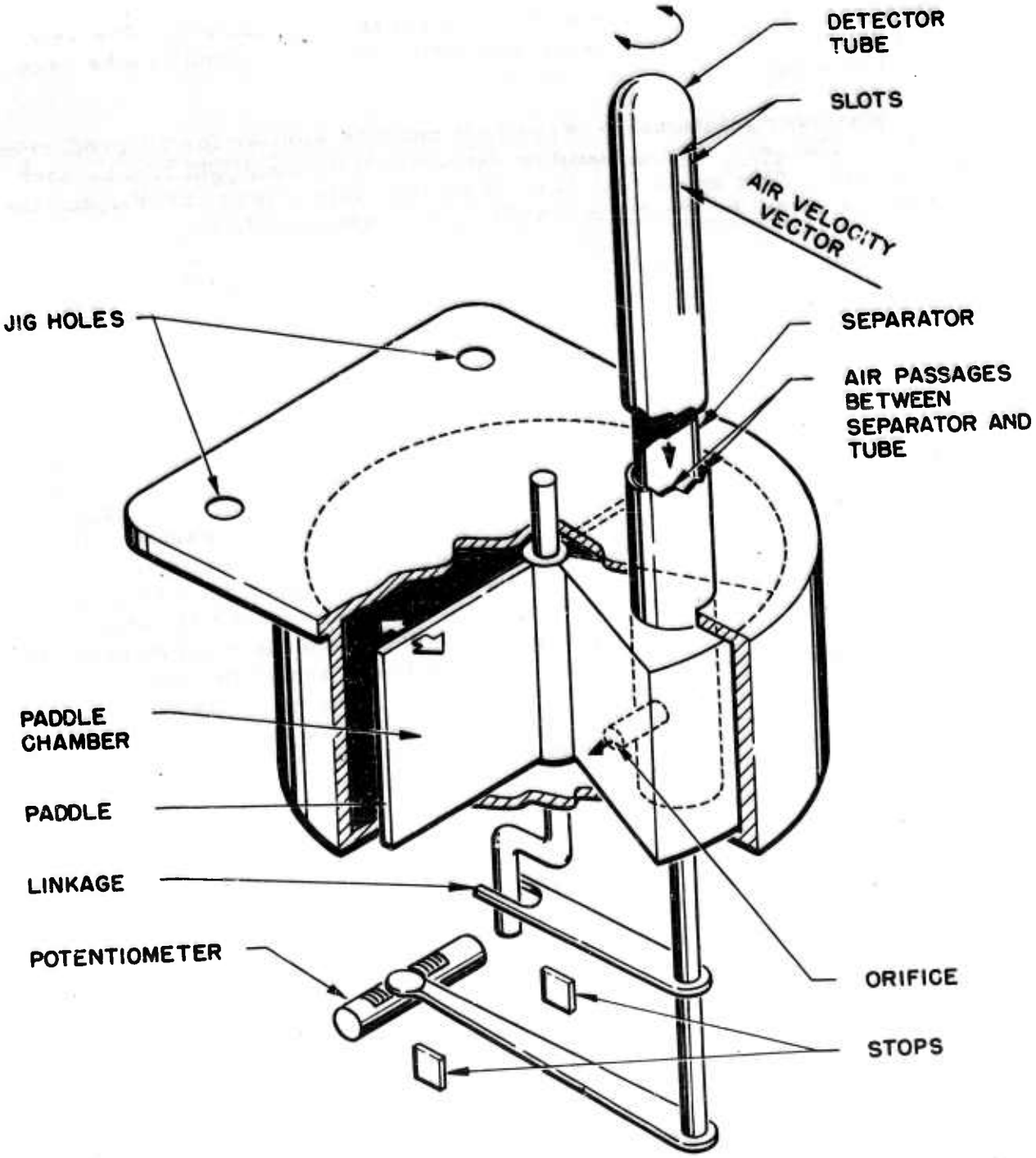

Fig. 22. Specialties, Inc., air stream direction detector

There is one difficulty in making this a rugged instrument. The movable cylinder must be mounted to move as freely as possible so as to have good sensitivity. This requirement makes it difficult to make a good seal around the moving cylinder to keep out dust and moisture.

The Young Instrument Company (Ref. 46 and 104) has made a successful null-pressure instrument using a movable head and a pressure sensor that responds to 0.002 in. of water pressure. This ensures 0.1 degree accuracy at "very low subsonic" speeds. The pressure sensor gives an on-off signal which is amplified and drives a positioning solenoid With this type of servo the system vibrates at 100 to 200 cps at null, with an amplitude less than 0.1 degree. The company also makes a dual unit with the head mounted on gimbals so as to measure angles of attack and yaw and another unit with a pitot-static tube attached to the head. This instrument is said to have been flown at Mach 0.75 and should work at higher speeds. It is also said to have operated satisfactorily from -38 F to 180 F.

It is felt that the main problems in using a null sensor to satisfy the contract requirements lie in the design of the mechanism to operate with the following restrictions:

1. The mechanism for moving the differential pressure head and measuring the angular travel must be enclosed in a cylinder of 2 in. to 3 in. in diameter. This is to make the system suitable for boom-mounting.
2. It should be able to withstand rough handling by maintenance crews, and the head should be able to move against aerodynamic forces and friction due to protective seals around the shaft bearings.
3. It should be able to withstand changes in external environment from, say, -60 F where icing would occur, to 540 F, which is the approximate skin temperature at Mach 3.0.

Items 1 and 2 require a design study to set up strength requirements and to see what types of mechanisms qualify. The Young instrument is a very compact design and illustrates what can be done.

To reduce the limit of temperature under which the mechanism operates requires temperature control. In other instruments heating wires have been installed in the head to prevent icing. However, none have encountered the problem of high skin temperatures. Some cooling seems a necessity for the mechanism for flight at Mach 3.0 for any length of time. It can also be assumed that any plane flying at this speed for any length of time needs some cooling for other avionics equipment and perhaps needs cooling for structural and aerodynamic reasons also. Therefore some small fraction of the airplane cooling system could be used for cooling the equipment in the boom.

An estimate was made of the amount of cooling required to see if any difficulty would be encountered in getting sufficient coolant through the boom. The estimate was made of the coolant rate with air as a coolant. It was assumed that the skin had a 1/8 in. thickness of asbestos to insulate the inside from the outside skin temperature. The dimensions of the cooled enclosure and skin area available for heat transfer are as shown in Fig. 21; air coolant rate is assumed as 3 cu ft/sec at an average temperature of 140 F and at 14.7 psi.

The calculation shows that 900 Btu/hr is the heat transfer rate. Assuming the air occupies one-third of the area inside the tube, the velocity would be 50 fps, with temperature rise of 54 degrees F. A circulating liquid could be the cooling medium. It is also possible to cool considerably by blowing a small amount of air over the outer surface. This alters the boundary layer so as to reduce the skin temperature with a minimum amount of cooling air. The method employed to cool depends mainly on what is available in the plane. The above values are of the nature of a preliminary estimate; however, they do show that a reasonable coolant rate can keep the mechanism at a reasonable temperature.

It should be mentioned that this heating and cooling require some control. However, this control should be simple, as extreme accuracy is not important. If such a device can be designed to overcome the environmental problems, some computer simplification, in comparison with the yaw-pitch pitot tube, is possible.

FORCE-SENSITIVE DEVICES

Lift Mechanization

General

A system which has been used with considerable success in fire control in present-day operational interceptor aircraft uses the mechanization of the lift equation of the airplane. In the light of the contract requirement for systems having "immovable sensors of minimum protuberance" this system warrants close examination, because it requires no additional external sensors.

The system may be likened to a vane system in which the entire airplane is the vane sensor and the forces on it are measured by inertial and pressure-sensing devices. The systems developed to date claim accuracies of the order of 0.25 degree in the altitude range of sea level to 60,000 ft and the Mach range of 0.3 to 1.05. However, certain refinements which take into account small-order effects previously neglected can make the increased accuracy possibilities attractive.

Basic Theory of Operation

A standard basic textbook on aerodynamic theory (Ref. 19) expresses the lift (L) developed by an airfoil by the equation

$$L = C_L S q$$

or

$$C_L = \frac{L}{Sq} \tag{20}$$

where C_L is the lift coefficient. S is the area of the lifting surface, and q is dynamic pressure. When the airplane is in trimmed flight, the vertical forces must balance; hence L is equal to weight times acceleration (Wn_Z) and Eq. 20 becomes

$$C_L = \frac{Wn_Z}{Sq} = \frac{m\,a_Z}{Sq} \tag{21}$$

By Ref. 19,

$$C_L = \frac{dC_L}{d\alpha}(\alpha - \alpha_0) \tag{22}$$

where $\frac{dC_L}{d\alpha}$ is the slope of the characteristic lift coefficient plotted as a function of attack angle (α) and α_0 is the angle of zero lift, or the intercept of lift coefficient when the attack angle is zero. Combining Eq. 21 and Eq. 22 and solving for α gives

$$\alpha = \frac{Wn_Z}{SqC_{L_\alpha}} + \alpha_0 \tag{23}$$

In Eq. 23, C_{L_α} is a shorter notation used to represent $\frac{dC_L}{d\alpha}$.

These equations are valid only in the linear region of the curve C_L vs. α.

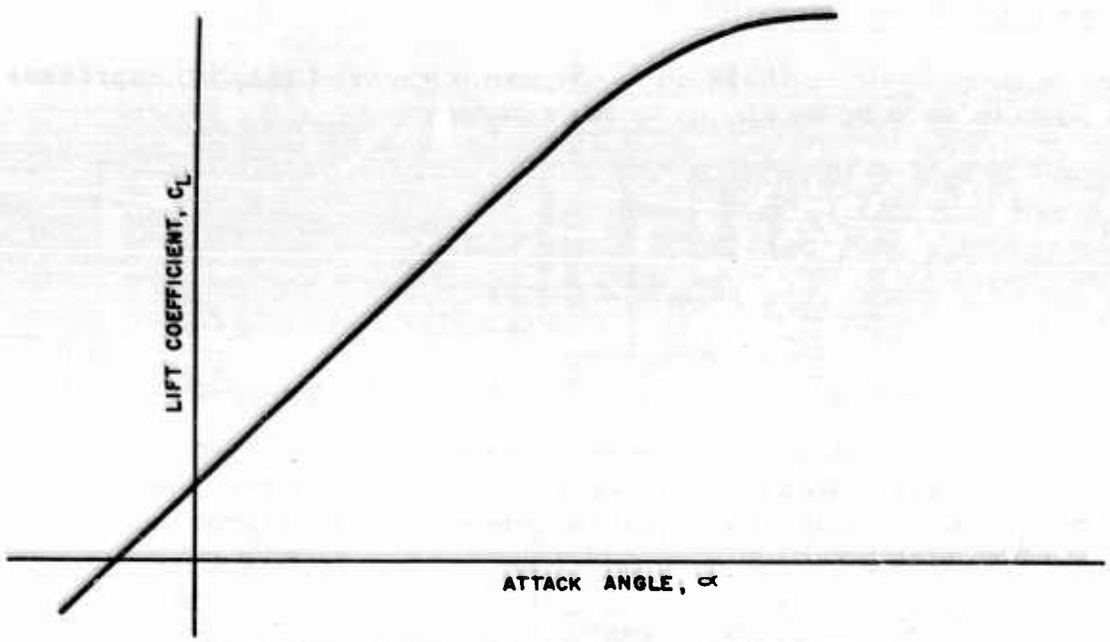

Fig. 23. Lift coefficient vs attack angle for a selected Mach number

Figure 23 shows a typical plot of lift coefficient vs. attack angle at a certain Mach number. Similar curves are usually available with Mach number the parameter, showing that the slope of the linear section and the intercept with the axis vary as functions of Mach number. It is apparent, therefore, that Eq. 23 is basically a slope-intercept form of equation in which the slope term $1/C_{L_\alpha}$ and the intercept term α_0 vary as functions of Mach number. As stated above, trimmed flight is assumed; untrimmed flight will be treated later.

It is impossible to measure dynamic pressure directly in flight. The nearest thing to this quantity is impact pressure, called q_i and related to dynamic pressure by the equation

$$q_i = q \cdot f_c(M) \tag{24}$$

where $f_c(M)$ is the compressibility factor given (Ref. 66) by

$$f_c(M) = 1 + \frac{M^2}{4} + \frac{M^4}{40} + \frac{M^6}{1600} + \ldots \qquad M \leq 1$$

$$= \frac{1.429}{M^2}\left[\frac{166.92\, M^7}{(7M^2 - 1)} - 1\right] \qquad M \geq 1 \tag{25}$$

The quantity q_i can be measured directly, as it is the differential pressure existing between the stagnation and static pressure sources of an aircraft airspeed system. Therefore, if Eq. 24 is solved for q and the expression obtained substituted into Eq. 23, we can write

$$\alpha = \frac{Wn_z}{Sq_i} f_1(M) + f_2(M) \tag{26}$$

where $f_1(M) = f_c / C_{L_\alpha}$ and $f_2(M) = \alpha_0$ for any Mach number. It is noteworthy that Eq. 23 may be reduced to practicability by use of the expression

$$\frac{q}{P_S} = 0.7\, M^2$$

where P_S is absolute (static) pressure. Solving for q and substituting in Eq. 23 gives

$$\alpha = \frac{Wn_z}{SP_S} f_1'(M) + f_2(M) \tag{27}$$

where $f_1'(M) = 1/0.7 M^2 C_{L_\alpha}$

This form is less desirable, as at high altitudes the quantity P_S in the denominator is tending toward zero and is therefore more difficult to measure than q_i in Eq. 26, which can never fall below a certain value in trimmed flight at ceiling. An additional advantage favors Eq. 26 in low-speed flight such as in landing, because $f_1(M)$ is essentially constant, in contrast to $f_1'(M)$, which has an M^2 term in the denominator and hence increases rapidly at low Mach numbers. The form of Eq. 26 will be assumed hereafter.

Effects of Aeroelasticity

A third term should be added to Eq. 26 to account for torsional deflection of the wings. A multitude of factors contribute to this term, the composite effect being as high as 10 percent of the total attack angle in some extreme cases (e.g., very thin wings of high aspect ratio). The noteworthy factors are

1. Wing camber
2. Differential thermal expansion of the upper and lower surfaces due to different stagnation temperatures

3. Pitching moments at certain Mach numbers due to variation in the moment coefficient for zero lift
4. External stores weight and distribution
5. Movable flow modifiers, such as spoilers and flaps
6. Variation of pitch moment with lift coefficient $\left(\frac{dC_m}{dC_L}\right)$
7. Moment due to weight being displaced from elastic axis
8. Moment due to center of pressure being displaced from elastic axis
9. Geometric effect of wing, such as with crescent or gulled wings for which there may be a drag-induced twist
10. Acceleration effect due to changing thrust, extending gear or flaps, executing pull-ups, etc.
11. Aeroelasticity

Several of these contributing factors are dependent on airframe and structural design details and can be treated only generally. Others, while not specifically defined, can be reduced to terms of cause. Item 10 is dynamic in nature and not of concern in trimmed flight. In any general case it is sufficiently accurate to say that the wing torsional effect on true attack angle is a function of wing loading and Mach number and may be expressed as

$$\alpha_t = f\left(\frac{Wn_z}{S}, M\right) \tag{28}$$

More explicitly, it is probable this may be written, and with sufficient accuracy, as

$$\alpha_t = \frac{K_1 Wn_z}{S} \cdot f_3(M) \tag{29}$$

since within the elastic limit of the wing the torsional deflection is proportional to wing loading and functionally related to Mach number.

In one application where the wing torsion contribution was mechanized, the quantity $f_3(M)$ was made constant and the total effect was then proportional to wing loading. Suitable accuracy was achieved. Equation 26 may then be expanded to

$$\alpha = \frac{Wn_z}{Sq_i} f_1(M) + f_2(M) + \frac{K_1 Wn_z}{S} f_3(M) \tag{30}$$

This is the general equation for a lift mechanization of an airplane in trimmed flight in the linear region of the lift coefficient vs. attack angle characteristic.

Consideration of Nonlinear C_{L_α} Characteristics

For some critical applications, e.g., air-to-air missile or rocket fire control systems, it is not wise to limit the operation to the linear region of the lift coefficient vs. attack angle characteristic. Analysis of the nonlinear region adds little difficulty.

Consider the curves of Fig. 24, wherein specific flight data on an F-86D type airplane at several Mach numbers have been approximated using the equation

$$C_L = f_a(M) + f_b(M)\alpha - f_d(M)\alpha^2 \tag{31}$$

Equation 31 is a mathematical approximation of Eq. 22, in which the first term, $f_a(M)$, is the zero lift effect and is usually very near zero. The second term, $f_b(M)\alpha$, represents the change in C_L per unit change of α, with Mach number as a parameter or the slope of the characteristic. The third term, $f_d(M)\alpha^2$, introduces the nonlinearity required to shape the curve in the high attack angle region, with Mach number a parameter.

Differentiation of Eq. 31 yields

$$\frac{dC_L}{d\alpha} = f_b(M) - 2\alpha f_d(M) = C_{L_\alpha} \tag{32}$$

Because $f_1(M)$ in Eq. 30 is $f_c(M)/C_{L_\alpha}$, we can substitute Eq. 32 into Eq. 30 to obtain

$$\alpha = \frac{Wn_z}{Sq_i}\left(\frac{f_c(M)}{f_b(M) - 2\alpha f_d(M)}\right) + f_2(M) + \frac{K_1 Wn_z}{S} f_3(M) \tag{33}$$

Equation 33 may be reduced to the form

$$\alpha = \frac{Wn_z}{Sq_i}\,\frac{f_c(M)}{f_b(M)}\left[1 - \frac{1}{\dfrac{2\alpha f_d(M)}{f_b(M)}}\right] + f_2(M) + \frac{K_1 Wn_z}{S} f_3(M) \tag{34}$$

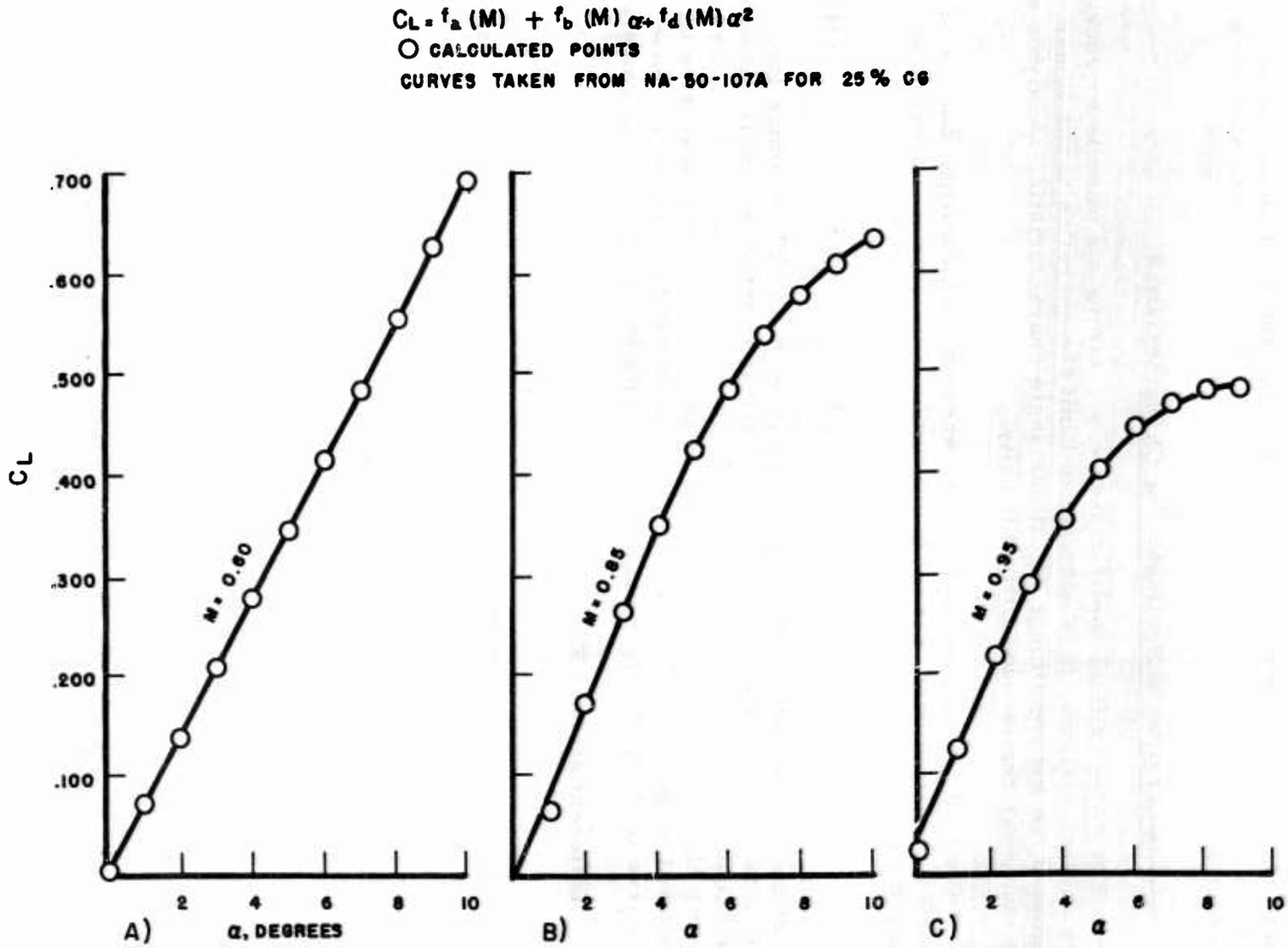

Fig. 24. Square-law approximation to trim lift coefficient, F-86D aircraft

Using the approximation $1 + x \approx 1/1-x$, which is acceptable for small x, this becomes

$$\alpha = \frac{Wn_z}{Sq_i} \frac{f_c(M)}{f_b(M)} + \frac{Wn_z f_c(M) \; f_d(M) 2\alpha}{Sq_i f_b(M)^2} + f_2(M) + \frac{K_1 Wn_z}{S} f_3(M) \quad (35)$$

From Eq. 35, if the small-order terms are all neglected,

$$\alpha \approx \frac{Wn_z}{Sq_i} \frac{f_c(M)}{f_b(M)} \quad (36)$$

which may be substituted into the second term of Eq. 35 with small error to derive

$$\alpha = \frac{Wn_z}{Sq_i} \frac{f_c(M)}{f_b(M)} + 2\alpha^2 \frac{f_d(M)}{f_b(M)} + f_2(M) + \frac{K_1 Wn_z}{S} f_3(M) \quad (37)$$

and, finally,

$$\alpha = \frac{Wn_z}{Sq_i} f_1'(M) + f_2(M) + \frac{K_1 Wn_z}{S} f_3(M) + f_4(M)\alpha^2 \quad (38)$$

where

$$f_1'(M) = \frac{f_c(M)}{f_b(M)} \text{ and } f_4(M) = \frac{2f_d(M)}{f_b(M)}$$

Equations 30 and 38 are seen to be similar, except for the effects of the nonlinearity of C_{L_α} in the first and fourth terms of Eq. 38. In general, this may be interpreted as saying that an improved computation of attack angle may be expected over the broad range of C_L if an additional function of Mach number and an α^2 term are introduced into the mechanization. This may or may not be necessary, depending upon the tactical operation expected of the aircraft.

Contributions of Displaced Accelerometers

An accelerometer mounted on an airframe normal to the XY-plane of the NACA body axis system experiences accelerations a_Z as expressed by

$$a_Z = \frac{F_z}{m} \cos \alpha + \frac{F_x}{m} \sin \alpha + e_X \ddot{\Theta} + e_Y \ddot{\Phi} + e_Z [\dot{\Theta}^2 + \dot{\Phi}^2] - e_X \dot{\Phi}\dot{\Psi} - e_Y \dot{\Psi}\dot{\Theta} \quad (39)$$

The aerodynamic forces along the x and z axes are given by

$$F_x = qS(C_T \cos \alpha - C_D) \quad (40)$$

$$F_z = -qS(C_T \sin \alpha + C_L) \quad (41)$$

where C_T is the coefficient of thrust, C_D the coefficient of drag, and S the area of lifting surface. During trimmed flight conditions, all first and second derivatives of the airplane attitude are zero, and Eq. 39 reduces to

$$a_Z = \frac{F_z}{m} \cos \alpha + \frac{F_x}{m} \sin \alpha \quad (42)$$

Substitution of Eq. 40 and 41 in Eq. 42 yields

$$a_Z = \frac{qS}{m}(C_T \cos \alpha - C_D) \sin \alpha - \frac{qS}{m}(C_T \sin \alpha + C_L) \cos \alpha$$

$$= -\frac{qS}{m}(C_D \sin \alpha + C_L \cos \alpha)$$

$$- \frac{C_L qS}{m} \left(\cos \alpha + \frac{C_D}{C_L} \sin \alpha \right) \quad (43)$$

It is seen that the thrust term does not appear in Eq. 43. Since the accelerometer is mounted perpendicular to the thrust line (along the X body axis), this could have been stated at the outset.

If we further limit the position of the accelerometer to being on the X body axis, the terms $e_Y \ddot{\Phi}$, $e_Y \dot{\Psi}\dot{\Theta}$, and $e_Z [\dot{\Theta}^2 + \dot{\Phi}^2]$ in Eq. 39 become

zero by virtue of the fact that e_Y and e_Z are zero for this location. Although Φ and Ψ can separately attain fairly large values, their cross product is generally small. Accordingly, the term $e_Y\dot{\Phi}\dot{\Psi}$ is assumed to have little effect on the total acceleration. Under these conditions, Eq. 39 can be written

$$a_Z = \frac{F_z}{m} \cos \alpha + \frac{F_x}{m} \sin \alpha + e_Y\ddot{\Theta}$$

$$= -\frac{C_L qS}{m} \left(\cos \alpha + \frac{C_D}{C_L} \sin \alpha \right) + e_Y\ddot{\Theta} \tag{44}$$

The lift coefficient of an airplane is sometimes given as

$$C_L = C_{L_\alpha} \cdot \alpha + C_{L_{\delta_T}} \cdot \delta_T + C_{L_{\dot{\Theta}}} \left(\frac{C\dot{\Theta}}{2V} \right) + \cdots \tag{45}$$

where δ_T is the deflection angle of the tail surface and C is a constant. For trimmed flight conditions, this reduces to

$$C_L = C_{L_\alpha} \cdot \alpha + C_{L_{\delta_T}} \cdot \delta_T \tag{46}$$

The tail surface deflection and the attack angle are related through the pitching moment equation

$$\ddot{\Theta} = \left[C_{m_0} + C_{m_\alpha} \cdot \alpha + C_{m_{\delta_T}} \cdot \delta_T + C_{m_{\dot{\Theta}}} \left(\frac{C\dot{\Theta}}{2V} \right) \right] \frac{qSC}{I_Y} \tag{47}$$

where I_Y is the moment of inertia about the Y body axis (pitching moment of inertia). During trimmed flight, this reduces further to

$$0 = C_{m_0} + C_{m_\alpha} \cdot \alpha + C_{m_{\delta_T}} \cdot \delta_T$$

since all derivative terms are zero. Solving for δ_T,

$$\delta_T = \frac{-(C_{m_0} + C_{m_\alpha} \cdot \alpha)}{C_{m_{\delta_T}}} \tag{48}$$

and substitution of Eq. 48 into Eq. 46 yields

$$C_L = \left[C_{L_\alpha} - \left(\frac{C_{m_\alpha}}{C_{m_{\delta_T}}}\right) C_{L_{\delta_T}}\right] \alpha - \left(\frac{C_{L_{\delta_T}}}{C_{m_{\delta_T}}}\right) C_{m_0} \tag{49}$$

The coefficient of the α term is the slope of the lift characteristic for trimmed flight, and the coefficient of the C_{m_0} term may be written as C/X_T where X_T is the distance of the tail force from the center of gravity. This permits writing Eq. 49 as

$$C_L = -\frac{C}{X_T} C_{m_0} + \left[C_{L_\alpha} - \left(\frac{C_{m_\alpha}}{C_{m_{\delta_T}}}\right) C_{L_{\delta_T}}\right] \alpha \tag{50}$$

Solving Eq. 21 for a_Z and substituting in Eq. 50, we have the acceleration expressed as

$$a_Z = -\frac{Sq}{m} \left\{ -\frac{C}{X_T} C_{m_0} + \left[C_{L_\alpha} - \left(\frac{C_{m_\alpha}}{C_{m_{\delta_T}}}\right) C_{L_{\delta_T}}\right] \alpha \right\} \tag{51}$$

for an airplane in trimmed flight, which is equal to 1 g.

If it is assumed in Eq. 45 that terms after the second have negligible effect on F_Z under all practical flight conditions, Eq. 44 becomes

$$a_Z = -\left[C_{L_\alpha} \cdot \alpha + C_{L_{\delta_T}} \cdot \delta_T\right] \frac{qS}{m} + e_Y \ddot{\Theta} \tag{52}$$

The substitutions cos $\alpha = 1$ and sin $\alpha = 0$ have been made for simplicity, as they have no bearing on the following development. Neglecting the term in Eq. 47 due to $\dot{\Theta}$ and substituting into Eq. 52, we have

$$a_Z = -\left[C_{L_\alpha} \cdot \alpha + C_{L_{\delta_T}} \cdot \delta_T\right] \frac{qS}{m} + \left[C_{m_0} + C_{m_\alpha} \cdot \alpha + C_{m_{\delta_T}} \cdot \delta_T\right] \frac{CqSe_Y}{I_Y} \tag{53}$$

and because $I_Y = k_Y^2 m$ where k_Y is the radius of gyration, the terms in Eq. 53 may be rearranged to give

$$a_Z = -\left[C_{m_0}\left(\frac{Ce_Y}{k_Y^2}\right) + \left(C_{L_\alpha} - \frac{Ce_Y^2}{k_Y^2} C_{m_\alpha}\right)\alpha + \left(C_{L_{\delta_T}} - \frac{Ce_Y}{k_Y^2} C_{m_{\delta_T}}\right)\delta_T\right] \frac{qS}{m} \tag{54}$$

If the accelerometer is located at a position e_Y such that

$$e_Y = \frac{k_Y^2}{C}\left(\frac{C_{L_{\delta_T}}}{C_{m_{\delta_T}}}\right) = \frac{k_Y^2}{X_T} \tag{55}$$

the term in Eq. 54 containing δ_T is reduced to zero, and it is not necessary to include the effect of δ_T to determine α. The acceleration equation is then

$$a_Z = \frac{qS}{m}\left[\frac{C}{X_T}\, C_{m_0} - \left(C_{L_\alpha} - \frac{C_{m_\alpha}}{C_{m_{\delta_T}}}\, C_{L_{\delta_T}}\right)\alpha\right] \tag{56}$$

which is the same as Eq. 51, obtained for trimmed flight conditions. The point $(e_Y, 0, 0)$ is called the center of percussion in the pitch plane of the airplane for a tail force.

The above treatment is somewhat cumbersome, and reference to the force and moment equations using a diagram may clarify the analysis to some extent.

Referring to the diagram below, the total lifting force on the airplane is $F_1 + F_2$, where F_1 is the force due to the wing and F_2 is that contributed by the tail surface when the airplane is trimmed. Similarly, r_1 and r_2 are the dimensions of the forces from the airplane cg.

Summing these forces gives

$$\Sigma_v = Wn_Z = ma_Z = F_1 + F_2 \tag{57}$$

and the moment equation as

$$\mathcal{M} = F_1 r_1 - F_2 r_2 = 0 \tag{58}$$

Substitution of Eq. 57 into Eq. 23 permits writing

$$\alpha = \frac{F_1 + F_2}{SqC_{L_\alpha}} + \alpha_0 \tag{59}$$

If, during untrimmed flight, we represent the disturbing tail force as F_3, acting to increase F_2 as shown in the second diagram, a new moment equation may be written:

$$F_1 r_1 - F_2 r_2 - F_3 r_2 = I_Y \ddot{\Theta} \tag{60}$$

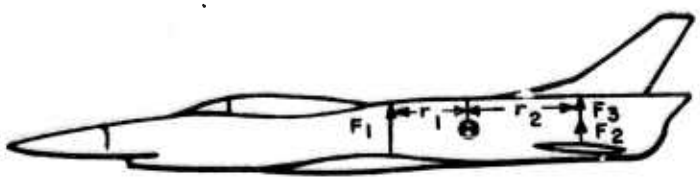

and since $F_1 r_1 - F_2 r_2 = 0$ from Eq. 57,

$$F_3 = -\frac{I_Y \ddot{\Theta}}{r_2} \tag{61}$$

The force equation for this untrimmed situation is

$$F_1 + F_2 + F_3 = Wn_Z \tag{62}$$

or

$$F_1 + F_2 = Wn_Z - F_3 \tag{63}$$

Substitution of Eq. 61 in Eq. 63 gives

$$F_1 + F_2 = Wn_Z + \frac{I_Y \ddot{\Theta}}{r_2} = Wn_Z + \frac{k_Y^2 W \ddot{\Theta}}{g r_2}$$

$$= W\left(n_Z + \frac{k_Y^2 \ddot{\Theta}}{g r_2}\right) \tag{64}$$

wherein the substitution $I = \frac{k^2 W}{g}$ has been made. The substitution of Eq. 64 into Eq. 23, as before, gives

$$\alpha = \frac{W\left(n_z + \frac{k_Y^2 \ddot{\Theta}}{g r_2}\right)}{q S C_{L_\alpha}} + \alpha_0 \tag{65}$$

Equation 65 is an expression of the attack angle of the airplane using information from an accelerometer located at the airplane cg. The accelerometer senses two contributing forces, one due to translation along the Z-axis (n_z) and the other due to rotation about the Y-axis $\left(\frac{k_Y^2 \ddot{\Theta}}{g r_2}\right)$. It is a well-known phenomenon that if an elongated body in equilibrium is subjected to a disturbing force at one end, it does not rotate about the cg, but around a different point called the center of percussion. The center of percussion is located at a distance from the center of suspension (cg) given by k_Y^2/u, where u is the distance from the center of suspension to the disturbing force. In Eq. 65, this is written k_Y^2/r_2, as it satisfies the above definition.

Therefore it is seen that if the accelerometer is located at the center of percussion (k_Y^2/r_2, or k_Y^2/X_T in Eq. 55), it will be insensitive to disturbing tail forces, but will be sensitive to translational forces. In this instance, the term $\frac{k_Y^2 \ddot{\Theta}}{g r_2}$ becomes zero, and Eq. 23 is accurate for either trimmed or untrimmed flight conditions.

A strong practical reason exists for location of the accelerometer at almost any other position than the cg of the airplane. Because of the long cylindrical form factor of turbojet engines, it seems that the cg of most single-engine airplanes invariably falls within the engine envelope. Most areas in the vicinity of the engine are subject to high ambient temperatures, a further inducement to keep instrumentation away from the engine. The center of percussion is forward of the cg, where suitable mounting provision can usually be made.

The computation of skid angle (β) is analogous to that for attack angle, except that it is simpler. The effect of aeroelasticity is negligible and there is no β_0 term due to symmetry of the airplane in the plane perpendicular to the Z-axis.

Practical Considerations

Although Eq. 30 is an accurate expression for attack angle, errors in addition to the inherent errors of the computer are introduced into the mechanization of this equation by several factors:

1. Variation of fuel gage indication with attitude.
2. Variation of airplane weight due to addition of external stores.
3. Variation of airplane weight and aerodynamic characteristics due to condensation during flight.
4. Variation of airplane weight due to moisture absorption on the ground during climatic changes.
5. Errors in total and static pressures as sensed by the pitot tube.
6. Variation of aerodynamic characteristics with cg position.
7. Variation of aerodynamic characteristics with external stores.
8. Variation of aerodynamic characteristics between airplanes and with aircraft aging.
9. Effect of cg position on computation during untrimmed flight conditions.
10. Effect of bomb bay doors, gears, flaps, dive brakes, etc.

It is possible to limit the errors introduced by factor 1 by utilizing an attitude-sensitive switch to de-energize the fuel gage indicator when unfavorable flight attitudes exist. This will cause the computed weight to be based upon the last known accurate fuel weight rather than upon one rendered incorrect by such contingencies.

The variation of airplane weight due to the addition of external stores (2) can be introduced via an airplane gross weight setting on the front panel of the computer. If, however, this additional weight is subject to variation during combat, some means must be provided for introducing the mass which remains in the airplane at all times into the weight circuit. It is possible to simplify this problem to some extent by operating instructions. For example, a standard operating procedure might be to use the fuel from the wing tanks first so that they would be empty when the airplane arrives at the expected combat area, thus eliminating change during combat.

Since aircraft are generally equipped with de-icing equipment, it is unlikely that an aircraft will enter combat in an iced condition. The effect of external moisture condensation is therefore not considered to be a serious problem.

The variation of weight of the airplane due to moisture absorption while on the ground (4) is very difficult to establish. The weighing

equipment for determination of this variation must be extremely accurate, as an error of slightly more than 1 percent can represent a bias error of 0.8 mils in the computation of jump angle for an F-86D airplane at Mach 0.8 and an altitude of 40,000 ft. It is suggested that a practical solution of this difficult problem may be found in the application of suitable load cells in conjunction with the field test equipment. It is felt that if the airplane does absorb some moisture through exposure to inclement weather, this absorption probably disappears very rapidly when the airplane is airborne.

The effects of pitot-static source errors (5) may be corrected implicitly as functions of Mach number and static pressure if the Mach range of the aircraft is sufficient to warrant concern. These effects are discussed in greater detail in the chapter entitled "Extension to Flight Data Computers."

The variation of aerodynamic characteristics with cg position (6) is a minor term but may be introduced into this mechanization if the errors due to neglecting it are found to be appreciable.

The effects of variation of aerodynamic characteristics with external stores (7) may be mechanized simply if this is required. The mechanization necessitates some interlock between the computer and the store jettison circuit which could introduce the appropriate bias change in a manner similar to that by which present computers accommodate flap-down conditions. However, there are few data available on these effects, and a flight test program would be required to determine them.

The only effect on aerodynamic characteristics expected from aging or from production differences between individual aircraft (8) is a change in the attack angle for zero lift. A suitable change in the bias setting compensates for this. It is believed that only a simple in-flight check is required. However, further study of this point may be desirable.

The effect of the position of center of gravity on the computation of attack angle during untrimmed flight conditions (9) is neglected in the mechanization, as the resulting system error is not greater than 0.1 degree at a 10-degree attack angle.

The effects of bomb bay doors, landing gear, flaps, dive brakes, etc., are similar to those of item 7. The Mach number range during which these effects may be applicable is limited, and it is generally noted that a bias shift of the C_{L_α} characteristic included as part of $f_1(M)$ will accommodate the variation. This shift may be introduced through relays actuated by the gear, flaps, dive brakes, or bomb bay door devices or by their control systems.

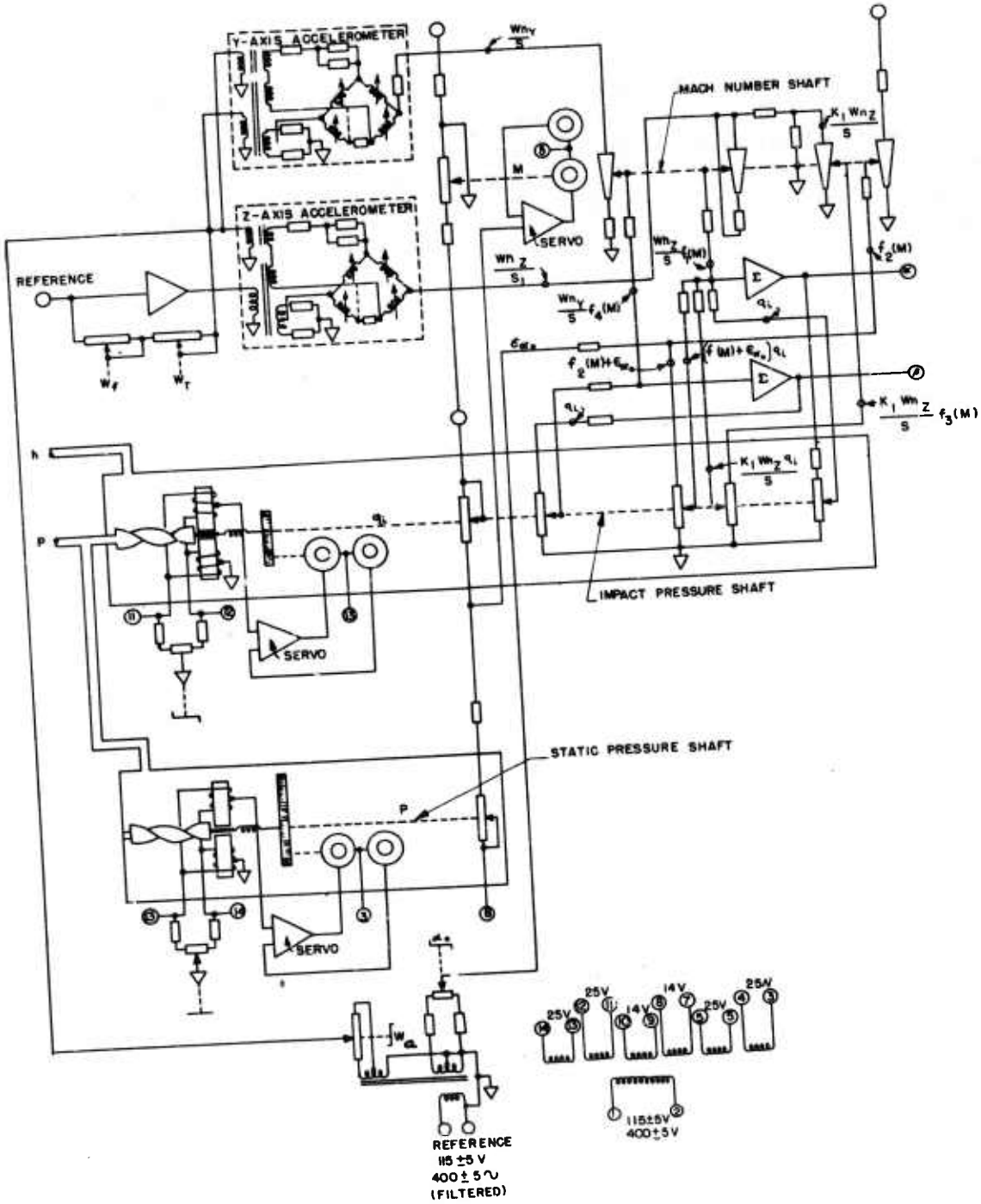

Fig. 25. Mechanization of attack and skid angles

Mechanization

The mechanization of attack angle as given by Eq. 30 is shown in Fig. 25, together with a similar mechanization of skid angle. The output is provided in the form of phase-polarized 400-cps voltages, which may be used in that form or servoed. If servoed outputs are required, it is probable that the servoamplifiers will replace the summing amplifiers shown.

For the first term of Eq. 30, the product of weight and acceleration is generated by exciting a variable reluctance accelerometer bridge with a voltage proportional to the total weight of the aircraft. This voltage is in two parts: a constant part proportional to the aircraft fixed weight and a variable part proportional to the variable weight, which consists of fuel, armament, etc. The fixed voltage is controlled by a handset potentiometer across a secondary of a transformer. The variable component is produced by varying the feedback resistance of an amplifier, which is excited by a reference voltage properly phased with the fixed weight component voltage. The amplifier feedback resistance is varied by switches in the rocket intervalometer or armament feed mechanism and also by a variable resistance element ganged to the remote indicator of the fuel gage, which provides a density-compensated indication of the fuel mass remaining.

As weight is expended, the feedback resistance is decreased and the amplifier output voltage diminishes. The voltage proportional to the fixed weight is applied to the primary of a transformer in the accelerometer, and the voltage proportional to the variable weight is applied to the primary of another transformer in the accelerometer. The secondaries of both these transformers are connected in series to provide a voltage proportional to the sum of the weight components. This voltage, representing the instantaneous total weight of the aircraft, is applied across the accelerometer bridge. The bridge output is thus made proportional to weight times acceleration, Wn_z. Two accelerometers are used, one oriented to measure a_Y and one to measure a_Z. The quantity S is introduced by selection of appropriate scale factors.

The output of the Z-axis accelerometer is loaded by two nonlinear potentiometers driven by the Mach number servo. The first of these is wound to produce the functional relationship

$$f_1(M) = \frac{f_c(M)}{C_{L_\alpha}} \tag{66}$$

so that the output of this circuit is $\frac{Wn_Z}{S} f_1(M)$, which is the first term of Eq. 30 except for division by q_i. This voltage is fed to the summing amplifier.

The second circuit loading the Z-axis accelerometer consists of a voltage divider to reduce Wn_Z by the factor K_1/S in the third term of Eq. 30. The nonlinear potentiometer excited from the voltage divider is wound to have the characteristic $f_3(M)$, which expresses the aeroelasticity vs. Mach number relationship. This potentiometer is loaded by a second potentiometer driven by the differential pressure, or q_i, servoed transducer. This multiplies the output of the $f_3(M)$ potentiometer by q_i to produce a voltage proportional to $\frac{K_1 Wn_Z q_i}{S} f_3(M)$, which is fed through a summing resistor to the attack angle feedback summing amplifier.

The second term of Eq. 30 is produced by a Mach number-positioned nonlinear potentiometer expressing the α_0 vs. Mach number characteristic The voltage output of this potentiometer is added to a bias voltage derived from a hand-set adjustment to introduce the variation of α_0 from airplane to airplane. The sum is used to excite a potentiometer positioned by q_i to develop $f_2(M)\, q_i$, which is fed through a summing resistor to the amplifier.

The three terms developed may be added together to give

$$\frac{Wn_Z}{S} f_1(M) + f_2(M)\, q_i + \frac{K_1 Wn_Z q_i}{S} f_3(M) = q_i \alpha \tag{67}$$

Division of all quantities being fed into the amplifier by q_i is accomplished through a potentiometer actuated by the servoed differential pressure transducer. This potentiometer comprises the feedback element of the attack angle summing amplifier, whose output voltage is now a representation of true attack angle, α. Thus Eq. 30 has been mechanized.

The development of the output voltage proportional to skid angle is identical to that of the first term of α, as the other effects are probably negligible. The equation is

$$\beta = \frac{Wn_Y}{S q_i} f_4(M) \tag{68}$$

In the mechanization of Fig. 25, use is made of closed-loop pressure transducers as discussed elsewhere in this report. These transducers are suitable for this application because of their inherent accuracy possibilities and because they make maximum use of the servoed shaft output feature discussed further in the chapter entitled "Extension to Flight Data Computers." The static pressure transducer contains an evacuated pressure-sensitive element, in this particular instance a twisted Bourdon tube, against which the ambient pressure is compared to obtain absolute barometric pressure (P_S). The differential pressure element is subjected to absolute pressure internally and to stagnation pressure (P_T) externally to produce $q_i = P_T - P_S$.

Mach number is mechanized in a self-balancing resistance bridge, two legs of which are variable resistance elements proportional to P_S and q_i, and physically located in the respective servoed transducers. A third leg of the bridge is constant. The followup leg consists of a nonlinear resistance element driven by the servomotor and having a functional characteristic given by

$$R = K_0[(1 + 0.2M^2)^{3.5} - 1] \text{ for } M \leq 1.0 \tag{69}$$

or

$$R = K_0 \frac{166.92M^7}{(7M^2 - 1)^{2.5}} - 1 \quad M \geq 1.0 \tag{70}$$

Through the choice of end resistors, the Mach number servo can be given the Mach number range desired.

The servoamplifiers used to drive the three servoes are identical. Rate generators are shown ganged to each servomotor to provide rate stabilization but because of the nature of the variables being servoed, it is doubtful whether they are required.

Error Contributions

The basic quantities in the computer required to mechanize the lift equation M and q_i, can be measured with suitable accuracy, probably to the order of 0.5 percent. It is also not extremely difficult to reduce the total computer error in attack and skid angle computations to less than 1 percent. These errors compose a small part of the total error that

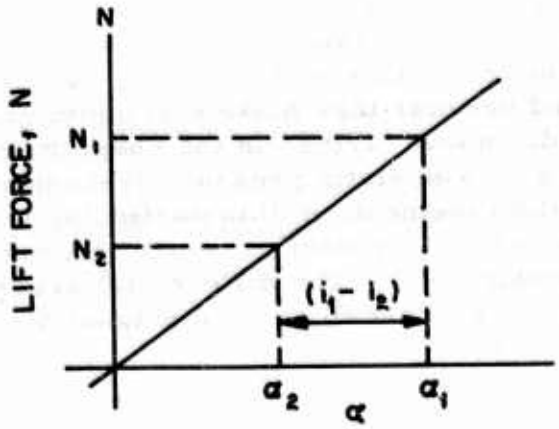

Fig. 26. Typical curve of lift force vs angle of attack for given m, q *and* h

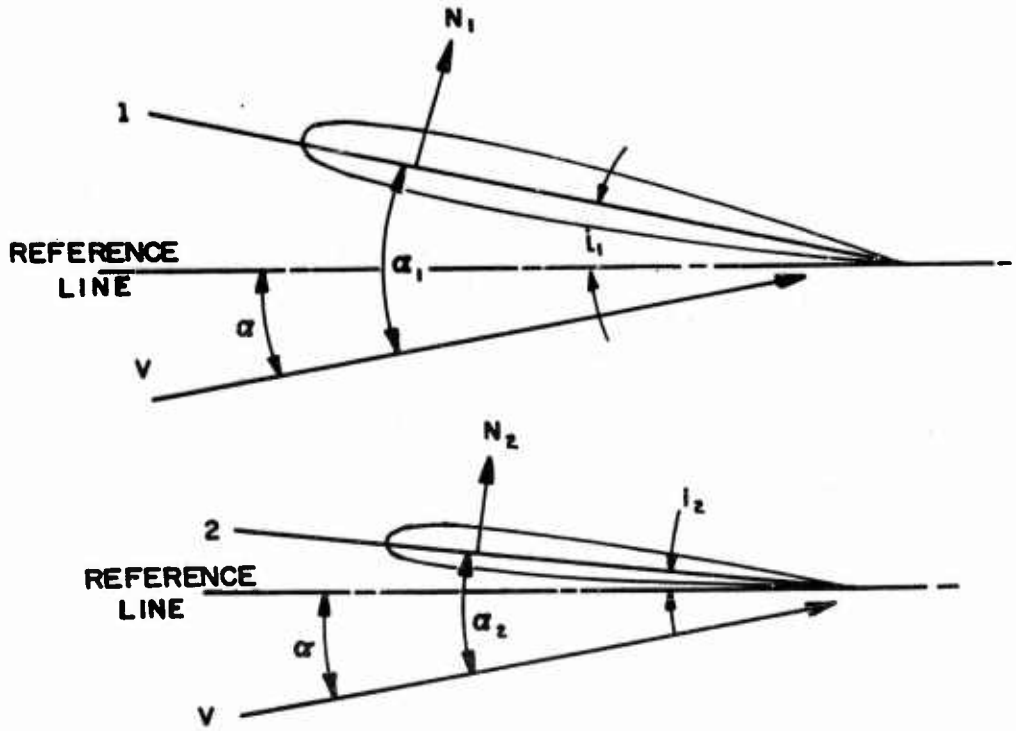

Fig. 27. Dual vane sensor showing reference angles

may be encountered. The items which are difficult to ascertain are the quantities $f_1(M)$, $f_2(M)$, $f_3(M)$, and K_1 and the weight and acceleration components The accuracy with which the accelerometers must be alined for a certain accuracy tolerance in attack angle is extremely critical and close, but not impossible. Weight can be determined with suitable accuracy if the variable components are properly instrumented.

The other quantities may be determined also with acceptable accuracy by utilization of flight test techniques which employ statistical reduction of flight test data and solutions of simultaneous equations of three unknowns. An accurate and reliable standard is required for comparison so that the error between true and computed attack and skid angles can be recorded. Suitable techniques and devices have been developed for this application in present-day supersonic aircraft, but need to be extended up to the limits defined by this study effort.

Force Vane Sensor

A small lifting surface can be used as an angle of attack sensor. The lifting force on the surface can be expressed generally as

$$F = qS[f_1(M) + \alpha_L f_2(M) + \alpha_L^2 f_3(M)]f_4(\beta) \tag{71}$$

The term $f_1(M)$ can be eliminated by using a symmetrical cross section. The term $\alpha_L^2 f_3(M)$ is necessary to take care of nonlinearities at high angles of attack. By measuring F and obtaining β, q, and M from a flight data computer, it is possible to compute α_L.

As with a pressure sensor, it is required that the shape and angular location be accurate and be maintained during use. The device for measuring force must be located near the force-sensing surface and, as shown in the chapter "Components," it is difficult to isolate it from environmental effects. An advantage of measuring force rather than pressure is that no long pressure lines are required, with the accompanying lag effects. On the other hand, if it is desirable to measure yaw also, two vanes are needed, with an additional protuberance from the fuselage.

Dual Vane Sensor

This system uses two restrained vanes to obtain angle of attack information independently of air flow parameters. The operation is based on the principle that the normal force acting on the vane (a symmetrical airfoil section) is directly proportional to the angle of attack of the airfoil. For moderate angles of attack, the plot of normal force, N, vs. the angle of attack, α (Fig. 26), is a straight line passing through the origin and having the slope N_α.

The proposed instrument measures directly the normal forces, N_1 and N_2, acting on two small lifting surfaces (Fig. 27). These surfaces have the same planform and cross-sectional shapes, so that the normal force curves are identical, within the limits of manufacturing tolerances. The surfaces are rigged at two different angles of incidence, i_1 and i_2, with respect to a reference line fixed in the airplane. When the airplane is flying at the angle α (with respect to the reference line), the angles of attack of the lifting surfaces are

$$\alpha_1 = \alpha + i_1 \tag{72}$$

$$\alpha_2 = \alpha + i_2 \tag{73}$$

The normal forces acting on the surfaces are

$$N_1 = C_{N_\alpha}(\alpha + i_1)Sqf(\beta) \tag{74}$$

$$N_2 = C_{N_\alpha}(\alpha + i_2)Sqf(\beta) \tag{75}$$

The difference between these forces is

$$N_1 - N_2 = C_{N_\alpha}(i_1 - i_2)Sqf(\beta) \tag{76}$$

Since from Eq. 75

$$C_{N_\alpha} = \frac{N_2}{(\alpha + i_2)Sqf(\beta)} \tag{77}$$

then

$$N_1 - N_2 = \frac{N_2}{\alpha + i_2}(i_1 - i_2) \tag{78}$$

Solving for the angle of attack,

$$\alpha = \frac{N_2}{N_1 - N_2}(i_1 - i_2) - i_2 \tag{79}$$

The relation may be simplified by letting $i_2 = 0$, giving

$$\alpha = \frac{N_2}{N_1 - N_2} i_1 \tag{80}$$

Knowledge of the incidence angles at which the surfaces are rigged and measurement of the normal forces in flight affords a simple method of obtaining angle of attack. This arrangement does not require corrections for Mach number, altitude, atmospheric properties, etc., because the direct measurement of normal force accounts for these variables.

It should be mentioned that bodies of revolution, rather than the vanes described above, may serve as sensing elements. Two cones rigged in the same manner as the two vanes could be employed. Cones have the advantage of being easier to construct accurately. The dimensions of such sensors can be small.

Because both sensing surfaces are identical in shape, they have approximately equal centers of pressure locations, regardless of Mach number. The surfaces must be mounted so that interference effects are either negligible or the same for each of the surfaces. Also, the effect of yaw must be such that $f(\beta)$ in Eq. 74 and 75 is the same for both vanes. Further investigation and wind tunnel tests will show whether this can be accomplished in practice.

The surfaces must be restrained to prevent motion during operation. The restraint may act parallel to the plane of symmetry along the X-axis of the airplane or normal to the plane of symmetry along the Y-axis. There is some advantage to arranging the axis parallel to the plane of symmetry, because a small rotation about this axis will not change the rigging angles, i_1 and i_2. This results in more precise measurements of the normal forces than if rotation occurs.

The two sensing surfaces could be mounted on a short boom located ahead of the shock wave produced by the nose of the airplane during supersonic flight. A second set of dual sensors is required to measure angle of yaw.

As can be seen, the dual vane sensor system is similar to the dual pressure sensor system and has many of the advantages and disadvantages of that system. If a force system is mounted on the end of a boom, the force-measuring device must be located in the small confines at the end of the boom. With a pressure sensor, the critical instruments can be located in the fuselage, but thus require pressure lines, which can introduce lag effects. On the other hand, a certain length of pressure line is advantageous to avoid the effects of pressure oscillations in the lines. Whether a dual pressure or a force vane system is more advantageous depends upon which of these problems can be solved more readily.

Null-seeking Vane

There are two possible ways of utilizing a null-seeking vane: one is to let the aerodynamic forces drive it to null, and the other is to servo-drive it to null. As both of these types have external moving parts, they do not meet the contractual requirements. However, it was thought worth while to mention them here because movable vane types are used on some present-day aircraft.

Free-floating types have been mounted on the end of booms and on the sides of the fuselage. They are made with sensitivities sufficient to sense α_L to 0.1 degree. Usually the angular position of the vane is converted into an electrical signal by a resistance or inductance transducer. To insure high sensitivity, it is necessary that the bearings and transducer have a minimum amount of friction. This reduction of friction encourages oscillations, but they can be minimized by so designing the vane that its natural frequency differs widely from that of the aircraft. Also, velocity damping can be used to minimize oscillations.

Free-floating vanes have the advantage that they are extremely simple, but it is difficult to design them to withstand rough handling and to provide isolation from the environment for the bearings.

A servo-nulling type, when subject to a lifting force, produces an error signal which causes a motor to rotate the vane and error sensor to an angle such that the lifting force is reduced to zero. This angular rotation is converted into an electrical signal proportional to α_L. The advantage of this system is that it does not depend on aerodynamic forces to provide torque. Time response is uniform at all airspeeds, as it is largely dependent upon the characteristics of the servo loop. It is also possible to damp out oscillations by suitable design of the servo loop.

Providing torque by a servomotor makes possible the use of seals to protect the internal parts from the outside environment. However, the error-sensing vane must be allowed to rotate freely a small amount to produce an error signal. If the error-sensing vane is pivoted on bearings, the same problems are encountered as in the free-floating vane.

On the other hand, a vane attached to a flexible support with embedded strain gages could be used as an error sensor and would eliminate the need for bearings. Care would be necessary in service use, as a bend in the vane would change the null position.

THERMODYNAMIC DEVICES

Hot-wire Anemometer

This device has been used in wind tunnel research to measure turbulence, which is a fluctuation in velocity and direction of flow. The device consists of one or more small wires mounted on a support at some angle θ to the air stream, shown below.

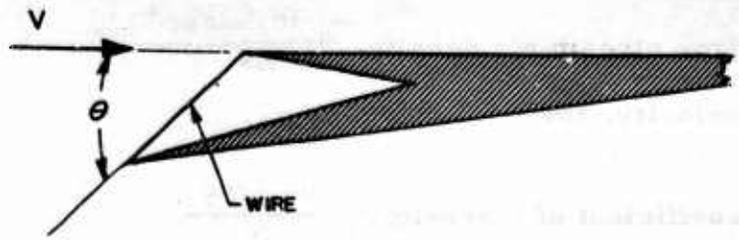

The wire is heated above the total temperature by electric current. The degree of cooling by the air flow is a function of the angle, θ, between the wire and the free stream velocity, as well as of velocity, Mach number, density, wire temperature, and total temperature. By knowing these flow properties, it is possible to compute θ and hence the angle of attack, α.

In wind tunnel work a small wire is used, usually approximately 0.0006 in. diameter by 1/8 in. long. This wire size is obviously too small for use on an airplane, and it is thought that a large-size wire would be practical from an environmental standpoint. A study was made to find how the voltage and current vary with angle of attack and with the other variables mentioned above. Also, it was desirable to know how large a wire can be used.

The equation (Ref. 55) describing the energy transfer from a wire immersed in a fluid whose flow vector is at right angle to the wire is

$$W = vi = \left(\frac{kl\,(T_w - T_g)}{1.08}\right) = \left[K_1 \left(\frac{\rho V d}{\mu}\right)^n + K_2\right] \tag{81}$$

where

W is energy in watts

v is volts

i is current in amperes

k is coefficient of heat conductivity of air, $\frac{\text{Btu}}{(\text{hr - ft}^2\text{ - deg F})/\text{ft}}$

l is wire length, ft

T_T is total temperature, degrees F

T_w is wire temperature, degrees F

ρ is free stream air density, $\frac{\text{lb}_f\text{ - sec}^2}{\text{ft}^4}$

V is velocity, fps

d is wire diameter, ft

μ is coefficient of viscosity, $\frac{\text{lb}_f\text{ -sec}}{\text{ft}}$

A review of the literature (Ref. 50, 53, and 55) gave some approximate values of K_1 and K_2. Also, V in Eq. 81 can be replaced by $V \sin \theta$. This is true when θ lies between 90 degrees and 25 degrees. At angles less than 25 degrees experimental results begin disagreeing with the above rule. Knowing these facts, the following approximate equations can be written for subsonic and supersonic flow:

$$\text{Subsonic flow} \qquad W = \frac{kl(T_w - T_T)}{1.08}\left[0.47\left(\frac{\rho V d \sin\theta}{\mu}\right)^{0.52} + 0.35\right]$$

$$\text{Supersonic flow} \qquad W = \frac{kl(T_w - T_T)}{1.08}\left(0.58\sqrt{\frac{\rho V d \sin\theta}{\mu}} - 0.8\right) \tag{82}$$

For supersonic flow ρ and V are evaluated in front of the shock wave, and μ and k are based on the total temperatures.

Table 1 shows the values of current, voltage, and sensitivity for a wire 0.1 ft long and 0.003 in. diameter (AWG No. 40) at an angle of 30 degrees between air stream and wire. This wire size should cause no difficulties with thermal lag. Values are given for four points of the flight envelope as shown in Fig. 2. The calculations are based on the wire being operated at a constant temperature. This condition was chosen because it allows the best sensitivity in all flight conditions and reduces thermal lag effects.

Table 1. Hot-wire sensor parameters for four points in flight envelope

Item	Point on envelope			
	1	2	3	4
Mach number	0.13	1.2	1.3	3.0
Altitude, ft	S. L.	S. L.	100,000	100,000
Reynolds number	244	1820	28.7	39
iv, watts	6.4	19	1.6	1.3
ΔW per $\Delta\theta = 0.1°$	0.01	0.03	0.004	0.003
$\Delta W/W$, percent	0.15	0.15	0.25	0.25
i	2.5	4.3	1.3	1.1
Δi	0.1	0.17	0.06	0.05
$\Delta i/i$, percent	4	4	5	5
V	2.5	4.3	1.3	1.4
ΔV	0.1	0.17	0.06	0.05
$\Delta V/V$, percent	4	4	5	5
Accuracy requirements for angle of attack rms error = ±0.1 deg				
Wire resistance, ohms	± 0.0016	0.0013	0.0025	0.0007
Percent	0.16	0.13	0.25	0.07
T_p, deg F	60	210	65	620
ΔT_p, deg F	± 0.65	0.5	1.0	0.3
Percent	0.9	0.26	1.5	0.053
q_i, psi	0.19	21	0.275	1.75
Δq_i, psi	0.0003	0.031	0.0004	0.0026
Percent	0.15	0.15	0.15	0.15
ΔM	0.0002	0.0018	0.0019	0.0045
Percent	0.15	0.15	0.15	0.15

No. 40 tungsten wire length 0.1 ft (1 ohm)
θ = 30 degrees

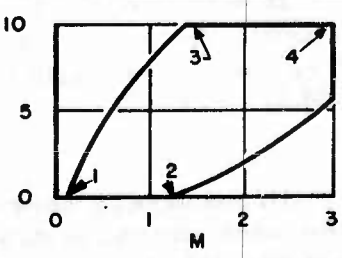

For maximum sensitivity as high a wire temperature as the wire material will stand is desirable. A wire temperature of 900 F was used because Ref. 53 showed that this was about the maximum temperature under which platinum-plated tungsten wire maintains a constant resistance. It is important that wire oxidation and/or evaporation not be allowed to alter the dimensions to the extent that the calibration is changed. This will be a problem with this type of instrument.

Discussion of Results

One noteworthy result shown in Table 1 is that for the extremes of flight conditions the voltage and current through the wire change by a factor of only four. The percentage change in volts and amperes for a 0.1-degree change in angle of attack remains approximately the same (4 to 5 percent). It should be noted that the sensitivities shown in the table are for a wire angle of 30 degrees with the free stream velocity vector. The sensitivity will fluctuate as the angle of attack varies about this point.

A single wire is used in the calculations. But two wires could be arranged (as shown below) in a bridge circuit to show differential resistance. This configuration helps to keep the sensitivity more constant with variations in α.

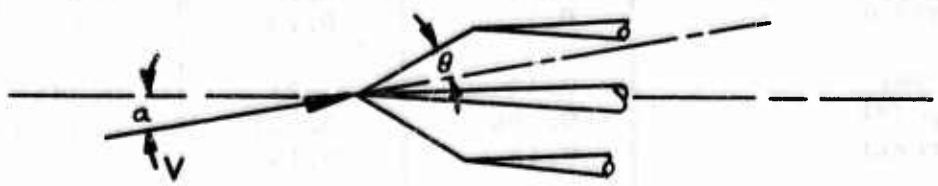

If wire length is increased, the resistance of the wire is increased, and hence the voltage across the wire. The percentage changes in voltage and resistance remain the same. Increasing the wire length increases the chance of collision with objects in the air. Installation problems may also increase.

From stress considerations it is desirable to increase the diameter of the wire, because drag is proportional to d but wire stress is proportional to $1/d^2$. Increasing d increases the percentage of change in power input to the wire per 0.10 degree by some factor less than the rate of increase of $\sqrt{d}$.

However, a greater effect of increasing the diameter of the wire is the decrease of the resistance ($r \sim 1/d^2$) of an already low-resistance device with resulting higher current and a lower potential across the wire. This low-resistance and low-voltage level seems undesirable from the standpoint of the associated electronics which must measure the voltage and current. If the signal voltage is too low, the signal is masked by tube noise in the amplifiers. With a very low resistance hot wire, errors are introduced by variation of lead resistance with temperature.

NACA (Ref. 53) also used 80 percent platinum and 20 percent iridium wire, which has about twice the resistance of tungsten at 900 F. However, its temperature coefficient of resistance is less by a factor of 5. This makes it difficult to measure wire temperature by changes in wire resistance.

If this device is to be developed, it is desirable to investigate materials with the following properties: high resistance, high temperature coefficient of resistance, high strength at high temperature, and resistance to corrosion or evaporation at high temperature.

As shown by Table 1, in order to know α (or θ) to 0.1 degree it is necessary to know the other factors affecting heat transfer to a similar degree of accuracy. This is a serious drawback, as small errors in total temperature, density, and velocity can combine to cause larger errors in the output. This also means that the output of the angle of attack sensor is dependent upon the operation of a flight data computer.

A possible mechanization of this sensor is discussed below. Equation 81 can be expressed more generally as

$$W = l f_1(T_f, T_w) \left[f_2(M) \sqrt{\frac{\rho V d \sin\theta}{f_3(T_f)}} + f_4(M) \right] \tag{83}$$

The terms can be rearranged to provide

$$\sin\theta = \frac{f_3(T_f)}{\rho V d} \left[\frac{W}{l f_1(T_f, T_w)\, f_2(M)} - \frac{f_4(M)}{f_2(M)} \right]^2 \tag{84}$$

The power input to the hot wire is $W = E^2/R$, where

E is voltage across the wire
R is resistance of the wire

In this application the wire will be operated at constant temperature. Therefore $f_1(T_F, T_w) = f_1(T_F)$.

If $K_1 = d$ and $K_2 = Rl$,

$$\sin\theta = \frac{f_3(T_F)}{K_1 \rho V}\left[\frac{E^2}{K_2 f_1(T_F)\, f_2(M)} - \frac{f_4(M)}{f_2(M)}\right]^2 \tag{85}$$

From Ref. 23,

$$V = \sqrt{\frac{K_3 T_F M^2}{1 + 0.2M^2}} \tag{86}$$

$$\rho = \frac{K_4 q_i}{V^2 f_5(M)} \tag{87}$$

where

q_i is differential pressure
$f_5(M)$ is compressibility factor
K_3, K_4 are constants

Combining these equations,

$$\sin\theta = \frac{K_5 f_6(T_T)}{q_i}\left[\frac{E^2 f_7(M)}{K_2 f_1(T_t)} - f_8(M)\right]^2 \tag{88}$$

where

$$K_5 = \sqrt{\frac{K_3}{K_1 K_4}},$$

$$f_6(T_T) = \sqrt{T_T}\ f_3(T_T)$$

$$f_7(M) = \sqrt[4]{\frac{M^2}{1+0.2M^2}}\sqrt{\frac{f_5(M)}{f_2(M)}}$$

$$f_8(M) = \sqrt[4]{\frac{M^2}{1+0.2M^2}}\sqrt{f_5(M)}\ \frac{f_4(M)}{f_2(M)}$$

The mechanization of these equations is presented in Fig. 28. The hot wire is kept at constant temperature by the feedback loop around the bridge circuit. If the temperature of the hot wire decreases, the bridge becomes unbalanced and the amplifier generates power to increase the temperature of the wire. The output voltage of the amplifier is thus

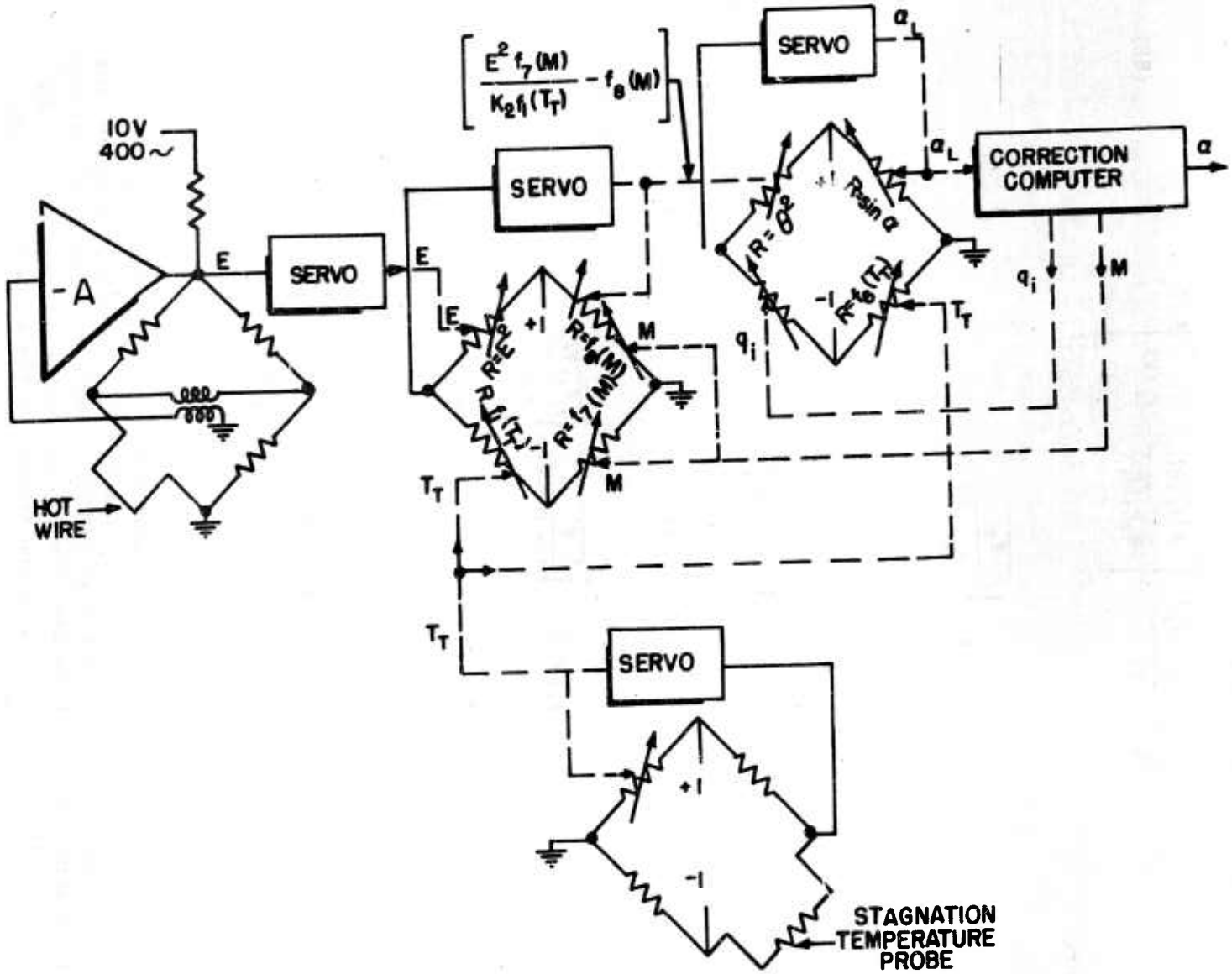

Fig. 28. Mechanization of hot-wire angle of attack indicator

proportional to the voltage across the hot wire. This voltage drives a servo which actuates a square-law rheostat in another bridge circuit. The remaining arms of the bridge are nonlinear rheostats, which generate $f_1(T_f)$, $f_7(M)$, and a linear rheostat, which is driven by a servo to balance the bridge. The shaft rotation of this servo is

$$\left[\frac{E^2 f_7(M)}{K_2 f_1(T_f)\, f_2(M)} - f_8(M) \right]$$

This servo drives a square-law rheostat in a bridge circuit in which the second arm is a linear rheostat driven by q_i, the third is a nonlinear rheostat which generates $f_6(T_f)$, and the fourth is a sine rheostat servo driven to balance the bridge. This bridge computes the local angle of attack, which is fed through the correction computer to obtain the true angle of attack. This computer is discussed on p. 108. T_f is obtained from a resistance temperature probe connected in a bridge circuit.

Actually, the temperature measured by the probe is related to the total temperature by $T_{probe} = T_f \left(\frac{1 + K_r 0.2 M^2}{1 + 0.2 M^2} \right)$, where K_r is the temperature recovery factor (usually $K_r \approx 0.98$). Because the two temperatures are very nearly equal, it would seem desirable to base the hot-wire anemometer equations on T_{probe} to avoid computing total temperature from T_{probe}. If this is done, the hot-wire and the temperature probe are calibrated at the same time; the mechanization then is based on T_{probe}.

AIR PARTICLE IDENTIFICATION

Smoke

In this system smoke particles are injected into the airstream, and the angle of attack is obtained by observing the downstream location of the stream line containing the smoke. There are several ways by which this system may be instrumented. In the system shown in Fig. 29, smoke is emitted from a line source and sensed by detectors 1 and 2. If the output of a detector is proportional to the amount of smoke crossing it, the angle of attack is given by

$$\tan \alpha_L = K \frac{D_1 - D_2}{D_1 + D_2} \tag{89}$$

where D_1 and D_2 are the outputs of detectors 1 and 2.

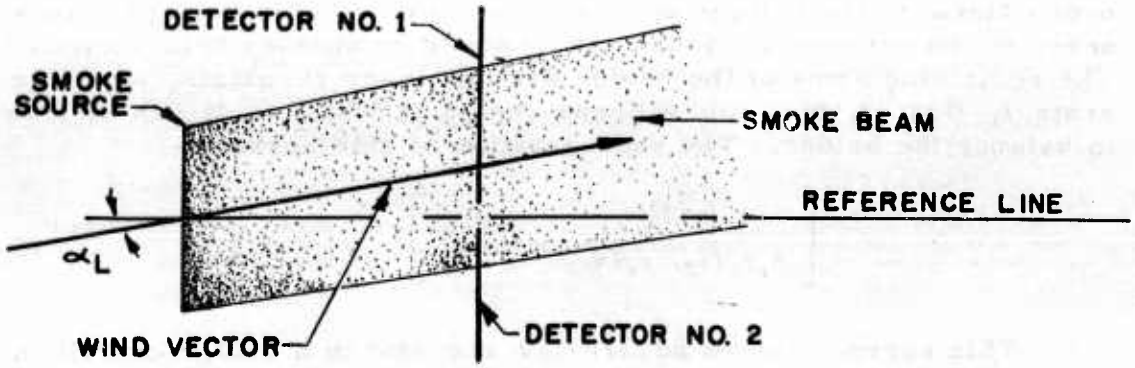

Fig. 29. Smoke particle system with fixed detector

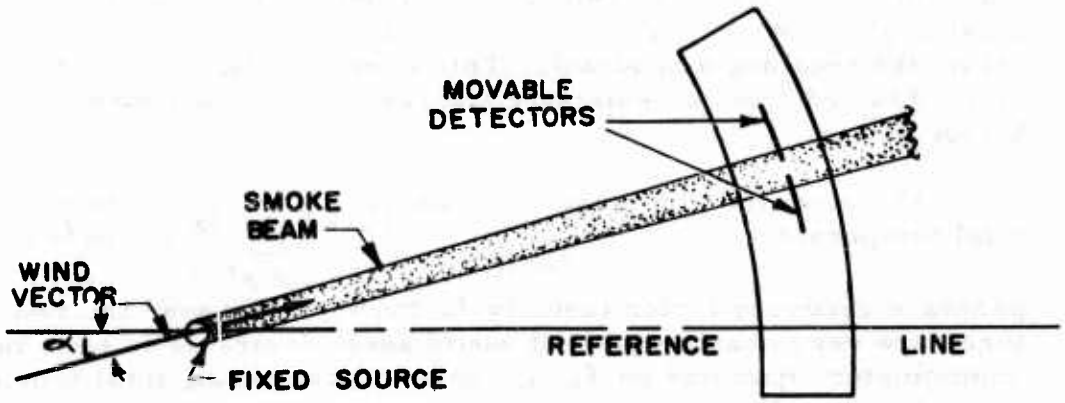

Fig. 30. Smoke particle system with movable detector

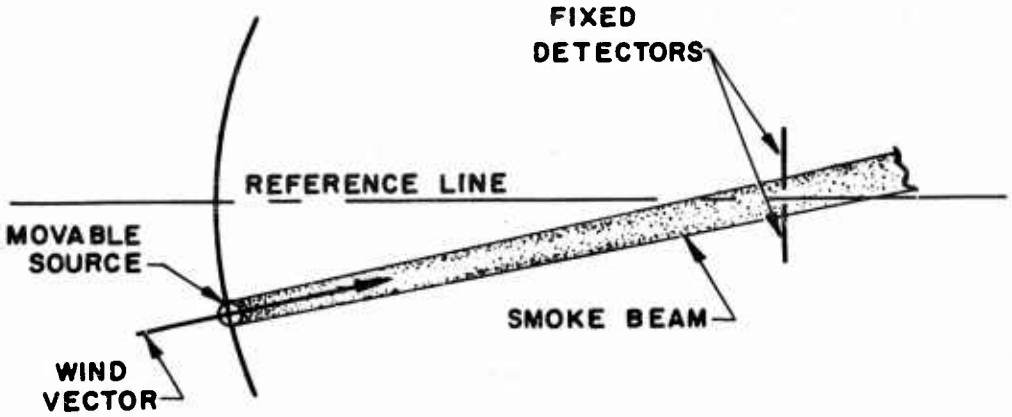

Fig. 31. Smoke particle system with movable source

Another method uses a point source of smoke and a movable pair of detectors (Fig. 30). The moving parts of this sensor may be protected from the airstream by a transparent window. The detector is servo-driven to track the smoke beam, and its orientation indicates angle of attack.

It is possible to use two fixed detectors and a movable source (Fig. 31). Here the source is servo-driven to obtain equal signals from the two detectors, and its position indicates angle of attack.

The advantage of the smoke system is that it indicates local angle of attack directly, without requiring high-accuracy pressure sensors and dividers. Of course, a correction computer is required to calculate the true angle of attack. A major problem of this system is the detection of smoke in clouds or at night. Photo cells can be used in an arrangement where they sense light reflected from the smoke, or heat detectors can be used to sense the temperature of the smoke. The smoke has to be injected far enough into the airstream to clear the boundary layer; and at the same time the smoke source, receivers, and their supports must not change the air flow. Frequent replacement of the smoke-producing material is required.

The smoke system is not considered desirable for a service instrument, as it is very difficult, if not impossible, to develop suitable techniques for injecting the smoke into the airstream and detecting it under all conditions.

Ionization

An ionization system also determines the angle of attack by marking the stream lines. In this case ions, rather than smoke particles, are used as markers. All the geometrical configurations discussed in the preceding section are applicable for an ion system.

Ions can be produced by radioactive substances and also by electrical discharges. An example of the use of a radioactive ion source is the Alphatron pressure gage manufactured by the National Research Corporation (Ref. 16). Here a small amount of radium in equilibrium with its decay products provides a source of alpha particles which are the ionizing agents.

Spark discharges, corona discharges, and precorona discharges also produce ions. Spark and corona discharges require high voltage, cause rapid deterioration of the discharge points, are apt to produce radio interference, and can be used only to generate pulses. Precorona

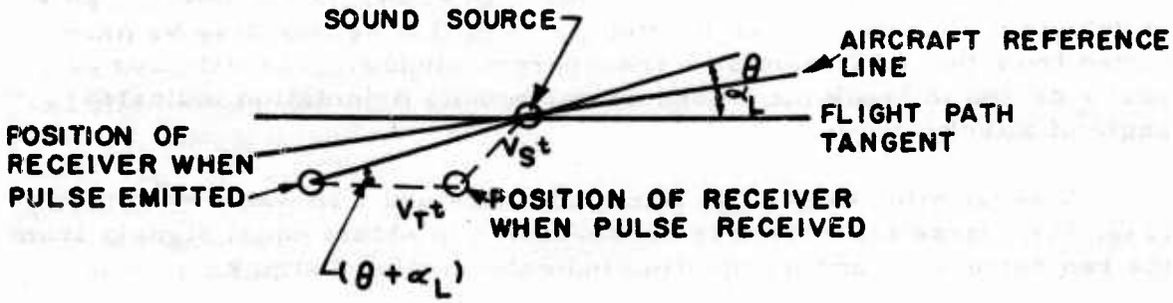

Fig. 32. Single-receiver sonic system

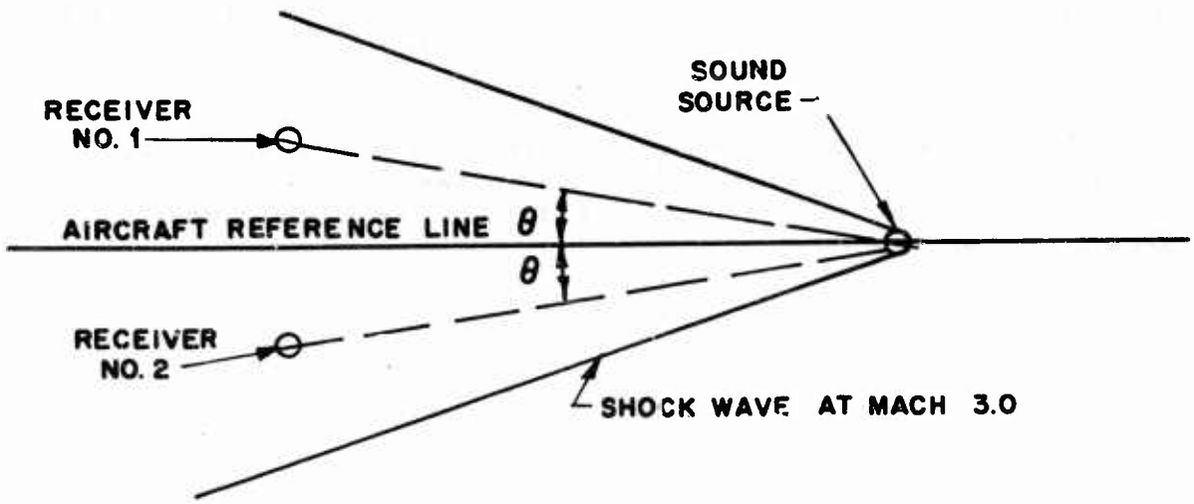

Fig. 33. Dual-receiver sonic system

discharges, on the other hand, require only moderate voltage, cause no deterioration of the discharge points, are less apt to produce radio interference, and can produce sine wave ion discharges. Sine wave ionization allows airspeed to be measured by observing the phase shift between the generated ion signal and that received at the detector.

The Cook Research Laboratories have built a velocity-measuring device using spark gap ionization. It has been tested in a supersonic wind tunnel up to Mach 1.7. A more detailed discussion of this instrument is presented in Ref. 21 and 25. Precorona sine wave discharge has been utilized by Eclipse-Pioneer in a subsonic airspeed indicator (Ref. 15).

Ions may be detected through the collection of ions in an electrostatic field or by the induction effect. It has been found that a greater detection signal can be obtained using the induction effect. If this effect is used, the detectors can be flush-mounted, shielded, and insulated "buttons"; or, in a movable detector, they can be protected from the air stream by an insulator.

An ion system provides local angle of attack directly and does not require a wide-range divider. A correction computer is required to obtain true angle of attack. The transmitter and receiver must not cause interference with the airflow, but at the same time the air outside the boundary layer must be ionized. This is a relatively untried system and requires considerable development. There is a chance that the discharge points, ion stream, or detectors might cause interference with the radar.

Sonic

It is possible to obtain angle of attack by measuring the time for a sonic pulse to travel between a source and receiver located in the air stream. From Fig. 32 it is seen that

$$V_S^2 t^2 = V_r^2 t^2 + f^2 - 2V_r t f \cos(\theta + \alpha_L) \tag{90}$$

where

V_S is velocity of sound
V_r is velocity of airplane
t is sound transit time
f is distance between source and receiver
θ is angle between fuselage reference line and line between source and receiver
α_L is angle of attack

Solving for the angle of attack,

$$\alpha_L = -\theta + \cos^{-1}\left(\frac{V_F^2 t^2 - V_S^2 t^2 + f^2}{2V_F t f}\right) \tag{91}$$

This system uses the velocity of the airplane and the speed of sound in obtaining the angle of attack. It is possible (Fig. 33) to use two receivers and to obtain the angle of attack without knowing the speed of sound. The angle of attack is given by

$$\alpha_L = \sin^{-1}\left[\frac{\left(\frac{t_1}{t_2} - \frac{t_2}{t_1}\right)\frac{f}{2V_F}}{\sqrt{t_1^2 + t_2^2 + t_1 t_2 (1 - \cos 2\theta)}}\right] + \tan^{-1}\left[\frac{t_1 - t_2}{t_1 + t_2}\cot\theta\right] \tag{92}$$

It is still necessary to measure the local velocity of the air stream. By using three receivers it is possible to eliminate the airplane velocity from the equation.

For the receiver to pick up the sound at Mach 1 or greater, the following equation must be satisfied:

$$\sin(\theta + \alpha) \leq \frac{1}{M} \tag{93}$$

At high Mach numbers this limits the range of attack angle that may be measured. For example, at $M = 3.0$, with $\theta = 15$ degrees, the maximum total measurable range of angle of attack is only 10 degrees.

In a sonic system the sound source has to be supported in a manner such that the supporting structure does not interfere (through creating shockwaves, turbulence, etc.) with the flow of sound pulses past the source and receivers. The system requires a considerable amount of electronic equipment, as it is necessary to generate sharp pulses, measure transit times, and compute local angle of attack from the transit times. Figure 34 is a block diagram of a possible system.

Cornell Aeronautical Laboratory has done a considerable amount of theoretical and experimental work on a sonic true airspeed and Mach number indicator. This work is presented in Ref. 27.

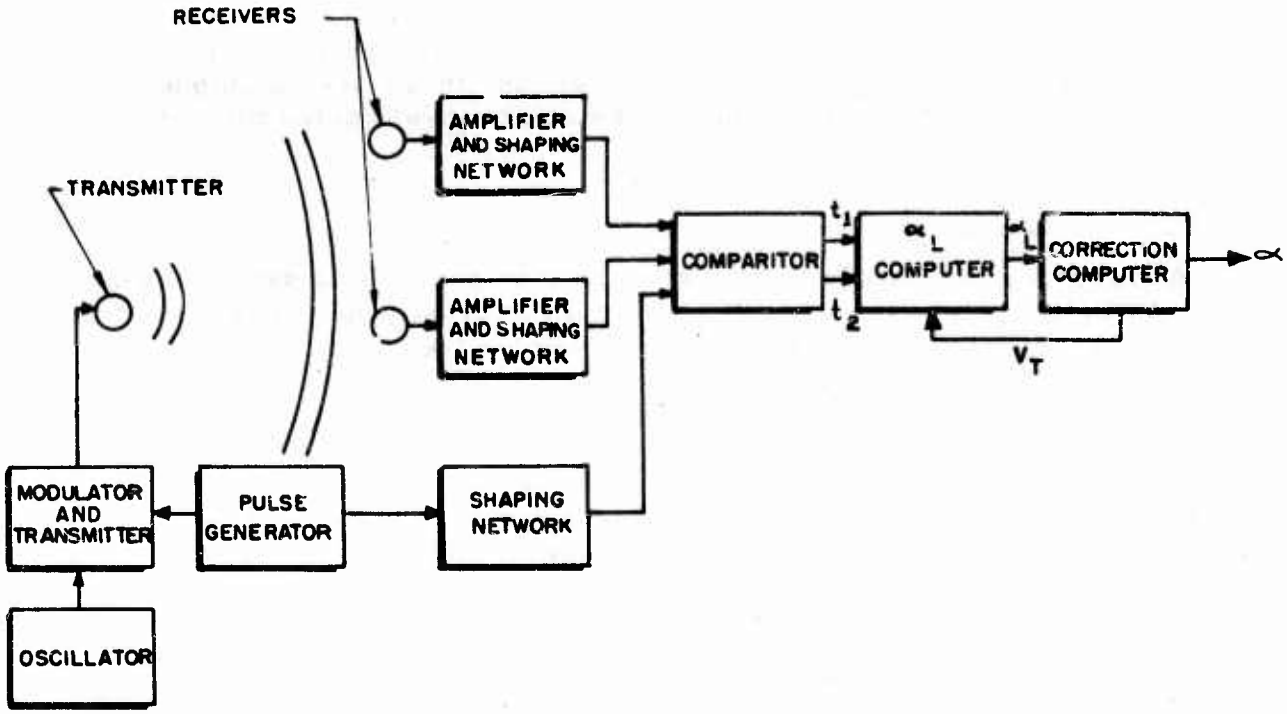

Fig. 34. Sonic angle of attack indicator

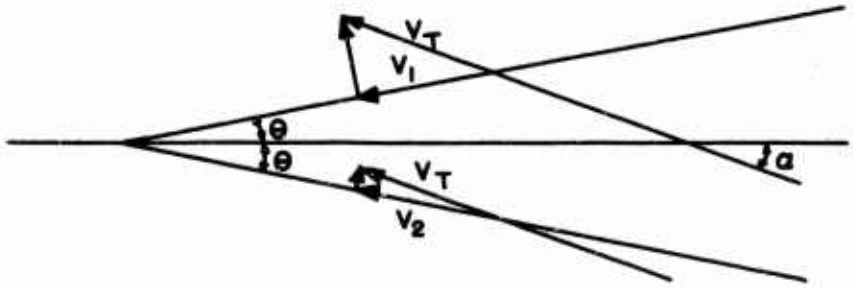

Fig. 35. Vector resolution of airspeed

The sonic method of measuring angle of attack requires extensive computing and measuring equipment, presents installation problems, and requires some transducer development. Because there are no unique advantages of this system over others, it was not investigated further.

Atmospheric Reflection

A study has been made to see whether it is possible to use atmospheric reflection of electromagnetic radiation to determine the true angle of attack. The system proposed uses the Doppler frequency shift of the reflected radiation to measure the velocity of the airplane with respect to the air mass. Figure 35 presents the geometry from which the equation for this system is developed. Here velocity, V_1, is the component of true airspeed resolved at an angle $+\theta$ with respect to the airplane reference line. Similarly, V_2 is the component resolved at an angle $-\theta$. These are the velocities measured by reflected radiation:

$$V_1 = V_T \cos(\theta + \alpha) = V_T(\cos\theta \cos\alpha - \sin\theta \sin\alpha)$$
$$V_2 = V_T \cos(\theta - \alpha) = V_T(\cos\theta \cos\alpha + \sin\theta \sin\alpha) \qquad (94)$$

By combining these equations,

$$V_2 + V_1 = 2V_T \cos\theta \cos\alpha$$
$$V_2 - V_1 = 2V_T \sin\theta \sin\alpha$$

from which

$$\tan\alpha = \frac{V_2 - V_1}{V_2 + V_1} \cot\theta \qquad (95)$$

By suitable gating of the transmitter and receivers it is possible to measure the radiation from only a portion of the air mass. It has been determined that light reflections from the air mass approximately 10 to 30 yd ahead of the airplane can be detected.

This system computes the true angle of attack without the use of a correction computer. Unfortunately, the Doppler shift is small, a fraction of an angstrom, and present equipment for measuring shifts of this order of magnitude is large and sensitive to vibration. Therefore this system is not suitable for airborne use. It is possible that in the future new equipment applicable to this problem will be developed as radar techniques are applied to the optical region of the spectrum.

SENSOR LOCATIONS

GENERAL

All of the systems studied, except lift mechanization and electromagnetic reflection, measure the local angle of attack at the sensor location and require a correction computer to convert this to true angle of attack. The difference between true and local angles of attack is called position error and is a function of Mach number, angle of attack, angle of yaw, and the location of the sensor. It is important to select the optimum location for a sensor because the complexity of the computer and the accuracy with which it computes true angle of attack are functions of sensor location.

Several possible sensor locations are discussed in this section. These locations are shown in Fig. 36, along with a tabulation of their advantages and disadvantages. In general, the position error is reduced if the sensor is mounted on a boom ahead of the aircraft, and the cross coupling between pitch and yaw is reduced if the sensor is mounted in a horizontal or vertical plane of symmetry. At subsonic speeds all locations have a position error, but at supersonic speeds pressure disturbances cannot be propagated upstream. The position error is zero for sensors located ahead of the aircraft shock wave. As a shock wave passes a sensor location, a large change in the local angle of attack occurs. A location is undesirable if the Mach number for shock wave passage varies with aircraft yaw and pitch.

WING

A sensor located on the wing is subject to large subsonic position errors. For example, Ref. 28 indicates that the subsonic position error for a 38-in. boom mounted on the wing of an F7F-1 is 1.6 degrees at zero angle of attack and increases linearly to 3.8 degrees at a 5-degree angle of attack. There are several sources of position error when the sensor is mounted outboard on the wing. Some of these errors are caused by wing deflections in flight and by permanent deflection of the wing as the aircraft ages. In addition, the Mach number for shock wave passage over the sensor varies with yaw angle. In most instances sensors must be located on both wing tips to average out the effects of cross flow.

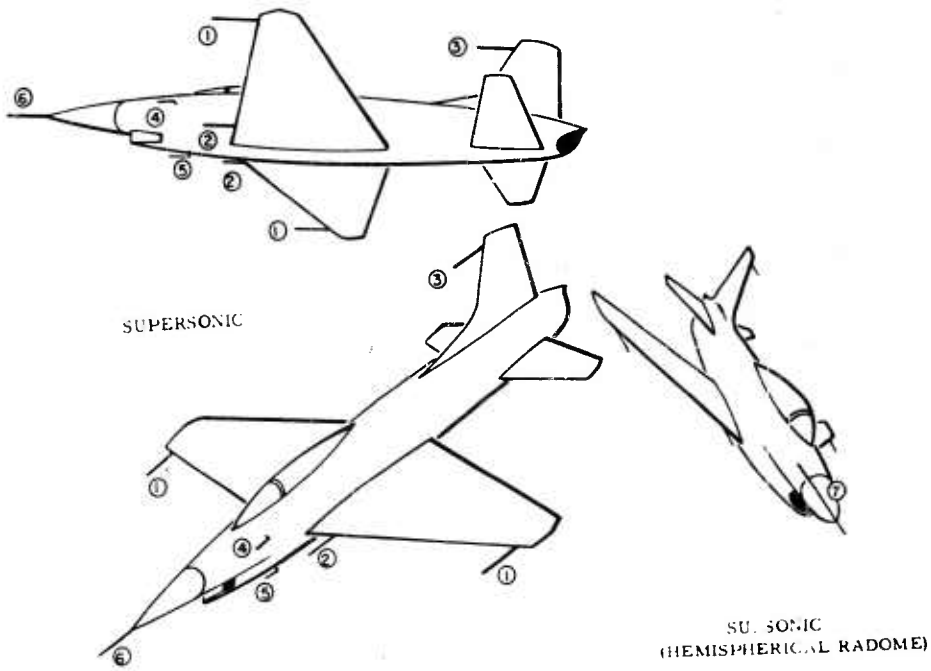

1. Position error, wing twist, and wing bending corrections required.
   Dual sensors required because of cross flow.
   Permanent set in wing.
2. Position error corrections required.
   Dual sensors required because of blanketing during yaw.
   Damage possible from flying debris off runway.
3. Fuselage and fin bending effects.
   Blanketed at moderately high attack angles.
   Probably no yaw corrections required.
   Position error corrections required.
   Turbulent flow: poor aerodynamic data.
4. Position error corrections required.
   Dual sensors required because of blanketing during yaw.
   Fuselage bending corrections required.
   Susceptibility to damage by ground personnel.
   Damage possible from flying debris off runway.
5. Position error corrections required.
   Fuselage bending corrections required.
   Susceptibility to damage by ground personnel.
   Damage possible from flying debris off runway.
   Affected by extended landing gear.
6. Subsonic upwash corrections required.
   No position error corrections supersonically.
   Fuselage bending corrections required.
   No yaw effects.
   Possible radar interference.
7. Upwash corrections required.
   No yaw effects.
   Possible radar interference.
   Fuselage bending corrections required.

NOTE
All have some degree of personnel hazard when the plane is on the ground. Location 3 is expected to present the least hazard.

Fig. 36. Comparison of possible external sensor locations

When the sensor is located on the inboard section of the wing it is in the distorted flow field of the fuselage, and sensors are required on both sides of the fuselage to eliminate blanketing and cross-flow effects when the aircraft is yawed. At supersonic speeds a number of shock waves are generated by protuberances on the fuselage, and these will cause changes in the local angle of attack as they pass the sensor location.

VERTICAL FIN

In most ways the position errors of a sensor mounted on the vertical fin are similar to those of a wing sensor, with pitch and yaw effects interchanged. There are some additional sources of error such as motion of the sensor due to fuselage deflections, turbulence from the fuselage, and buffeting at high angles of attack. Some sensors located on the fin are always aft of the shock wave and thus have position errors throughout the entire flight envelope.

FUSELAGE

The following discussion does not include the fuselage nose location, which is presented in the next section. The position error for other fuselage locations is greater than that for wing locations. Subsonically, Ref. 5 indicates that the position error for a probe located 9 in. aft of the fuselage nose on a 0.1 scale model of an F9F aircraft is 2.2 degrees at zero angle of attack and increases linearly to 6.1 degrees at a 5-degree angle of attack. The sensor always has a supersonic position error, as it is located behind the aircraft shock wave at all speeds. This supersonic position error is difficult to analyze because it may be affected by protuberances forward of the sensor or even by skin rippling.

Because the sensor must extend beyond the boundary layer, it should be mounted on a forward section of the fuselage where this layer is thin. Previous work (Ref. 28) has shown that the best fuselage location is in the horizontal (xy) plane of the fuselage reference line. Such a location requires symmetrical mounting of a sensor on each side of the fuselage to eliminate blanketing and cross-flow effects when the aircraft is yawed. If the system is not required for negative angle of attack it is possible that one sensor underneath the fuselage will be sufficient. Such a sensor would be subject to damage from debris flying off the runway during takeoff and landing.

FUSELAGE NOSE BOOM

An ideal location, from considerations of sensor operation alone, is on a fuselage nose boom because the supersonic position error is zero and the subsonic error is small. For example, the subsonic position error for a 36-in. boom mounted on the nose of an F7F-1 aircraft is zero for a zero angle of attack and increases to only 1 degree at a 5-degree angle of attack (Ref. 28). Because the boom can be fairly short its cross section need not be very large to provide structural rigidity. The chief objection to a fuselage nose location is that it may create radar interference if the aircraft has a nose radar installation.

Radar Interference with Subsonic Radomes

Subsonic radomes are normally hemispherical or oblately ellipsoidal in shape, such configurations providing small boresight errors and good power transmission. A boom on the axis of such a radome causes serious boresight errors and power losses. A boom located along the side of the radome and projecting ahead of the main shock wave does not necessarily affect radar performance and provides good sensor location for appropriate polarization of the radar energy.

Tests of such a boom on the F-100 aircraft were performed by NAA. The radome used was more streamlined than the usual subsonic radome, but the results are qualitatively pertinent. These tests showed that the change in radiation pattern due to installation of the boom was not measurable in those portions of the pattern having a power level of 1 percent or greater. Limitations of the equipment used prevented measurements for power levels less than 1 percent.

Radar Interference with Supersonic Radomes

With the advent of supersonic aircraft, it became necessary to streamline the radome to minimize drag and to reduce radome erosion. The resulting high-fineness-ratio, conical, or ogival radomes have considerable boresight errors and power transmission losses. Where a transmission null, or even a blind spot, exists along the radome axis, a boom or a metal plate mounted in the nose of the radome actually increases the power transmitted in this direction. An investigation to determine the probable effect of mounting a boom on a streamlined supersonic radome has produced the following information:

1. NAA radar engineers believe, from their experience and preliminary computations, that a small sensor on the radome tip will not produce excessive interference when used with a practical supersonic radome.

2. Radar engineers at Hughes Aircraft Company state that they anticipate no difficulty from a sensing device on the aircraft nose forward of the radar. Their opinion is undoubtedly based upon their experience in developing a radome and fire control system for the Convair F-102A (which has a nose boom on its radome) and upon the test data which follow.

a. Test measurements of Mach number, true airspeed, and angles of attack and yaw were made with a sensor on the tip of a boom mounted on a conical radome. For accurate flight data, the shortest boom possible was 18 in., tapered down from a base diameter of 2.5 in. The boom and sensor contributed no detrimental effects on the accuracy and boresighting of the radar as the radome had a 4.0-in. blind spot forward along its axis; actually, mounting of the boom on the radome removed this blind spot.

b. Boresight errors of the order of 3 to 4 mils were experienced with a 3.5-in. diameter boom on an F-102 radome. These were considered acceptable errors.

3. The McMillan Laboratories have actively studied distortions in radar fields due to radomes and other objects in the near field. The following information has been obtained from them: some of it in reports, and some from conversations with their personnel.

a. Tests on a 15-degree conical radome with walls having high reflection ratio showed a minimum or null area in the pattern along the radome axis of symmetry. This null effect was the same when the radome was slightly truncated and the tip left open, indicating that the tip shape is relatively unimportant. An extensive series of experiments was made to discover the effects of covering the open tip with a disk. It was found that the null in the center of the pattern may be made to disappear, or at least to decrease, by the use of a metal disk of proper size and location; however, the pattern was still slightly distorted. Test results were similar for high-fineness-ratio cones and ogives. It is believed that the power loss in the center of the pattern is caused by adverse reflection of the radar beam from the radome walls.

b. Tests of a hemispherical radome with de-icing wires in the radome grating (structural ribs) showed that the wires caused no noticeable boresight shift.

c. A 30-degree conical radome with a total head orifice in the apex of the cone and nonmetallic pressure lines within the grating was found to have a boresight error of 0.05 degree per degree of antenna rotation.

The preceding data indicate that, with high fineness ratio, supersonic radomes, mounting the sensor on a fuselage nose boom does not seriously reduce radar performance.

COMPONENTS

SENSORS

Pressure Sensors

In studying angle of attack systems that use pressure sensors, it was thought worth while to investigate the range of pressures to be measured to provide 0.1-degree accuracy over the wide range of the flight envelope. Also, a search of the literature was made to find out what methods are available for measuring pressure over a wide range and with a high degree of accuracy.

All of the pressure angle of attack systems measure a differential pressure, $\Delta P = P_1 - P_2$, and some divide ΔP by $P_T - P_S$ to get the first-order term in the computations of local angle of attack. Most of the experimental information on pressure angle of attack sensors is given in terms of $\frac{\Delta P}{P_T - P_S}$ vs. α_L, from which a representative value of $\frac{\left(\frac{\Delta P}{P_T - P_S}\right)}{d\alpha_L}$ could be obtained. Knowing this and the flight envelope, it was possible to get the following range of pressures to be measured and to estimate the accuracy required for an error of 0.1 degree in angle of attack:

Static pressure (absolute) 0.15 to 15 psi (±0.00025 psi)
Total pressure (absolute) 0.42 to 37 psi (±0.00025 psi)
P_1 and P_2 (for ±15 degree range of α_L) 0 to ±9 psi (±0.00025 psi)

The extreme accuracy of ±0.00025 psi is needed to sense α_L to 0.1 degree while flying at 90 knots. If it is decided that the 0.1-degree accuracy is not needed over the entire flight range, this requirement can be reduced.

Many methods are available for measuring low pressures accurately, but only three basic gages were found that showed possibilities for measuring all values from sea level to 100,000 ft: an ionization gage, the General Electric molecular gage, and the conventional displacement or force-type gages using bellows, diaphragms, or bourdon tubes.

The ionization type has been developed by the National Research Corporation (Ref. 16). This gage uses alpha particles from radium to ionize the gas. The resulting ionization current between two charged electrodes is a function of pressure. With this instrument some temperature and water vapor content corrections are necessary.

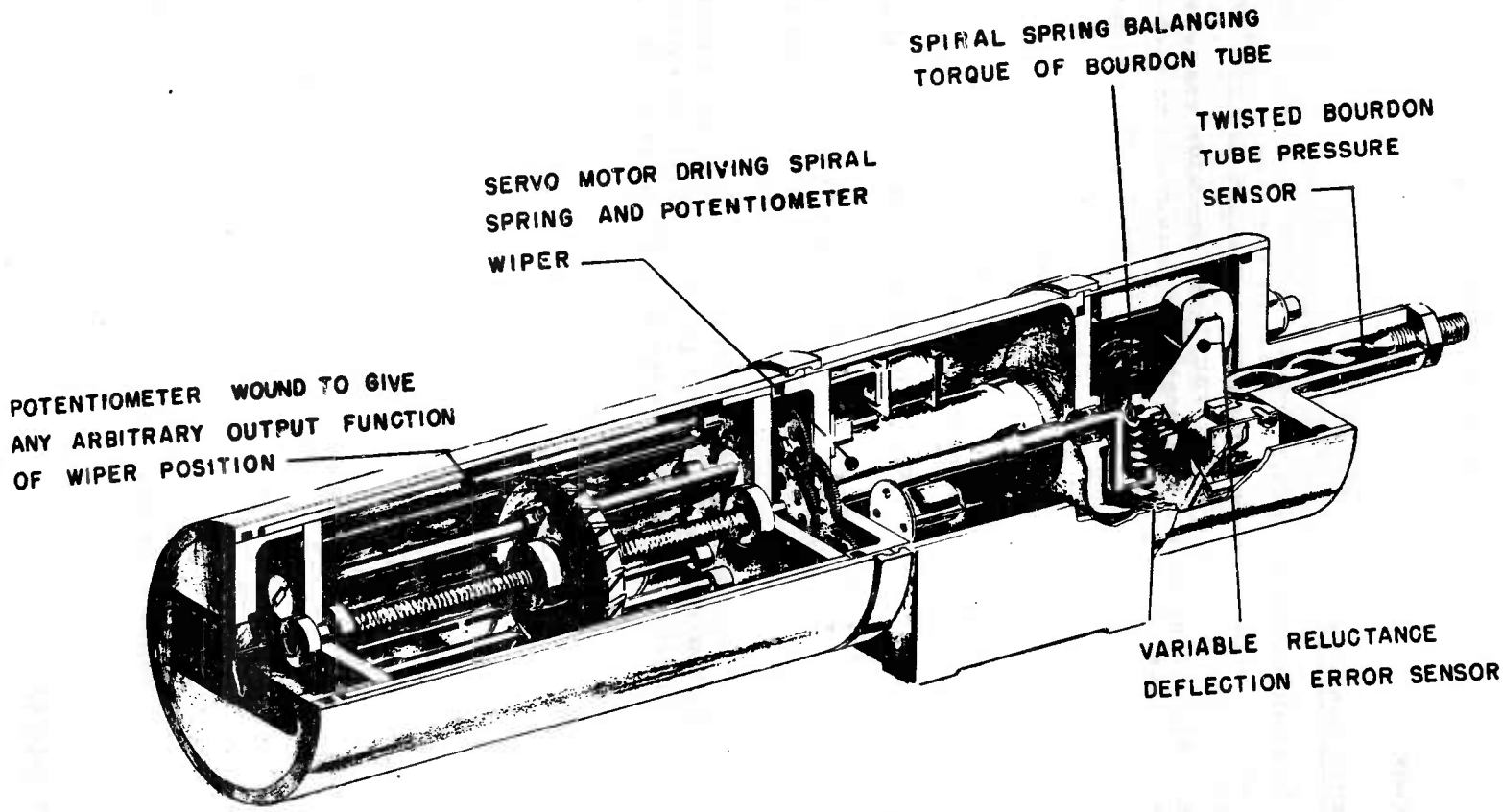

Fig. 37. Closed-cycle pressure transducer

This gage is sold commercially with a range from 0.000002 psi to 20 psi. Present information indicates that over some of the range the same output is given by two different pressures. This increases the complexity of measuring pressure. Also, the current resulting from the ionization is small and needs amplification to be used in a computer circuit. The ionization sensing element is very rugged, but overall dependability is determined, to a large degree, by the associated electronics.

The molecular vacuum gage is manufactured by General Electric Company. The air whose pressure is to be measured is set in motion by a simple centrifugal blower and directed against a stationary turbine. The torque produced by the turbine is a function of gas pressure and turbine speed. It is expected that the readings of this gage must be corrected for temperature and for the presence of anything, such as water vapor, that changes the molecular weight of air.

The centrifugal blower may be run at constant speed, allowing the torque to vary; or the torque may be held constant and the motor speed varied. The latter method is preferable, as it does not require a constant frequency for constant motor speed. Electromechanical speed and torque transducers are required to convert these quantities into voltages for the computer. Although this gage is manufactured only in a range from 0 to 0.4 psi, there appears to be no reason why it could not operate over a greater range.

Displacement-type gages are made in a variety of forms, but they all measure pressure directly by the deformation of a bellows, diaphragm, or bourdon tube. It is doubtful that such a pressure sensor could be made adaptable to aircraft use over the above ranges with ±0.00025-psi accuracy. That is, the metal would have to be sufficiently flexible to measure a deflection for 0.00025 psi, but be able to deflect to 140,000 times this amount without any measurable hysteresis or zero drift effects.

This problem may be solved by a force-balance system where the deflection element is allowed to deflect only enough to cause an error signal. This error signal is amplified and used to apply a force to balance the pressure force of the deflecting element. In this way the pressure displacement element is not allowed to deform to such an extent that hysteresis and other errors occur.

NAA has developed pressure transducers (Fig. 37) which balance the torque of a twisted bourdon tube by a spiral spring. The number of rotations of the spring needed to balance the pressure torque is the output signal. This transducer is sensitive to somewhere between 0.00036 and 0.0007 psi. References 9 and 38 describe a diaphragm gage and a nine-turn bourdon tube which are sensitive to 0.0002 psi.

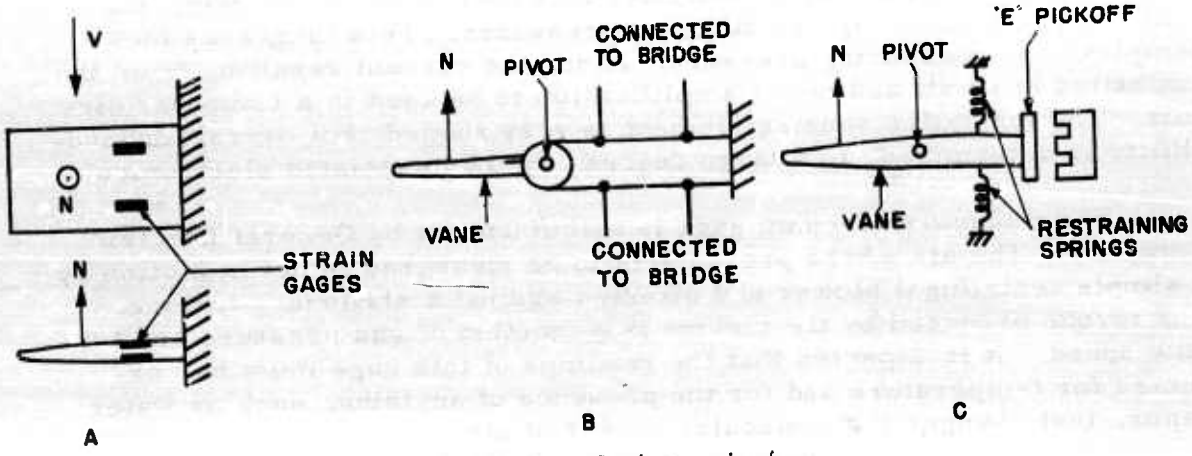

Fig. 38. Methods of measuring force

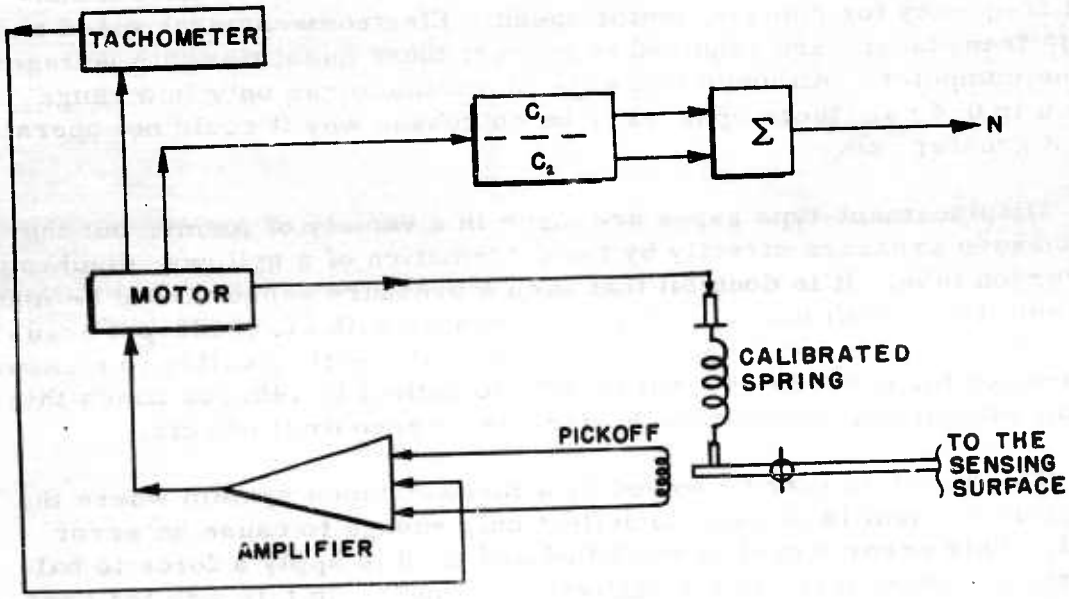

Fig. 39. A sensitive force-measuring system

Because displacement gages measure pressure directly, no compensation is needed except for those effects due to thermal expansion of mechanical parts. These effects can be automatically compensated for by a choice of suitable materials.

An advantage of the diaphragm bellows or bourdon-type gage is that one gage can be used to measure the difference between two pressures. It thus takes the place of two gages of the ionization or molecular type. The maximum error allowed in measuring pressure can be increased, or, in other words, fewer errors are introduced by the pressure transducers. The ranges of pressure and errors using differential pressure gages are shown below:

$(P_T - P_S)$	0.19 to 29 psi	(±0.0005 psi)
$(P_1 - P_2) = \Delta P$ (for $\alpha_L = \pm 15^{\circ}$)	0 to ±18 psi	(±0.0005 psi)

An additional benefit is realized when the differential pressure forces can be connected directly to a mechanical divider, as discussed in the portion of this chapter entitled "Computers."

In view of the above facts, it would seem possible and desirable to use displacement-type pressure elements with the pressure angle of attack sensors. Special pressure transducers must be developed, but present knowledge and skills indicate that they can be built.

Force Sensors

The force sensors required must measure force to a high degree of accuracy over a large range. In doing this the sensor must be restrained from motion, so as to keep out unwanted effects. One way is to attach the sensing and restraining elements together in a single unit. Figure 38, A shows a system where strain gages are used to measure bending.

Another possible procedure is to provide the sensing surface with a hinge along the X-axis. In this arrangement two preloaded strain gage wires restrain the surface (Fig. 38, B). The normal force adds to the tension of one wire and relieves the tension of the other. Two such strain gage wires built into a bridge provide temperature compensation, as well as intelligence for the normal force. An "E" pickoff and a restraint (Fig. 38, C) could also be used. "E" pickoffs are expected to afford a wider range output signal for a given displacement than will strain gages. The systems shown in Fig. 38 allow the force sensor to

move a slight amount. If these are used they must be designed for a limited movement that will not introduce errors.

A more sensitive, but more complicated, restraint can be obtained by using a servo arrangement (Fig. 39), which functions in the following manner. When a load is applied to the vane, causing it to deflect, the electrical pickoff detects an error and immediately signals the amplifier and the electric motor. The motor deflects the calibrated spring in such a way as to develop a force which restores the vane to zero deflection. The deflection of the spring is thus directly proportional to the force N.

The spring calibration factor is determined empirically. In deflecting the spring, the motor revolves; these revolutions are counted on a coarse counter, C_1, which, through proper gearing, is connected to a fine counter, C_2. The readings from the coarse and the fine counters are summed and fed into the computer. A tachometer connected with the motor provides a derivative term for damping. Systems such as this produce accurate results and are currently used in many instruments.

The mechanical spring discussed above can be replaced by other means, such as an electrical torquer, to provide stiffness to the system. The current, I, in the torquer is then proportional to the normal force on the vane. A derivative term, dI/dt, provides the damping of the system. The speed of response of this type system is greater than that of a system utilizing an electric motor.

All of the above methods for measuring force must be able to sense the change in force due to a 0.1-degree change in angle of attack, a change especially small at low speeds. The ratio of accuracy required to the range of force to be measured is of the same order of magnitude as that for the pressure sensors, approximately 1 part in 50,000. The systems shown in Fig. 38, A and B use strain gages to measure the deflection of a member, but present experience with strain gages indicates that they would be unsuitable for this use. System C uses an "E" type pickoff, which, it is believed, affords better sensitivity than strain gages.

The system shown in Fig. 39 could be designed to produce the desired results. However, the systems shown in both Fig. 38 and 39 require a friction-free bearing for maximum sensitivity. This brings up the problem of sealing the bearing against external environment while still maintaining the pivot as frictionless as possible. In this respect the restrained vanes have the same problem as movable vanes.

Acceleration Sensors

The only system which requires knowledge of acceleration is mechanization of the lift equation. In the computer previously presented, it is assumed that a passive-type inductive pickoff accelerometer is used. By adding the fixed and variable components of weight in the accelerometer, the computer is simplified. It is believed that the simple and reliable passive-type accelerometers are sufficiently accurate for the lift mechanization application.

The accuracy of resistive pickoff accelerometers is limited by the resolution problem . Strain-gage types are used in flight test only because calibration and output voltage amplification can be tolerated there. The inductive pickoff accelerometer is linear, not limited by resolution, and provides a large output voltage. It is therefore considered to be a superior passive-element-type accelerometer.

Closed-loop or force-balance accelerometers are worthy of consideration because of their inherent accuracy potentialities and the form of the output intelligence. One of these types, manufactured by the Donner Scientific Company, uses a D'Arsonval current-sensitive meter movement with an unbalanced mass arm attached. Balance between two opposing torques is produced, one torque being proportional to the acceleration of the unbalanced mass and the opposing torque proportional to the current in the meter movement coil. The coil and mass assembly is prevented from deflecting under acceleration by sending through the meter coil a current of such magnitude and in such a direction that an opposing torque is produced of precisely the same magnitude as the torque due to acceleration.

If the applied acceleration is varied, the current through the meter coil is likewise varied to maintain the torque balance condition. With the provision that the torque due to current is proportional to current in the position of zero deflection of the mass, the equivalence of opposing torques ensures that acceleration normal to the pointer and to the pivot axis is measured by the current in the coil necessary to maintain zero deflection. Because the torque balance is established by a d-c current flowing in the coil of the meter movement, the situation is ideal for introduction into the control coil of a magnetic amplifier device. A d-c voltage can be obtained as the voltage drop across a precision wire-wound resistor in the coil circuit.

Another closed-loop instrument, developed by North American Aviation, Inc., employs a principle similar to that of the Donner instrument described above. This instrument is of the precision type and

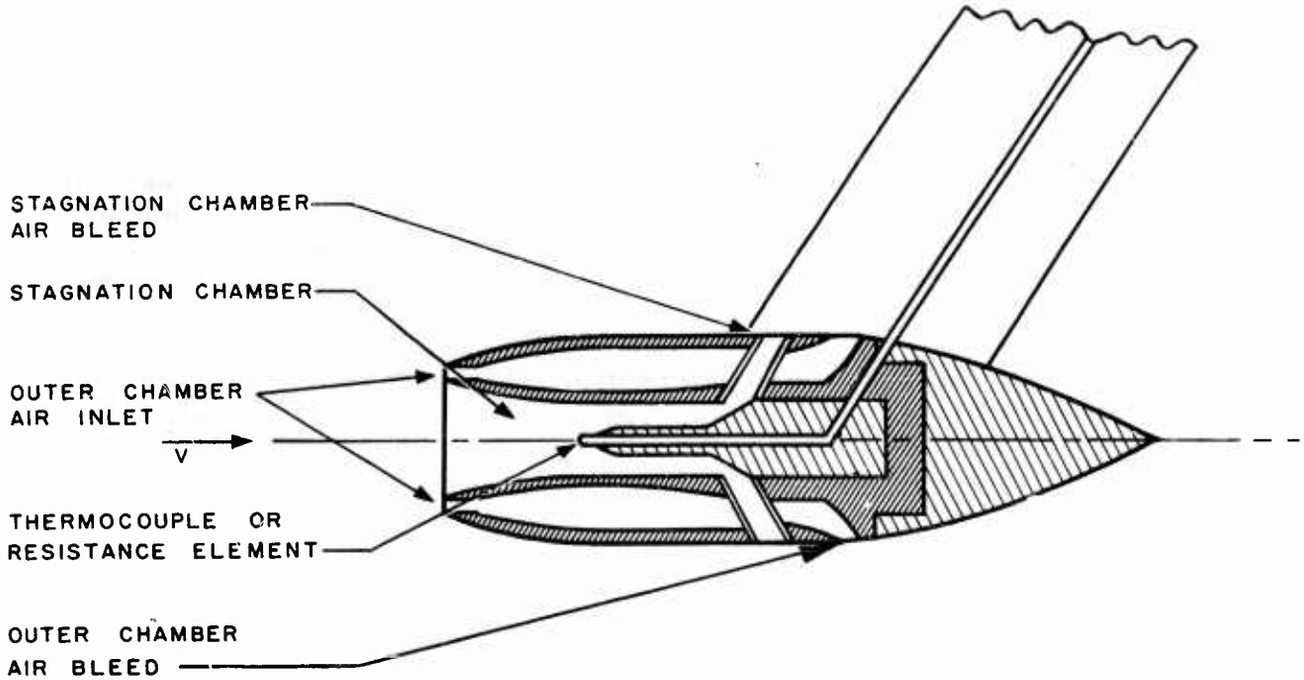

Fig. 40. Stagnation temperature probe

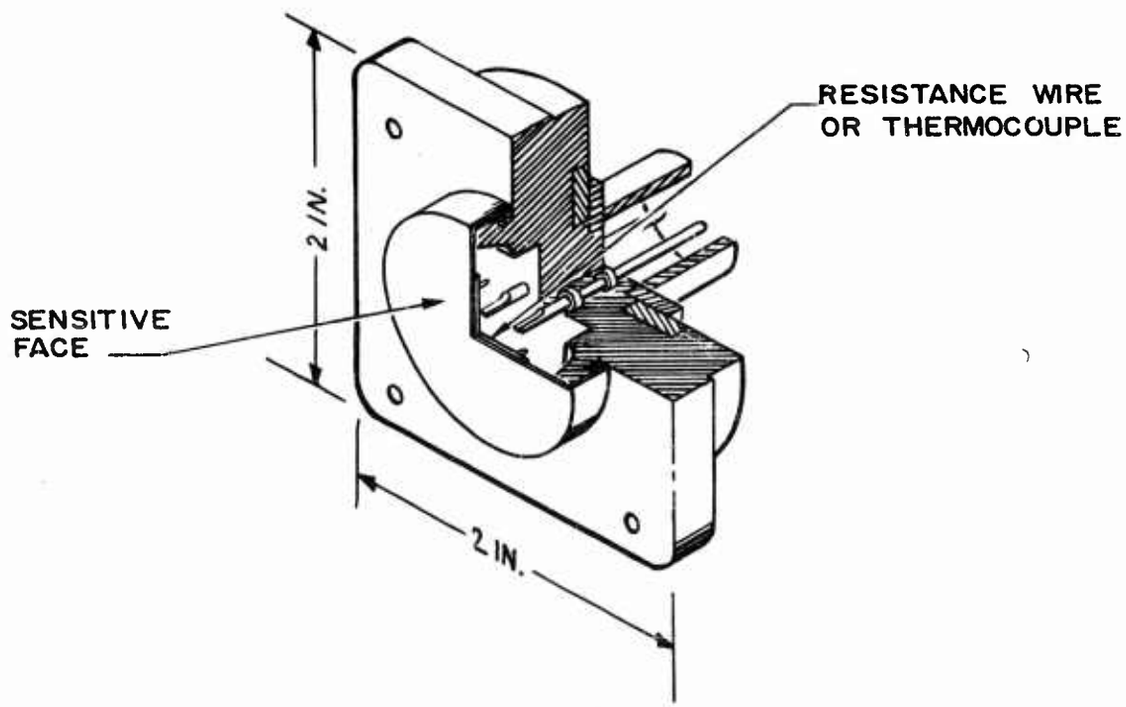

MOUNTED SO SENSITIVE FACE OF PROBE IS FLUSH WITH AIRPLANE SKIN. PREFERRED LOCATION ON BOTTOM ℄ BETWEEN WING ROOTS

Fig. 41. Flush-mounted temperature probe

provides excellent performance. Its normal application is the measurement of distance traveled through double integration of acceleration components. The seismic element consists of a spring-restrained, rotatable motor frame which supports an unbalanced mass. The unknown torque, developed by acceleration perpendicular to the mass arm and to the motor axis, is opposed by the reaction torque of the armature driven by the followup amplifier. The current in the armature is then a measure of this acceleration. A variable reluctance pickoff amplitude modulates a 400-cps carrier, in contrast to a capacitance pickoff, which produces frequency modulation of an r-f oscillator in the Donner device.

Temperature-probing Sensor

Air temperature is needed for the calculation of angle of attack with the hot-wire anemometer and for use with a flight data computer if true airspeed or air density is required. Some of the possible ways of measuring air temperature are by stagnation probe, flush-mounted probe, vortex thermometer, or infrared methods.

The stagnation and flush-mounted probes convert a portion of the velocity energy of the air into a temperature rise. The probe temperature is related to the total temperature by

$$T_{probe} = T_t \left(\frac{1 + K_r 0.2 M^2}{1 + 0.2 M^2} \right) \tag{96}$$

where K_r is the temperature recovery factor.

The temperature measured by a stagnation probe is close to the total temperature: that is, the value of K_r is close to unity. For a given probe K_r varies slightly with Mach number and altitude. The general construction is a two- or three-walled cylinder open at the forward end. Figure 40 shows a two-walled probe. The air is allowed to flow slowly through the inner and outer cylinders, its rate of flow controlled by holes in the rear. A resistance or thermocouple element is located in the inner cylinder to convert air temperature into an electrical signal. The purpose of flow through the outer cylinder is to maintain it near the total temperature, so as to reduce radiation from the inside thermocouple or resistance element to the outside and to reduce radiation from the sun to the inside elements.

This probe is subject to icing, which can be prevented by locating heating wires in the outside surface. Care must be taken in this design that no error is introduced into the temperature readings. This type of

probe is usually located on a nose boom or some such location to get as unobstructed a sample of the free stream as possible. It is simple in construction and when designed skillfully gives good accuracy and time response.

The flush-type probe consists of a small, flat plate with some resistance wire cemented to the back of it. The plate is mounted flush with the fuselage skin and insulated from it. Figure 41 shows a typical design. The same equation applies to this type probe as to the stagnation type. However, the value of K_r is not so near unity and varies considerably with Mach number, altitude, and location on the fuselage. For this reason in-flight calibration is required. The probe shown has a large time response because of the comparatively large mass of metal used for sensing temperature. This could be minimized by reducing the size and thickness of the metal. It is also subjected to radiation from the outside and can radiate heat itself. As it can be located in the skin of the fuselage, it is not subjected to icing.

The vortex thermometer measures the static air temperature. It does this by cooling the air sufficiently to bring it down to the static temperature. It works on the principle that the air at the center of a vortex is at a reduced pressure and hence at lower temperature than the air at the outside of the vortex. Because the vortex is fed by air directly from the air stream, its velocity is a function of the free stream velocity; hence the cooling is a function of the free stream velocity. By proper design this cooling effect counteracts the heating effect of slowing down the free stream air, thus allowing a thermometer to read static temperature. Reference 75 describes an axial flow vortex thermometer with an accuracy of ±0.2 degree F up to 435 knots. It is uncertain how well this principle will work at higher speeds, where compressibility effects predominate.

The infrared method of measuring free air temperature, as the name implies, measures the infrared radiation from the air in a cone of space ahead of the aircraft. It is theorized that the radiation from air far ahead of the aircraft (several miles) is attenuated greatly and will not contribute much to a reading. Also, the radiation from the air that is affected by the aircraft will add little because of the small amount of air contributing to the total radiation received. Therefore most of the radiation will come from air 1/4 to 1 mile ahead of the aircraft. This radiation should provide an indication of the free air temperature. This device was described in Ref. 8 when it had been developed only to the laboratory stage and had not been flight-tested to prove the theory fully.

Both the vortex thermometer and the infrared thermometer require a computer to provide total temperature, which is needed by the hot-wire anemometer. However, a flight data computer needs free air temperature to compute the speed of sound, which, in turn, is required to obtain true airspeed.

At present the stagnation probe appears to be developed to the extent that it can be built very rugged, is simple in construction, and should give accurate results.

COMPUTERS

A computer for the true angle of attack system must perform the operations of addition, subtraction, multiplication, division, and function generation. It should have a computing speed fast enough to compute angle of attack during maneuvers of the aircraft and an overall accuracy of 0.1 degree, which is about 0.25 percent of the full-scale output. An electromechanical analog computer is well suited for this application, as it provides the required speed and accuracy and, at the same time, is small and economical.

In the majority of systems considered, the local angle of attack is computed as a quotient in which the denominator is proportional to dynamic pressure and the numerator may be proportional to the differential pressure between two orifices, to the product of aircraft weight and acceleration, or to the normal force on a vane. This is the most critical calculation to mechanize, as dynamic pressure has a variation of 150 to 1 over the desired flight range and must be indicated to an accuracy of 0.002 percent of full scale. The accuracy of the quotient (local angle of attack) is reasonable: at most, 0.25 percent.

The following computing methods have been studied for possible application.

Mechanical Computers

The techniques of mechanical computation are particularly useful in a computer with pressure inputs because computations can often be accurately and easily performed in the input transducer. An example is the subtraction of pressures in a bellows pressure transducer, where one pressure is applied to the inside of the bellows and the other to the outside. The resulting displacement of the bellows is proportional to the difference of the pressures.

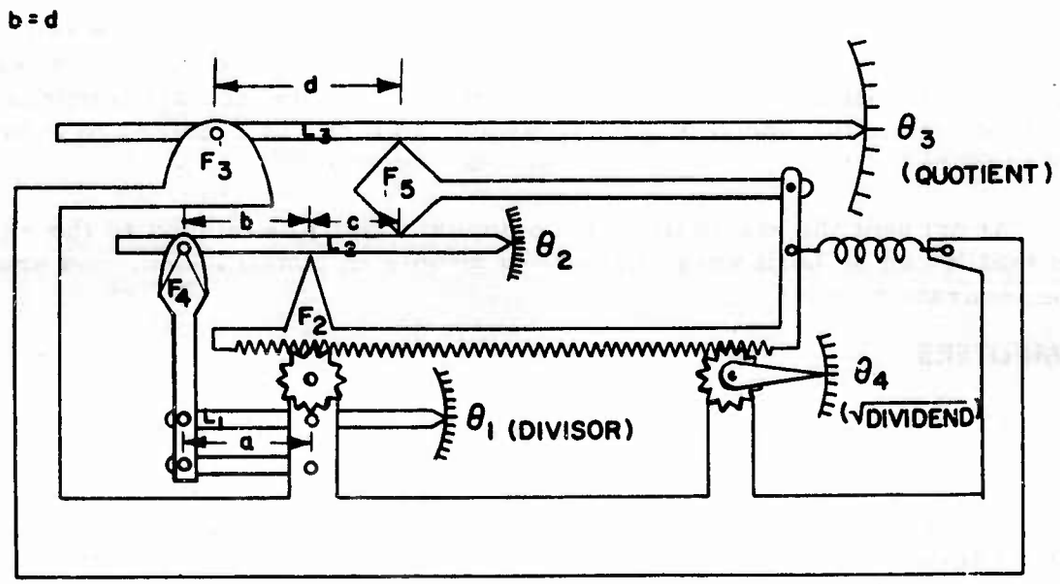

Fig. 42. Compound lever quotient computer

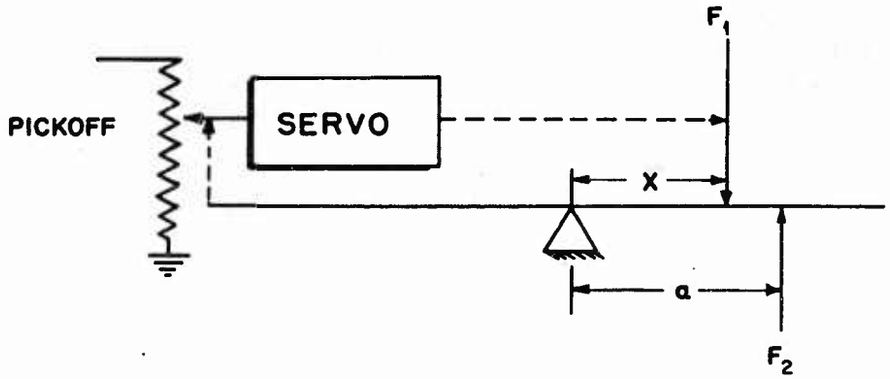

Fig. 43. Force-balance divider

This method is obviously superior to one in which two pressure transducers are used to produce electrical signals which are then subtracted electrically. A divider can be constructed using a simple variable lever when the range of the denominator is less than 10 to 1. If the range is greater than this, a compound lever can be used. Figure 42 is a schematic of a compound lever quotient computer described in Ref. 31. The compound computing levers are L_1, L_2, and L_3, with their respective fulcrums located at F_1, F_2, and F_3. F_4 and F_5 are knife edges whose function is to transmit motion from one lever to another. Fulcrum F_2 is not fixed, but is subject to translation (integrally with lever L_2) by means of the gear-rack system. The lever lengths a and c are fixed in value. Lengths b and d are always equal and of a magnitude fixed by the position of the fulcrum F_2. The output is

$$\theta_3 = ac\,\frac{\theta_1}{b^2} = K\,\frac{\theta_1}{\theta_4^2} \tag{97}$$

where

$$K = \frac{ac}{K_1} \text{ and } b = \sqrt{K_1}\,\theta_4$$

If θ_4^2 is made proportional to the divisor this mechanism will function as a divider. Reference 31 describes such a divider in which inputs θ_1, the dividend, and θ_4, the divisor, are from spring-strained bellows. A nonlinear spring is used to make θ_4^2 proportional to the divisor. This unit shows promise of working over a 50 to 1 pressure range.

Levers can be used in force-balance systems. Figure 43 is a schematic of such a divider. The inputs to this divider are F_1 and F_2. Lever arm a is fixed while lever arm X is variable. The lever is maintained at zero deflection by means of a pickoff and servomotor, which varies X to keep the forces balanced. It is readily seen that $X = aF_2/F_1$. One disadvantage of this divider is that the line of application of F_1 must be variable. This is difficult to accomplish in practice.

A force balance divider used in the dual sensor system is presented in Fig. 44. The inputs to this divider are the two forces F_1 and F_2, which are applied to two computing levers. A servo moves a pair of rollers to balance the forces from the levers. For balanced forces,

$$\frac{F_1 l_1}{a + X} = \frac{F_2 l_2}{X}$$

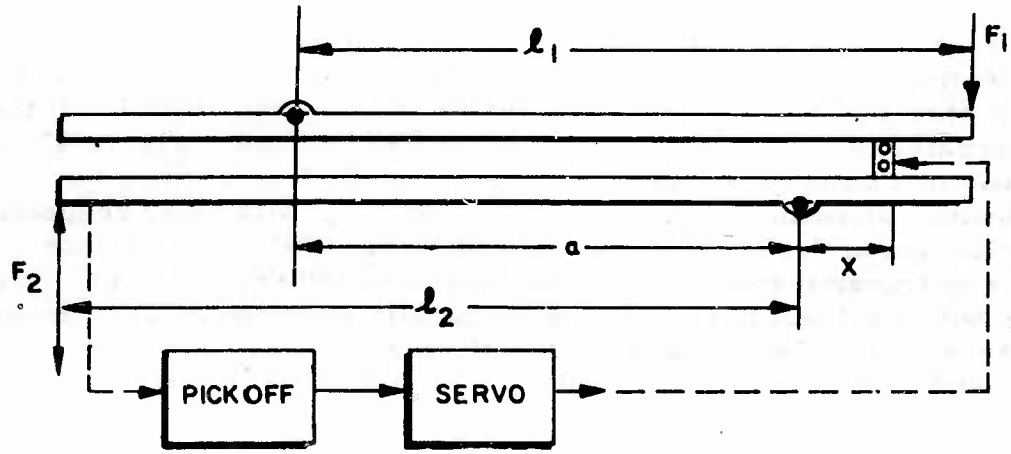

Fig. 44. Dual sensor system using force-balance divider

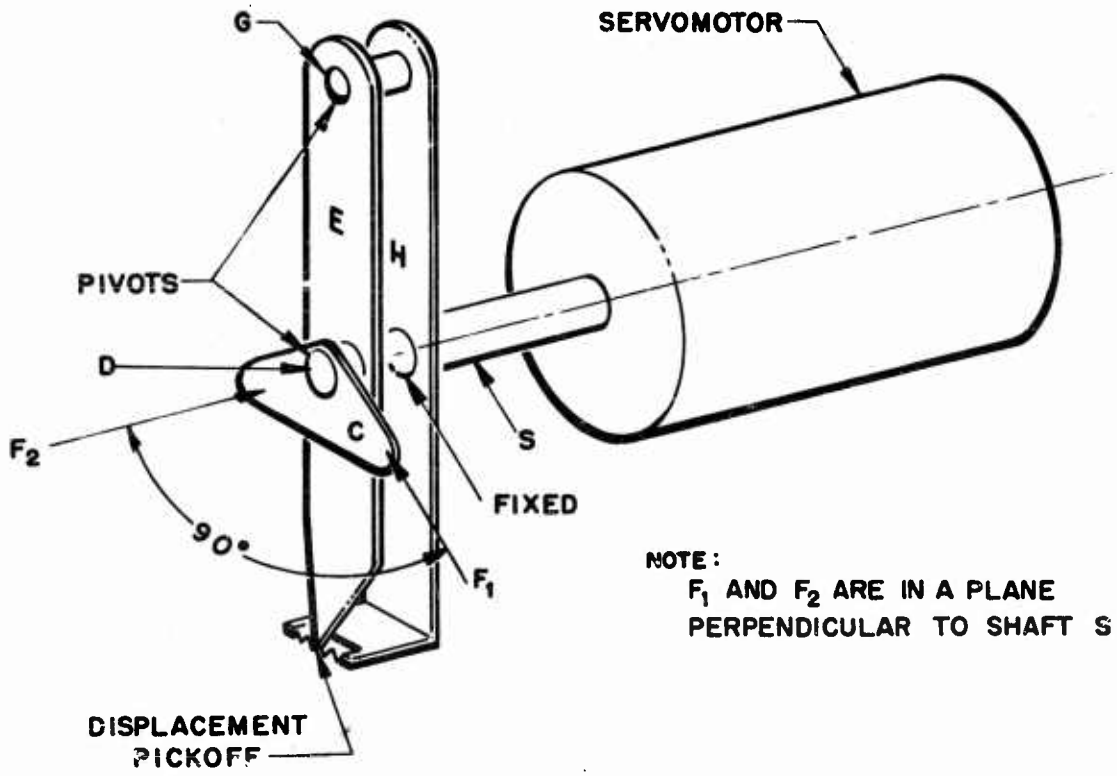

Fig. 45. Vector-resolution divider

Solving for X,

$$X = \frac{F_2 l_2 a}{F_1 l_1 - F_2 l_2} \tag{98}$$

By letting $l_1 = l_2$, Eq. 98 becomes

$$X = \frac{F_2 a}{F_1 - F_2} \tag{99}$$

If F_1 is produced by the differential pressure ΔP_{1-2} and F_2 by ΔP_{5-6}, then X in this equation becomes $\frac{\Delta P_{5-6} a}{\Delta P_{1-2} - \Delta P_{5-6}}$, similar in form to the fraction of Eq. 14.

Another mechanical divider calculates the resultant angle of a vector addition. If two forces acting at right angles to each other are added vectorially, the angle of the resultant force is given by

$$\tan \theta = \frac{F_1}{F_2} \tag{100}$$

A method for mechanizing this equation is presented in Ref. 2, and a schematic of this is shown in Fig. 45. In this mechanism forces F_1 and F_2 are applied at right angles to each other. The vector sum of these forces, transmitted through pivot D to linkage bar E, causes it to rotate around pivot G. The resulting displacement of the pickoff drives the servomotor rotating shaft S and linkage bar H to return the pickoff to zero. In this manner a shaft rotation is established proportional to arc tan F_1/F_2, and the linkage configuration constrains the forces F_1 and F_2 to zero displacement. The arc tangent can be converted into a tangent by means of a nonlinear linkage, nonlinear potentiometer or a loaded potentiometer.

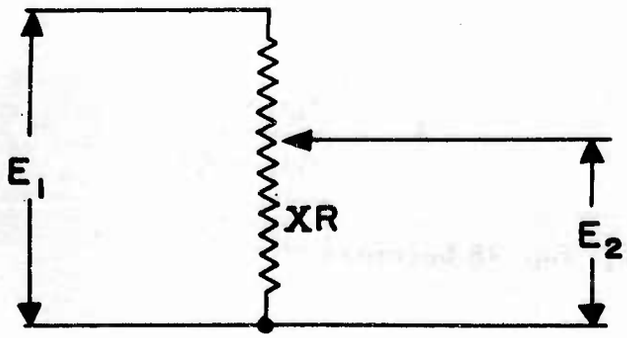

Fig. 46. Function generator as divider

Potentiometer Computers

Potentiometers can be used for many computing operations. If the potentiometer in the circuit of Fig. 46 is linear, $E_2 = XE_1$. If the potentiometer resistance is a nonlinear function of wiper position, with $R_X = f(X)$, this circuit acts as a function generator and $E_2 = f(X)E_1$. By making $f(X) = 1/X$ the circuit functions as a divider.

In general, the wiper of the potentiometer will be positioned by a servo system. Frequently one servo can position several potentiometers, with a resulting saving in space. The accuracy of this method of computation depends upon the accuracies of the potentiometer and servo system. Linear potentiometers with accuracies of 0.1 percent of full scale can be obtained at a nominal cost. If required, potentiometers with linearity of 0.005 percent of full scale are available. The input impedance of the circuit driven by the potentiometer loads it. If the ratio of input impedance to potentiometer impedance is low, significant errors are introduced.

To maintain loading errors less than 0.005 percent, the input impedance of the circuit should be at least 300 times the impedance of the potentiometer. There are compensation methods available. However, as the effect of loading errors is cumulative and applies to the servo loop also, it is difficult to obtain multipliers with overall accuracies better than 0.02 to 0.03 percent of full scale.

The accuracy of a nonlinear potentiometer depends upon the function to be matched. In general, it varies from 0.1 to 1 percent of full scale.

When a reciprocal potentiometer is used as a divider, the percentage accuracy of the quotient is equal to the accuracy of the potentiometer setting referred to that setting, rather than to full scale. If a reciprocal potentiometer having a full-scale accuracy of 1/10 percent is used for division, the accuracy of the quotient when the divisor has a value of 1/150 of its maximum value is $1/10/150$, or 15 percent of the full-scale quotient.

A multiplier may be used for division if it is connected as part of a feedback loop shown in Fig. 47. When a servo multiplier is used there are two possible configurations, which are shown in Fig. 48 and 49. If the servo is not included in the feedback loop, the circuit of Fig. 48 applies. This is essentially an operational amplifier with variable feedback and is discussed later. When the servo is included in the feedback loop, Fig. 49 applies. Here potentiometer P_2 functions as an automatic gain control to keep the gain of the servo loop constant for all values of y. Without this, the servo gain would vary by the same factor as the denominator. Because the potentiometer setting determines the quotient directly when the x and y inputs are accurate, the accuracy of the circuit is determined by the accuracy of potentiometer P_1. A 0.1-percent potentiometer gives a quotient accurate to 0.1 percent of full scale.

A servo-balanced bridge circuit can be used for both multiplication and division. The circuit and equation are presented in Fig. 50. If two 0.01-percent potentiometers are used for division, with a divisor range of 150 to 1, the accuracy of the quotient is $1.5\sqrt{2}$, or about 2 percent of full scale. The accuracy can be improved by range-switching of R_4 and the sensors.

Another type of computer uses logarithmic potentiometers. The standard method of subtracting logarithms is not directly applicable, as it does not allow the numerator to change sign. Figure 51 is a schematic diagram of a logarithmic divider in which the numerator may change sign. P_1, P_2, and P_3 are nonlinear potentiometers. P_2 is wound so that

$$R = R_T 10^{K_1 \theta} \tag{101}$$

where

- R is resistance from wiper to ground
- R_T is total resistance of potentiometer
- θ is angular position of the wiper
- K_1 is a constant

P_1 and P_3 are wound so that

$$R = R_T 10^{-K_1 \cdot \theta} \tag{102}$$

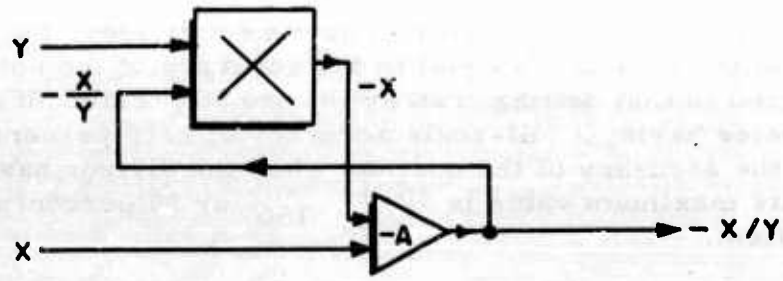

Fig. 47. Multiplier used as divider

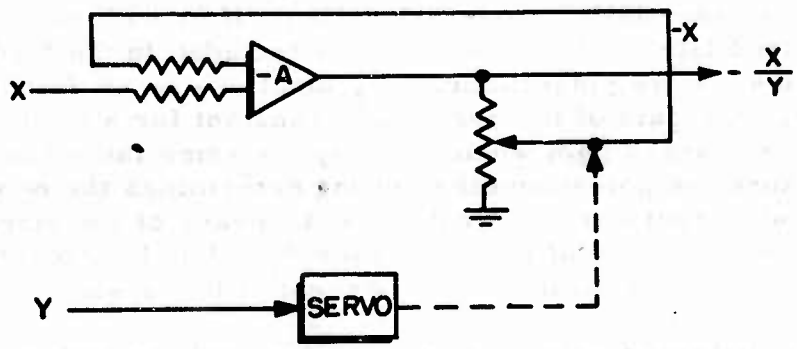

Fig. 48. Servo multiplier with servo not in feedback

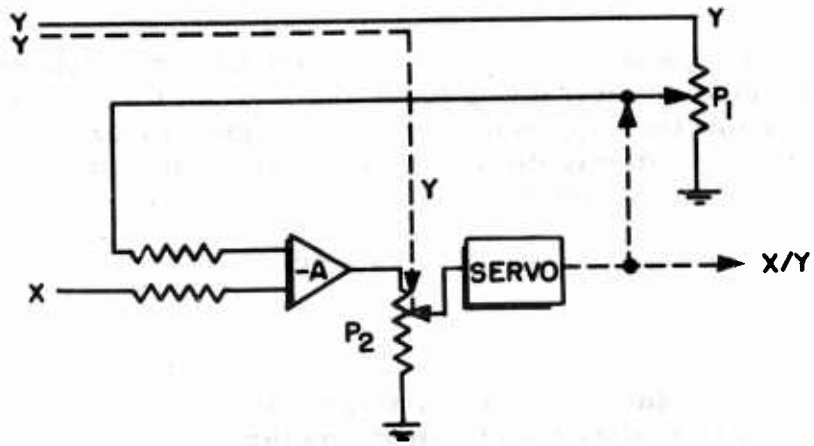

Fig. 49. Servo multiplier with servo in feedback

$$R_3 = \frac{R_1 R_4}{R_2}$$

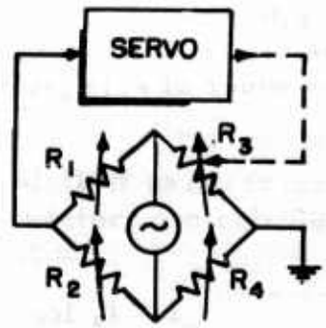

Fig. 50. Servo-balanced bridge circuit

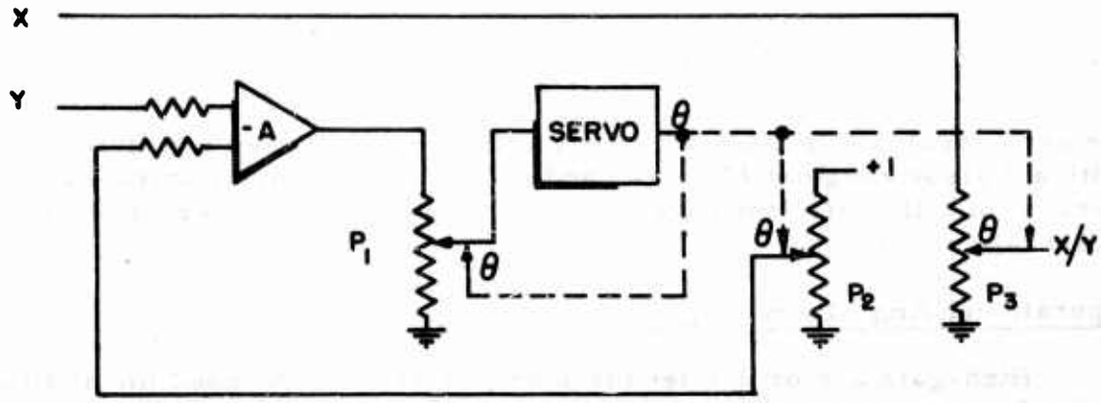

Fig. 51. Logarithmic divider

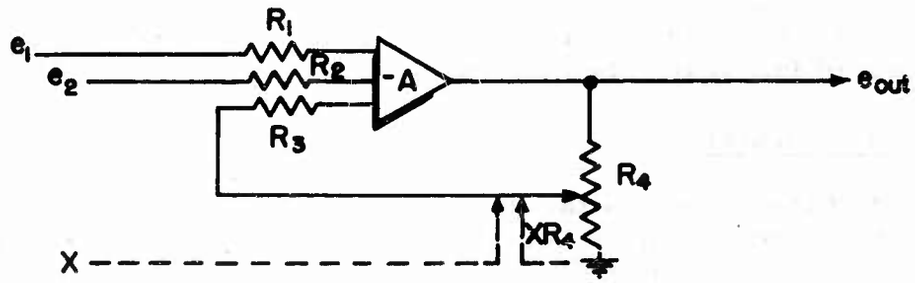

$$e_{out} = -\frac{R_3}{X}\left(\frac{e_1}{R_1} + \frac{e_2}{R_2}\right) \text{ if } \begin{array}{l} A \gg 1 \\ R_3 \gg R_4 \end{array}$$

Fig. 52. Variable feedback high-gain amplifier

P_1 functions as a gain control to keep the servo gain constant. Feedback from P_2 maintains the shaft rotation of the servo proportional to log Y. The voltage on the wiper of P_3 is given by

$$e_0 = (X)\ 10^{-K_1\theta} \tag{103}$$

Since

$$\theta = K_2 \log Y$$

therefore

$$e_0 = K\frac{X}{Y} \tag{104}$$

An error analysis indicates that when the circuit is used for division with a divisor range of 150 to 1, and when P_2 and P_3 are accurate to 0.1 percent of full scale, the quotient is accurate only to 20 percent of the full-scale reading.

Operational Amplifiers

High-gain a-c or d-c feedback amplifiers may be used for addition, multiplication, and division by varying the impedance of the feedback loop. The circuit and equation are given in Fig. 52.

An error study has been made of this circuit functioning as a divider with R_1, R_2, and R_3 fixed and $e_2 = 0$. If e_1 and X are accurate and R_4 has 0.01-percent full-scale linearity, the accuracy of the quotient will be 1.5 percent of full scale when the range of the divisor is 150 to 1.

Correction Computer

Most of the angle of attack indicators studied measure the local angle of attack and therefore require a correction computer to compute the free-stream angle of attack. Studies by Cornell Aeronautical Laboratory (Ref. 91) show that the free-stream angle of attack for sensors located on a nose boom is given by

$$\alpha = \alpha_L - f_4(\alpha_L) - Mf_5(\alpha_L) - M^2 f_6(\alpha_L) + \frac{\dot{\alpha}K}{V} \tag{105}$$

where f_4, f_5, and f_6 are arbitrary functions and K is a constant.

With the sensor mounted ahead of the nose of the aircraft, f_4 , f_5, and f_6 become zero at supersonic speeds and .

$$\alpha = \alpha_L + \frac{\dot{\alpha} K}{V} \tag{106}$$

To correct the local angle of attack it is necessary to have Mach number available in the computer; therefore the calculation of Mach number is included in this mechanization.

For the condition $0 < M < 1$,

$$\frac{P_T}{P_S} = \left(1 + \frac{\gamma - 1}{2} M^2\right)^{\frac{\gamma}{\gamma - 1}} \tag{107}$$

If $\gamma = 1.40$ this may be rearranged to give

$$\frac{q_i}{P_S} = (1 + 0.2M^2)^{3.5} - 1 = f_7(M) \tag{108}$$

where

γ is the ratio of specific heats of gas

f_7 is a specific function of Mach number

For the condition $M > 1$,

$$\frac{P_T}{P_S} = \frac{(\gamma + 1)^{\frac{\gamma+1}{\gamma-1}} M^{\frac{2}{\gamma-1}}}{(8\gamma M^2 - 4\gamma + 2)^{\frac{\gamma}{\gamma-1}}} \tag{109}$$

This may be written in the form

$$\frac{q_i}{P_S} = f_8(M) \tag{110}$$

At $M = 1$, $f_7(M)$ and $f_8(M)$ form a continuous function. Therefore

$$\frac{q_i}{P_S} = f_9(M), \quad M > 0 \tag{111}$$

where

$$f_9(M) = f_7(M), \; 0 < M \leq 1$$

$$f_9(M) = f_8(M), \; M > 1$$

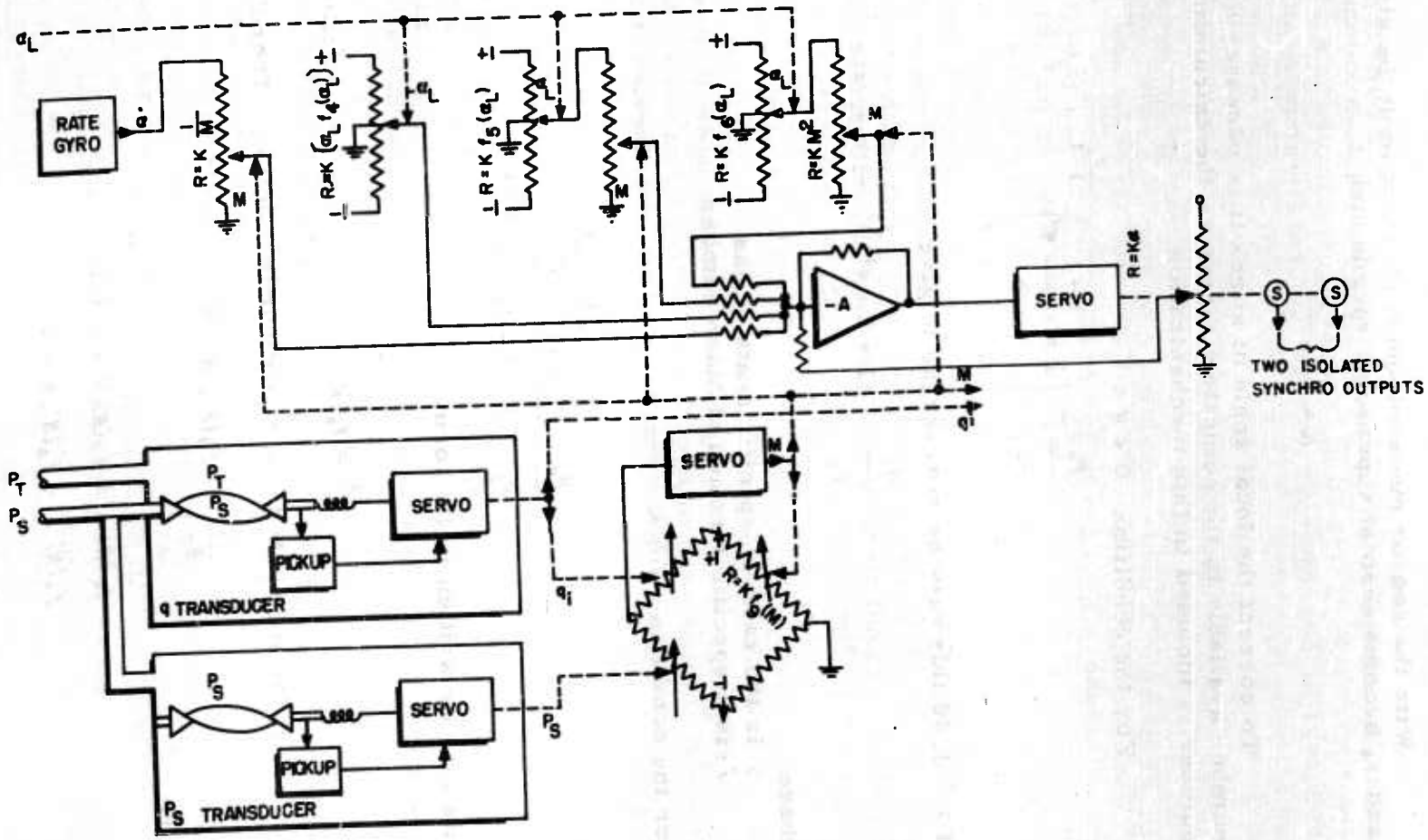

Fig. 53. Mechanization of correction computer

The mechanization of the correction computer is presented in Fig. 53. This computer is designed for a sensor location on a nose boom. Correction computers for other sensor locations are considerably more complex, as they must provide compensation for local flow disturbances in supersonic flight. This is not required with a nose boom installation. In this mechanization the following assumptions have been made:

1. The term $\frac{\dot{a}K}{V}$ may be expressed as $\frac{\dot{a}K}{KM}$.

2. The static pressure line is compensated so that the correct value of P_S is measured. (Static pressure compensation is discussed in the next section.)

The inputs to the correction computer are local angle of attack, pitching rate, and static and total pressure. Twisted bourdon tube pressure sensors are shown, in which a servomotor drives a spring to maintain the tip of the bourdon tube in the null position.

Mach number is computed in a bridge circuit in which one resistor is fixed, another is a linear rheostat set by static pressure, a third is a linear rheostat set by dynamic pressure, and the fourth is a nonlinear rheostat with $R = Kf_9(M)$. A servomotor drives this rheostat to balance the bridge, and thus the shaft position of the servo is proportional to Mach number. The Mach number servo also drives potentiometers used in the calculation of both local and true angle of attack.

The local angle of attack input is from a servo and positions three function potentiometers. One of these furnishes voltage to a square-law potentiometer positioned by Mach number and another provides voltage to a linear potentiometer positioned by Mach number. The true angle of attack is computed by summing the outputs of the Mach potentiometers, the output of the local angle of attack potentiometer, and the output of a reciprocal potentiometer positioned by Mach number and excited by the output of a pitching rate gyro.

Without the potentiometer, $R = K\alpha$, the output of the amplifier, is an amplitude-modulated 400-cps signal proportional to α. Adding the voltage from the potentiometer makes this output zero when the output shaft is positioned at some angle proportional to α. Thus the two synchros can be used to indicate α remotely.

EXTENSION TO FLIGHT DATA COMPUTERS

GENERAL

The growing trend toward integration of requirements for flight data and toward obtaining these data from a single computer package is closely allied with computation of attack angle, particularly when the accuracy goal is 0.1 degree. To obtain this accuracy, it becomes necessary to include small-order effects that are negligible in many less accurate applications, and since these effects are functions of aerodynamic quantities, it is apparent that flight data are essential. All the systems for determination of attack angle require flight data, if not for computation of the basic terms, at least for introduction of correction terms. True, the accuracy required of the flight data is less in the second case, but in integrated systems the accuracy must be suitable for the most demanding requirements, which may not always be those of the attack angle problem.

Because movable external flow sensors are not permitted in this study problem, measurement of the direction of local air flow at any selected position on the airframe by this technique is eliminated. If local air flow angle can be measured, the true attack angle may be determined with acceptable accuracy for present-day fire control applications by introducing corrections to the local angle which are functionally related to Mach number.

Some angle of attack systems are basically measuring systems while others are basically computing systems. The systems which have promise of application within the specified boundary conditions have two basic sources of error:

1. Inaccuracies in such basic measuring devices as accelerometers, pressure sensitive elements, temperature probes, and force pickoffs, or in their installation.
2. Basic data mechanized in the computer, which may introduce errors in the form of arbitrary functions of the several aerodynamic quantities.

Errors in group 1 can be reduced to the necessary precision only through the medium of improved sensors. It is important to select the systems which use the best available instruments and which may possibly suffice with less instrument accuracy. Those in group 2 are determined through

flight test in the final analysis, and, again, instrumentation becomes an important factor. The accuracy with which these functions can be determined is much less than the accuracy of the computer which mechanizes the functions because increased computer accuracy is merely refinement of technique. The argument that measuring systems are superior to computing systems, or vice versa, is beside the point in this instance, without due consideration for all of the sources of error, as they both rely basically on the measurement of a number of quantities and upon the mechanization of arbitrary functions of aerodynamic quantities. It becomes apparent that the promising solutions will probably contain errors due to both factors.

STATIC ERROR COMPENSATION

One of the errors which becomes more acute as aircraft approach and exceed the transonic region is the error in static pressure source. This error is due to misalinement, compressibility, and shock wave effects, which can combine to produce a resultant error in static pressure of 10 percent or more in some instances. This error is reflected in each computation that includes static pressure, impact pressure, Mach number, or true airspeed relations; therefore the desirability of eliminating it is obvious. Since the errors are inherent in the source, only partial improvement can be realized by redesign and relocation of the pressure source pickoff. One remaining possibility is to compensate the pressure line for errors in the source. This method permits the designer more freedom in selecting the location of the source to accord with such other factors as drag, structure, radar interference, and local flow effects.

Two methods of introducing the compensation may be considered. The first, using electrical repeaters from correct quantities mechanized in the computer, is usually ruled out because of the loss of flight information in the event of computer failure. Although the simplest, it is not the most reliable solution. The second method consists of introducing into the static pressure line a decrement of pressure to offset the source error. It assumes that the error is repeatable and a continuous, single-valued function of common aerodynamic quantities and, further, that the error function can be determined with acceptable accuracy from flight test processes.

This system has the desirable feature of utilizing standard pressure-actuated flight instruments and can be made fail-safe in such a manner that de-energizing the source of pressure correction only relaxes the system to the conventional uncompensated condition. Some form of static pressure compensation is believed to be mandatory if the 0.1-degree

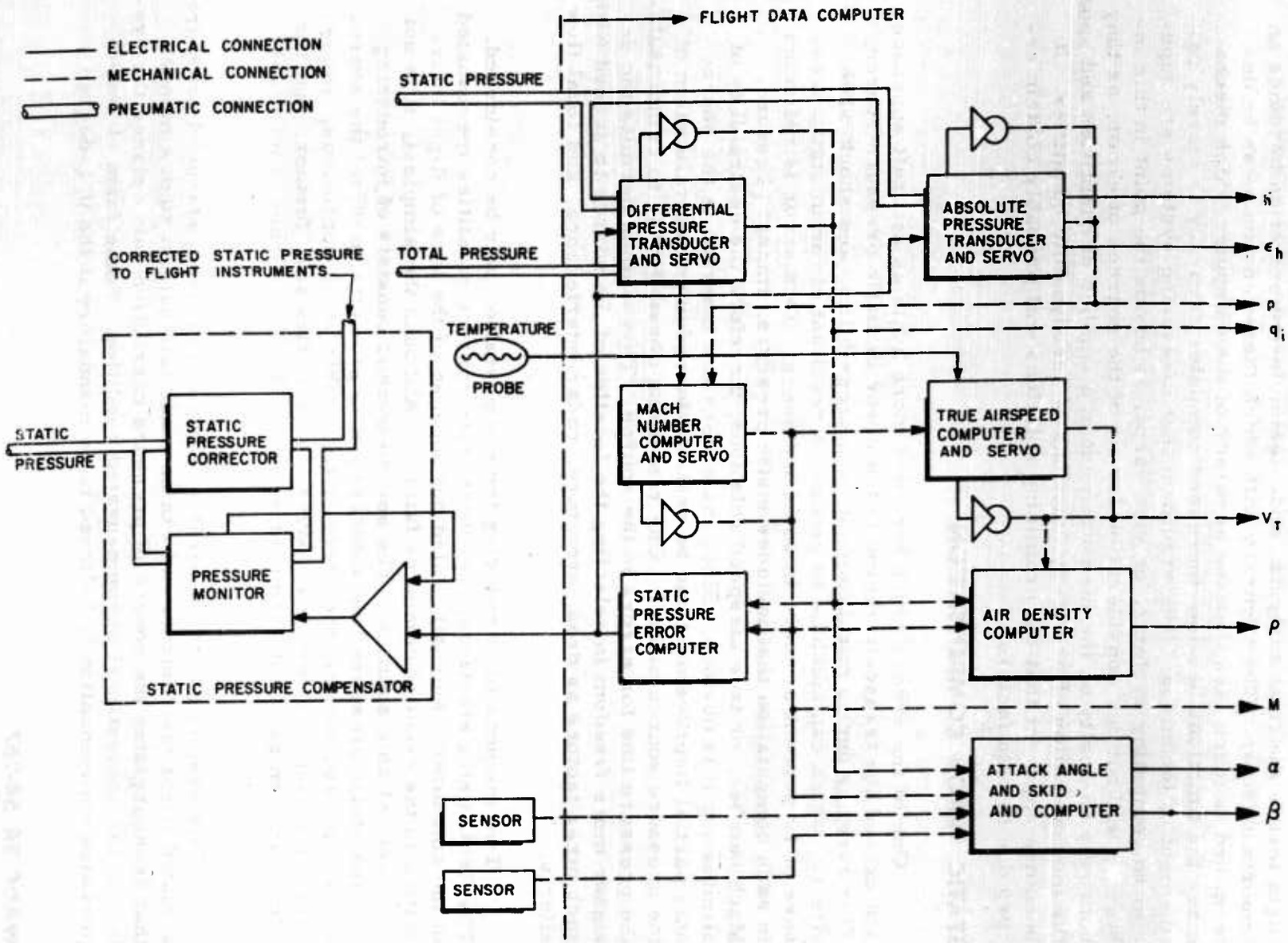

Fig. 54. Integrated flight data computer block diagram

accuracy is to be obtained for the attack angle output. It is not mandatory in all systems to develop an actual pressure, but since the error must be mechanized, it seems desirable that advantage be taken of this fact to correct the pilot's flight instruments.

INTEGRATED FLIGHT DATA COMPUTER

Certain logical assumptions can be made to define a hypothetical system. The assumption that the attack angle information is required for solution of a fire control or bombing problem suggests the need for true airspeed, and possibly air density, information. If no yaw damper is provided in the flight control system, the computation of skid angle is required. Automatic pilot tie-in may specify altitude-hold and rate-of-climb intelligence, in addition to the basic static and differential pressure quantities.

These assumptions round out a basic flight data system which has the defined function of providing true attack angle to an accuracy of 0.1 degree, plus the expanded facility for static pressure error compensation and fire control - flight control tie-in. Figure 54 illustrates the block flow diagram of such an instrumentation system. The more basic quantities — absolute (static) pressure, p ; impact differential pressure, q_i ; Mach number, M ; and true airspeed, V_T — are servoed to obtain accurate shaft rotations proportional to these quantities. The remaining variables — attack angle, α ; skid angle, β; air density, ρ ; altitude rate, h ; and altitude error, ϵ_h — are supplied as voltages.

Variations of the computer shown in Fig. 54 are almost unlimited. The only purpose here is to suggest the logical diversification of the functions performed by the angle of attack computer and their incorporation into an integrated package. The greater utility will benefit overall weapon efficiency, reliability, and performance.

ACCURACY REQUIREMENTS

It is worth while to examine the accuracy requirements of a true angle of attack indicator, as cost and complexity increase rapidly as the error is reduced below 0.25 degree. The information accuracy required is dictated by the performance of the system with which it is used. Probably the most critical requirement is that set by a fire control system; therefore this discussion will be concerned with such a system.

FIRE CONTROL SYSTEM ERRORS

Errors Normally Neglected

In the design of present fire control systems a number of small-order effects are neglected. If system accuracy is such that angle of attack data are required to an accuracy of 0.1 degree, it is probable that some of the following must be considered.

1. A modern fighter aircraft is never completely stable in trimmed flight, especially at high altitudes where aerodynamic damping is low. The dynamic pitching, yawing, and rolling oscillations of the aircraft impart momentum to the rocket while it is in the launcher. This momentum affects its trajectory.
2. Because a finite time is required for the rocket to ignite and travel through the launching tube the angle of attack at the moment the rocket leaves the launcher may be different from that introduced into the fire control computer.
3. An error will be introduced if a portion of the rocket flight path crosses through gusts. This is especially important if the gust is encountered during the rocket burning time.
4. At supersonic speeds an error is introduced as the rocket passes through the aircraft shock wave.

Other Errors

In the attempt to obtain an accurate system it is natural to require the ultimate accuracy from each element of the system. However, if this accuracy can be obtained only through greatly increased complexity and expense, it is wise to re-evaluate the accuracy requirement in terms of the accuracy consistent with other elements in the system. A fire

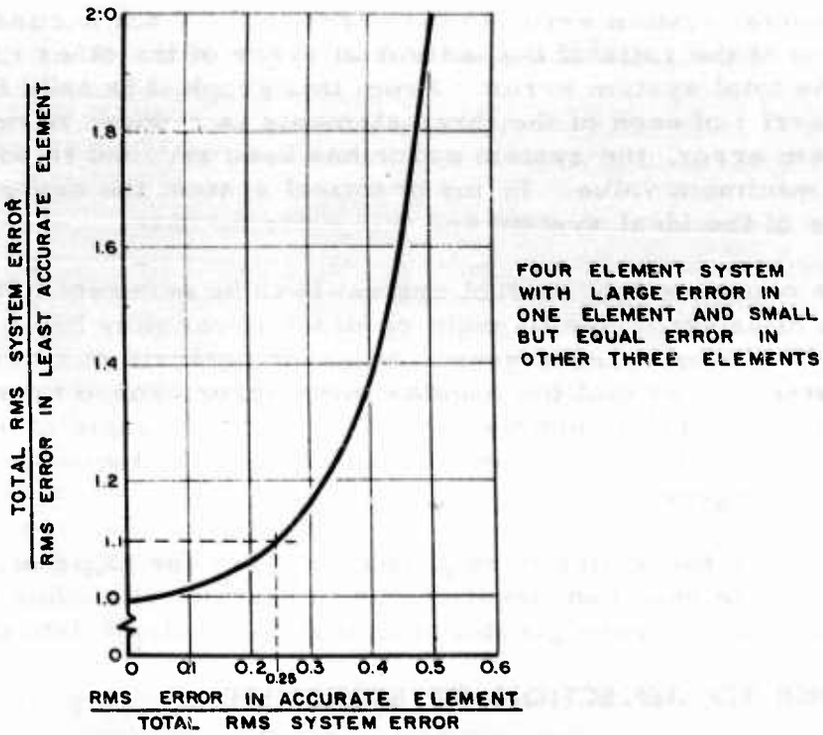

Fig. 55. Variation of total system rms error with rms error in accurate element

control system is assumed to comprise radar, fire control computer, flight data computer, and pilot or autopilot. At the present state of development there are errors in all of the elements of the system, and it is not reasonable to require extreme accuracy from one element while tolerating poor accuracy from another.

The rms error of the complete fire control system is the square root of the sum of the squares of the rms errors of the individual elements of the system. In an ideal system the component errors are small and contribute equally to the total system error. A system composed of four elements, like this one, has a total rms error equal to twice the rms error of an element. In other words, the rms error of each element need be no better than one-half desired system rms error. In practice the errors of the elements are different, and in an extreme case one element may have a large error and the other three have small errors which again contribute equally. Figure 55, a curve for this case, shows

the ratio of total system error to the error in the least accurate element as a function of the ratio of the individual error of the other three elements to the total system error. From this graph it is seen that if the individual error of each of the three elements is reduced to one-fourth of the system error, the system error has been reduced to within 10 percent of its minimum value. In any practical system the errors lie between those of the ideal system and this extreme case.

If the complete fire control system is to be accurate to 0.5 degree, the system miss error due to angle of attack error may be as large as one-fourth of 0.5 or 0.125 degree. An error analysis of a typical fire control system shows that the angular miss error caused by an error in angle of attack is approximately half of the error in angle of attack. Therefore the actual error in angle of attack may be twice this, or as much as 0.25 degree.

This is the theoretically required accuracy for angle of attack. This analysis has been conservative, as in practice the other components in the system have errors greater than that of the flight data computer.

ERRORS DUE TO DEFLECTION OF STRUCTURE

As the airplane goes through various flight maneuvers the air loads and g loading on the structure will vary. This will cause some deflection of the structure between the angle of attack sensor and the fuselage reference line. To what extent this deflection will cause errors in angle of attack must be determined by flight test. It is expected that a short nose boom with mounted sensor can be designed to have negligible deflection.

It is also necessary to know to what extent the nose section of the aircraft deflects with reference to the fuselage reference line. If a deflection of a magnitude to cause objectionable error is found, an additional term or terms must be added to the correction computer.

VARIATION OF ACCURACY WITH DYNAMIC PRESSURE

Most of the angle of attack systems studied require division by dynamic pressure, with their accuracy a function of dynamic pressure. The best accuracy occurs at the upper end of the dynamic pressure range. This fact is consistent with the fire control problem, as combat occurs in the upper portion of the aircraft speed range. Because angle of attack systems naturally have greater errors for low speeds than high, the cost and complexity of a system are reduced if the accuracy tolerance can be relaxed for the low-speed portion of the flight envelope.

FLIGHT TEST ERRORS

One of the problems in the design and evaluation of a high-accuracy angle of attack system is obtaining accurate flight test information. In all the systems studied, flight tests of the aircraft are necessary to obtain the basic data required for the design of the computer; therefore the accuracy of the system depends upon the accuracy of the flight test data. Upon completion of a system, flight test calibration is used to check its accuracy.

Two basic methods are available for flight test calibration. In one the attitude and flight path angles of the aircraft are measured and the angle of attack computed as their difference; in the other a free-floating vane mounted in the undisturbed flow region ahead of the aircraft measures the angle of attack directly. Techniques used to measure the attitude of the aircraft include photographing a ground reference from the aircraft; measuring aircraft attitude directly by a gyro, pendulum, or other inertial instrument; and simultaneously photographing the aircraft from the ground and the ground from the aircraft. The flight range through which the attitude and flight path methods can be used is severely restricted, and these methods are subject to errors of the same order of magnitude as the desired maximum error specified in this contract.

The most accurate method of calibration uses a free-floating vane on a 6- to 8-ft nose boom. Tests by the NACA and NAA (Ref. 57 and 23) indicate that a vane this far forward of the aircraft suffers less than 0.1-degree error from the aircraft. Of course, it is necessary to correct the results for floating angle of the vane, upwash around the boom, and bending of the boom. Floating angle can be determined by wind tunnel tests, upwash can be determined theoretically or by wind tunnel tests, and the boom tip inclination can be measured by photographing the deflection of a light beam reflected from the tip of the boom. NAA has developed this technique to an accuracy of ±0.05 degree. This method allows calibration over the entire flight envelope.

Unfortunately, free-floating vanes on a long nose boom cannot be used with a nose boom sensor because of interference between the two booms. One possible technique is to use free-floating vanes to calibrate a lift mechanization system which can then be used as a reference for calibrating the nose sensor.

Requirement	System																
	Lift mechanization	Yaw-pitch pitot tube	Nose location of pressure ports*	Dual sensors	Dual differential pressure ports yaw-pitch pitot tube	Single vane	Dual vane	Wedge	Wing	Spencer	Null-seeking pitot tube	Null-seeking vane	Atmospheric reflection	Hot wire	Ionization	Sonic	Smoke
Probability of attaining desired accuracy	good	good	good	good	good	good	good	good	good	good	good	good	fair	poor	poor	poor	poor
Meets requirement of no moving parts exposed to air stream	yes	yes	yes	yes	yes	yes	yes	yes	yes	yes	no	no	yes	yes	yes	yes	yes
Will measure yaw by re-orientation of sensor	yes	yes	yes	yes	yes	yes	yes	yes	no	no	yes	yes	yes	yes	yes	yes	yes
Sensor resistance to damage	excellent	good	good	good	good	good	good	poor	fair	fair	poor	poor	good	poor	good	good	good
Relative computer size and complexity *	9	16	16 (or less)	9	9	16	9	16	16	12	9	9	very large	16	--	--	large
Aerodynamic drag **	none	low	none	high	low	low	high	low	none	none	medium	low	low	low	low	low	low
Maintenance required*	slight	slight	slight	slight	slight	slight	slight	slight	slight	slight	slight	slight	slight	moderate	moderate	slight	considerable
Without external sensor (except pitot-static tube)	yes	no	yes	no	no	no	no	no	yes	yes	no	no	no	no	no	no	no
External sensor includes pitot-static tube	no	yes	no	yes	yes	no	no	no	no	no	yes	no	no	no	no	no	no
Will measure angles of yaw and attack with only slight addition	yes	yes	yes	yes	yes	no	no	no	no	no	yes	no	no	no	no	no	no

* The number in this row is the total number of amplifiers and servos required in the mechanization of the system.

** Terms used in referring to sensor drag are relative, as the drag of any sensor is very small compared to the drag of the airplane.

Table 2. Comparison of systems investigated

SUMMARY AND CONCLUSIONS

The important characteristics of the systems studied have been tabulated and are presented in Table 2. The systems are presented in approximate order of their suitability, with their characteristics presented in order of importance. A number of characteristics common to all systems have not been included in the table but are discussed below.

1. Ease of installation by the contractor. The installation problems are similar for all systems. The sensors must be located accurately, but bias adjustments in the computer compensate for small misalinements. One flight test for each installation determines the proper bias setting.
2. Ease of operation. All systems have an ON-OFF switch and operate with no other attention from the pilot.
3. Suitability for all types of aircraft. All of the systems studied require a change in the computer for each aircraft model. The items to be changed can be incorporated into plug-in units so that these changes can be easily made.
4. Total and static pressure measurement. All of the systems require total and static pressure information for use in the computer. In some cases this information can be obtained from extra orifices in the sensor; in others the information may be obtained from the standard instrument source of these pressures.

An examination of Table 2 indicates that seven systems meet the following contractual requirements:

1. Probability of having an error of less than 0.1 degree of true angle of attack during normal flight conditions.
2. No moving parts external to the aircraft or exposed to environmental conditions.
3. Suitability for measuring angle of yaw through reorientation of the sensing element and necessary mechanization modification.
4. Good resistance to environmental conditions.

The systems which do not meet these requirements have been discarded for the following reasons. The smoke particle method was rejected because it was believed difficult to get a well-defined smoke stream with which to detect angle of attack to 0.1 degree. The sonic method requires extensive electronic equipment and offers no advantages over other

systems. The atmospheric reflection method has the advantage of measuring angle of attack of the airplane with respect to undisturbed air, but the complexity and development required rule out this method. The ionization method improves the smoke particle method by using an unlimited source of praticles, which should be easier to detect. But there is some doubt about how the flow is influenced by the structure between the ionization source and detector and about how accurately the detector locates the stream of ions. There is also the question as to what effect the ion stream has upon the radar.

The null-seeking devices have been discarded because each has an external moving part. The wing system cannot be reorientated to measure yaw and requires complicated correction functions.

After eliminating the systems discussed above, the following remain:

1. Lift mechanization
2. Yaw-pitch pitot tube
3. Yaw-pitch pitot tube with dual differential pressure port
4. Nose pressure ports
5. Dual pressure sensor
6. Force vane sensor
7. Dual vane sensor

Of these systems the dual vane sensor, the force vane sensor, and the dual pressure sensor can be eliminated because any advantages they have over the remaining systems do not compensate for their disadvantages. The only possible advantage of the force systems is the elimination of pressure lines and accompanying lag effects, which are not expected to be serious. An inherent problem in boom-mounted vanes is that the force-measuring device must be mounted in the small confines of the boom and is exposed to wide temperature variations. Also, the force-measuring devices available must allow a slight movement of the sensor, which is not desirable. Finally, computer complexity for the force systems is the same as for the equivalent pressure systems.

There appears to be no advantage of the dual pressure sensor system over the dual pressure port yaw-pitch pitot tube providing that the latter system works according to theory. The dual pressure sensor system has the disadvantage of possible interference effects of one sensor on the other and, in subsonic flow, of the interference of the supporting structure on the sensor. In addition the dual sensors, separated by some distance, present a bulky angle of attack sensor.

There remain for further consideration the following:

1. Lift mechanization
2. Yaw-pitch pitot tube
3. Yaw-pitch pitot tube with dual differential pressure port
4. Nose pressure ports

Present information is not sufficient to say which of these is best. Until the lift mechanization is applied to a particular airframe, it is difficult to say exactly how complicated the computer will be. This system has the advantage of requiring no external sensors except the pitot-static tube, which is already required for the aircraft instrument system. It does require accurate measurement of airplane takeoff weight and an account of airplane weight during flight. While in previous systems of this type it has not been necessary to weigh the plane to the accuracy required here, it is felt that this weighing can be accomplished without great inconvenience.

The point in favor of the yaw-pitch pitot tube is that, as a pitot-static tube is needed anyway, there is no serious inconvenience in specifying the special shape and adding the extra ports to obtain the additional angle of attack information. By adding an extra pair of ports to the yaw-pitch pitot tube, one obtains a dual pressure port yaw-pitch pitot tube. The resulting computer simplification justifies the extra ports on a yaw-pitch pitot tube. By mounting either type of pitot tube on a short boom ahead of the nose, the local flow corrections are minimized.

The shape of the head used on the yaw-pitch pitot tube will be based upon factors which must largely be determined from wind tunnel tests at high Mach numbers and by ease of manufacturing.

The degree to which the local flow corrections are minimized by the boom and the amount of radar interference determine the relative merits of the nose-boom-mounted pitot tubes vs. a nose location of pressure ports. If the boom imposes undesirable radar interference, does not decrease significantly the local flow corrections, and/or imposes a maintenance personnel hazard, the nose location of pressure ports appears more feasible. The nose location implies a suitable and reliable nose shape upon which to locate the ports without contributing any radar interference. It is felt that there is a strong possibility of achieving this.

Both the lift mechanization and the yaw-pitch pitot tube have been developed for subsonic aircraft, but at the present state of development it is impossible to say which of the four systems is best for supersonic

flight. It is therefore recommended that these four systems be investigated further until it becomes clear which has the best characteristics, with the understanding that, except for the lift mechanization, the systems are similar and require similar hardware.

A nose boom location is recommended for the yaw-pitch pitot tubes because it has been shown that greatest accuracy can be obtained from such a sensor location. This location should not seriously interfere with the radar in supersonic aircraft having high-fineness-ratio, conical, or ogival radomes. For aircraft with a hemispherical radome, a boom sensor located beside the radome will probably not cause serious radar interference and is recommended. In addition to providing suitable angle of attack data, these locations will furnish improved static and stagnation pressure information for the aircraft instrument system.

Free-floating vanes on a long nose boom should be used in the flight test program for determining the computer constants and for evaluation and calibration of the lift mechanization system. The calibrated lift mechanization system can then be used as a reference in evaluating the yaw-pitch pitot tube system.

It is recommended that the computers for these systems be developed in a form that will allow their expansion into flight data computers with a minimum of additional components. It is also recommended that the accuracy requirements be re-examined in an attempt to relax them as much as possible, especially in the low-speed portions of the flight envelope. This will reduce the complexity and cost of the system.

NOMENCLATURE

a	acceleration
a_Y	acceleration along aircraft Y axis
a_Z	acceleration along aircraft Z axis
a, b, c	dimensions of computer lever arms
C	constant
C_D	drag coefficient
C_{D_0}	zero lift drag coefficient
C_{D_π}	proper drag coefficient
C_L	lift coefficient
C_{L_α}	lift curve slope, $\frac{dC_L}{d\alpha}$
$C_{L_{\delta_T}}$	lift curve slope of tail surface, $\frac{dC_L}{d\delta_T}$
$C_{L_{\dot\theta}}$	lift curve slope due to pitching velocity
C_m	pitching moment coefficient
C_{m_0}	pitching moment coefficient for zero angle of attack
C_{m_α}	rate of change of pitching moment coefficient with α, $\frac{dC_m}{d\alpha}$
$C_{m_{\delta_T}}$	rate of change of pitching moment coefficient with δ_T, $\frac{dC_m}{d\delta_T}$

$C_{m_{\dot{\theta}}}$	rate of change of pitching moment coefficient with $\dot{\theta}$, $\frac{dC_m}{d\dot{\theta}}$
C_P	specific heat at constant pressure
C_{P_α}	$d\left(\frac{P_1 - P_S}{q_t}\right)/d\alpha$
C_T	aircraft thrust coefficient
C_V	specific heat at constant volume
c	wing chord length
D	aerodynamic drag
D_1, D_2	output of smoke particle detectors
d	wire diameter
E_n $n = 1, 2, 3 \ldots$	computer voltages
e_X, e_Y, e_Z	distances between accelerometer and aircraft cg along X, Y, and Z axes, respectively
F_c	compressibility factor
F_n $n = 1, 2, 3 \ldots$	force
F_x	force along flight path axis
F_z	force perpendicular to flight path axis
f	distance in sonic transit time sensor
f_c	compressibility factor
g	acceleration of gravity
h	altitude

$\dot{h}$	altitude rate
i	current
I_Y	moment of inertia about Y axis
K_n $n=0,1,2,3\ldots$	various constants
K_r	temperature recovery factor
k	coefficient of heat conductivity for air
k_Y	radius of gyration, $\sqrt{\frac{I_Y}{m}}$
L	aerodynamic lift
L_n $n=1,2,3,\ldots$	computer levers
l	hot wire length
M	Mach number
m	mass of aircraft
N_n $n=1,2,3\ldots$	force normal to vane
n_Y	$\frac{a_Y}{g}$
n_Z	$\frac{a_Z}{g}$
P_L	pressure at lower orifice of sensor
P_n	pressure at specific sensor port
P_S	free-stream static pressure
P_{S_i}	indicated free-stream static pressure

P_T	total pressure; in supersonic flow, the total pressure behind the shock wave
P_U	pressure at upper orifice of sensor
ΔP	differential pressure
ΔP_{a-b} $a=1,2,3\ldots$ $b=1,2,3\ldots$	differential pressure between two ports of a sensor
ΔP_α	differential pressure between angle of attack sensing ports
ΔP_β	differential pressure between angle of yaw sensing ports
q	dynamic pressure, $1/2\ \rho V^2$
q_i	indicated, or compressible, dynamic pressure $(P_T - P_S)$
$R,\ R_T$	variables defined by Eq. 101
R_n $n=1,2,3\ldots$	resistance
$r_1,\ r_2$	distances of wing and tail forces, respectively, from cg
S	area of lifting surface
s	distance between source and receiver
T	static temperature
T_{probe}	temperature measured by a temperature probe
T_T	total temperature
T_w	wire temperature
t	sound transit time

t	wing thickness
u	distance from center of suspension to disturbing force
V_S	velocity of sound
V_T	true airspeed
v	voltage
W	weight
w	power in watts
XYZ	reference axis system affixed to aircraft (Fig. 1)
xyz	reference axis system affixed to flight path (Fig. 1)
X_T	distance between tail force and center of gravity
α	angle of attack of aircraft relative to surrounding air mass
α_L	local angle of attack at location of sensing element
α_{L_1}	local angle of attack at sensor 1
α_{L_2}	local angle of attack at sensor 2
α_0	angle of attack for zero lift
α_t	angle of attack due to wing twist
β	angle of yaw of aircraft relative to surrounding air mass
β_L	local angle of yaw at location of sensing element
β_0	angle of yaw for zero sideslip
γ	ratio of specific heats, $\frac{C_P}{C_V}$

δ_T	deflection angle of tail surface
ϵ_h	altitude error
Θ, Φ, Ψ	angular rotations about Y, X, and Z axes, respectively
θ	general angle, used in several discussio
λ	angle defined in Fig. 19
μ	coefficient of viscosity
ρ	air density

REFERENCES

1. Allen, H. Julian, Estimation of the Forces and Moments Acting on Inclined Bodies of Revolution of High Fineness Ratio. RM A9126, National Advisory Committee for Aeronautics, Washington, 14 November 1949.

2. Alternate Proposal for a High Performance Mach Number Computing System, G. M. Giannini & Co., Pasadena, California, 4 October 1954.

3. Bartlett, G. E. and Peterson, J. W., Wind Tunnel Investigation of a Double-wedge Airfoil at Subsonic Speeds. BBR 53, Johns Hopkins University, Baltimore, Maryland, August 1946.

4. Bers, Lipman, On a Method of Constructing Two-Dimensional Subsonic Compressible Flows Around Closed Profiles. TN 969, National Advisory Committee for Aeronautics, Washington, March 1945.

5. Bogdan, L. and Segel, L., Wind Tunnel and Theoretical Investigations of Position Error Variation with Angle of Attack and Mach Number for Two Typical Fuselage Sensing Locations. Report No. IK-705-P-3, Cornell Aeronautical Laboratory, Buffalo, New York, 18 June 1952.

6. Brink, Paul L., The Determination of the Angles of Attack and Skid from the Measurement of Aircraft Accelerations. Report No. 1392, U. S. Naval Ordnance Plant, Indianapolis, Indiana, 28 September 1951.

7. Cochran, Roy J., Flight Test of Two Experimental Vortex True Free Air Temperature Systems. TN WCT-54-9, Wright Air Development Center, Wright-Patterson Air Force Base, Ohio, March 1954.

8. Cary, A. F., Final Report on an Experimental Evaluation of the Infrared Method of Measuring Free Air Temperature at Supersonic Speeds. Report No. F-2015-4-1, Franklin Institute Laboratories for Research and Development, Philadelphia 3, Pennsylvania, August 1949.

9. Cook, D. B. and Danby, C. J., "A Simple Diaphragm Micromanometer," Journal of Scientific Instruments, July 1953.

10. Cooper, M. and Webster, R.A., The Use of an Uncalibrated Cone for Determination of Flow Angles and Mach Numbers at Supersonic Speeds. TN-2190, National Advisory Committee for Aeronautics, Washington, March 1951.

11. Cover, J.H., Witte, N.F., and Seeley, L.W., Angle of Attack and Skid Measurements for Aircraft Rocket Fire Control Purposes. U.S. Naval Ordnance Test Station, China Lake, California, 23 November 1951.

12. Crawford, David J., Flight Check of Null-Pressure Type Angle of Attack and Yaw Indicator. MCRFT 2279, Flight Test Division, Air Material Command, Dayton, Ohio, 31 March 1950.

13. Davis, T., Development and Calibration of Two Conical Yawmeters. Meteor Report No. UAC-43, United Aircraft Corporation, East Hartford, Connecticut, October 1949.

14. Denison, M.R., Heat Transfer Coefficients and Insulated Wall Temperatures in High Speed Flow. PDM-123, North American Aviation, Inc., Downey, California, 9 September 1954.

15. Description of Ionization Type True Airspeed Indicator, Eclipse-Pioneer Division, Bendix Aviation Corporation, Teterboro, New Jersey, August 1948.

16. Development, Design and Construction of a High Altitude Altimeter 140,000 to 500,000 Feet. Report No. R-2, National Research Corporation, 70 Memorial Drive, Cambridge 42, Massachusetts.

17. Driver, P.C., Evaluation of Two Types of Airstream Direction Detectors for Measurement of Angle-of-Attack and Skid. TM 4527-20, Aviation Ordnance Department, U.S. Naval Ordnance Test Station, China Lake, California, December 1949.

18. Du Mond, J.W.M. and Pickels, W.M., "Superiority of a Knudsen Type Vacuum Gage for Large Metal Systems with Organic Vapor Pumps: Its Design and Operation," Review of Scientific Instruments, November 1935.

19. Dwinnell, James H., Principles of Aerodynamics, McGraw-Hill Book Company, Inc., New York, 1949.

20. Eckman, Ro[illegible]ald P., Industrial Instrumentation, John Wiley & Sons, New York, 19[illegible]

21. Electronic True Airspeed Indicator (Progress Reports No. 1 to 6), Cook Research Laboratories, Chicago, April 1947 to October 1947.

22. EM-370, Calibration Device for Attack Angle Computers in Production Airplanes. North American Aviation, Inc., Downey, California, 30 March 1953.

23. EM-404, Summary Description of the Flight Data Computer Aero X4A, North American Aviation, Inc., Downey, California, 20 July 1953.

24. Ferri, Antonio, Supersonic Flow Around Circular Cones at Angles of Attack. Report 1045, Langley Aeronautical Laboratory, Langley Field, Virginia, 1951.

25. Final Report, High Range True-Airspeed Indicator. Contract No. W33-038-ac-16652, Cook Electric Company, Chicago, 17 November 1947.

26. Fischer, H. S., Supersonic Wind-tunnel Test of the NIKE Angle-of-Attack, Indicator Moment Model. Report No. SM-13948, Douglas Aircraft Company, Inc., Santa Monica, California, 8 March 1951.

27. Flight Line Computers (Theoretical Studies). Report No. IH-431-P-3. Cornell Aeronautical Laboratory, Buffalo, New York, 17 February 1947.

28. Flight Line Computer (Final Report). Report No. IH-431-P-28, Cornell Aeronautical Laboratory, Buffalo, New York, 15 September 1949.

29. Flight Line Computer (Progress Reports November 1946 to December 1948). Cornell Aeronautical Laboratory, Buffalo, New York.

30. Flight Line Computer (Phase A Report). Report No. IH-705-P-1, Cornell Aeronautical Laboratory, Buffalo, New York, 31 January 1951.

31. Flight Line Computer (Phase B Report). Report No. IH-705-P-2, Cornell Aeronautical Laboratory, Buffalo, New York, 2 January 1952.

32. Flight Test Report No. 26 for Week Ending 6 January 1951 for Model YF-86D Airplane. NA-51-33, North American Aviation, Inc., Los Angeles, California, 10 January 1951.

33. Gracey, W., Coletti, D.E., and Russell, W.R., Wind-Tunnel Investigation of a Number of Total-Pressure Tubes at High Angles of Attack: Supersonic Speeds. TN 2261, National Advisory Committee for Aeronautics, Washington, January 1951.

34. Gracey, W., Letko, W., and Russell, W.R., Wind-Tunnel Investigation of a Number of Total-Pressure Tubes at High Angles of Attack: Subsonic Speeds. TN 2331, National Advisory Committee for Aeronautics, Washington, April 1951.

35. Gracey, W., Pearson, A.O., and Russell, W.R., Wind-Tunnel Investigation of a Shielded Total-Pressure Tube at Transonic Speeds. TM L51K19, National Advisory Committee for Aeronautics, Washington, 22 January 1952.

36. Greatbatch, Wilson, A Symposium on Flight Data Measuring Equipment for Aircraft Fire Control Systems. Report No. IH-820-P-1, Cornell Aeronautical Laboratory, Buffalo, New York, 1 September 1952.

37. Gross, N. and Lane, P.N.R., "An Accurate Wire Resistance Method for the Measurement of Pulsating Pressures," Journal of Scientific Instruments, January 1953.

38. Heiland, C.A., "New Precision Barometer and Barograph," Mechanical Engineering, December 1951.

39. Hottel, H.C. and Kalitinsky, A., "Temperature Measurement in High-Velocity Air Streams," Journal of Applied Mechanics, March 1945.

40. Howland, W. Lavern, "Measurement of Ambient Air Temperature in Flight," Preprint No. 106, Institute of the Aeronautical Sciences, A Sherman M. Fairchild Publication Fund Paper, New York, no date.

41. Huston, W.B., Accuracy of Airspeed Measurements and Flight Calibration Procedures. TN-1605, National Advisory Committee for Aeronautics, Washington, June 1948.

42. Investigation of Possible Methods for Measuring Air Speed Parameters Through the Transonic and Supersonic Range. F-2015-5A, The Franklin Institute, Philadelphia, 15 August 1949.

43. Investigation to Determine Most Practical Method of Obtaining Free Air Temperature at Transonic and Supersonic Speeds (Interim Report). Report No. F-2015-4, The Franklin Institute, Philadelphia, Pennsylvania, 31 December 1948.

44. Johnson, M. C., Supersonic Wind Tunnel Tests of a SPARROW Angle of Attack Indicator. Report No. SM-14051, Douglas Aircraft Company, Inc., Santa Monica, California, 29 August 1951.

45. Johnson, W. H., Supersonic Wind Tunnel Tests of a Hemispherical Yaw Meter at a Mach Number of 1.71. MR 473, Ballistic Research Laboratories, Aberdeen Proving Ground, Maryland, 25 March 1948.

46. Kass, Philip, "Two in One Unit for Yaw and Attack Angles," Aviation Week, January 5, 1953.

47. Keith, Melvin, Consideration of a Wedge-shaped Vane as an Airflow Direction Measuring Instrument for Aircraft Fire Control Purposes. TM 154, U.S. Naval Ordnance Test Station, China Lake, California, 4 October 1951.

48. Kollsman and Giannini, Experimental Sensitive Angle of Attack Indicators. NAES-INSTR-75-49, Naval Air Material Center, Philadelphia, 10 November 1949.

49. Kovasznay, Laszlo, Calibration and Measurement in Turbulence Research by the Hot-Wire Method. TM-1130, National Advisory Committee for Aeronautics, Washington, June 1947.

50. Kovasznay, Leslie S. G., The Hot-Wire Anemometer in Supersonic Flow, Journal of the Aeronautical Sciences, 17 (September 1954).

51. Lawrence, James C. and Landes, George L., Applications of the Constant Temperature Hot-Wire Anemometer to the Study of Transient Air Flow Phenomena. Paper No. 52-12-5, Proceedings of the Instrument Society of America, 1952.

52. Litting, C. N. W. and Taylor, W. K., "An Automatically-Controlled Knudsen Type Vacuum Gage," Proceedings of the Institute of Electrical Engineers, Vol. 99, Monograph No. 36, 1952.

53. Lowell, Herman H., Design and Applications of Hot-Wire Anemometers for Steady-State Measurements at Transonic and Supersonic Airspeeds. TN-2117, National Advisory Committee for Aeronautics Washington, July 1950.

54. Marlow, D.G. and Nisewanger, C.R., A Method for the Instantaneous Measurement of Velocity and Temperature in High-Speed Air Flow. NOTS 161, U.S. Naval Ordnance Test Station, China Lake, California, 20 October 1948.

55. McAdams, W.H., Heat Transmission, McGraw-Hill Book Company, Inc., New York, 1942.

56. McClanahan, H.C., Jr., Wing-Flow Investigations of a 45° Cone as an Angle of Attack Measuring Device at Transonic Speeds. RM L51E16, National Advisory Committee for Aeronautics, Washington, 11 July 1951.

57. McFadden, N.M., Holden, G.R., and Ratcliff, J.W., Instrumentation and Calibration Technique for Flight Calibration of Angle of Attack Systems on Aircraft. RM A52I23, National Advisory Committee for Aeronautics, Washington, 5 December 1952.

58. McFadden, N.M., Rathert, G.A., and Bray, R.S., Flight Calibration of Angle of Attack and Sideslip Detectors on the Fuselage of a 35° Swept-Wing Fighter Airplane. RM A52A04, National Advisory Committee for Aeronautics, Washington, February 1952.

59. Miller, LCDR Rupert S., Smoke Puff Method for Measuring Angle of Attack. Report N11-204, Naval Air Test Center, Patuxent River, Maryland, no date.

60. Minutes of the Symposium on Angle of Attack and Skid Measurements for Aircraft Rocket Control. U.S. Naval Ordnance Test Station, China Lake, California, 18 May 1951.

61. Minutes of the Conference on Angle of Attack and Skid Measurement for Fire Control Purposes, U.S. Naval Ordnance Test Station, China Lake, California, 14 January 1952.

62. Mitchell, J.L. and Peck, R.F., An NACA Vane-Type Angle of Attack Indicator for Use at Subsonic and Supersonic Speeds. RM L9F28a, National Advisory Committee for Aeronautics, Washington, 16 August 1949.

63. "Molecular Vacuum Gage," General Electric Bulletin GEC-986.

64. Munnikhuysen, R.D., Electronic True Airspeed Indicator, Engineering Revision Memorandum Report MCR EXE-655-1553A, AAF Material Command, 28 January 1948.

65. "Navy Buys Specialties, Inc., Angle of Attack Unit," Aviation Week, August 18, 1952.

66. Notes and Tables for Use in Analysis of Supersonic Flow (Staff of Ames Aeronautical Laboratory).TN-1428, National Advisory Committee for Aeronautics, Washington, December 1947.

67. Obert, Edward F., Elements of Thermodynamics and Heat Transfer, McGraw-Hill Book Company, Inc., New York, 1949.

68. Ollivier, Louis and Tricebock, D. J., "Precise Pressure Measurement," Electrical Manufacturing, August 1953.

69. Ormsby, Robert B., Jr., An Angle-of-attack and Angle-of-yaw Indicator Using a Direct-reading, Simple Strain-gage Circuit on Sting Balances. Aero-855, The David W. Taylor Model Basin Aerodynamics Laboratory, Navy Department, Washington, February 1954.

70. Parry, D.H. and Steele, D.I., Kollsman Giannini Experimental Sensitive Angle of Attack Indicators, NAES - INSTR-75-49, Naval Air Material Center, U.S. Naval Base Station, Philadelphia, Pennsylvania, November 1949.

71. Patterson, John L., A Miniature Electrical Pressure Gage Utilizing A Stretched Flat Diaphragm. TN-2659, National Advisory Committee for Aeronautics, Washington, April 1952.

72. Pilny, John M., A Small Pirani Gage for Measurement of Nonsteady Low Pressure. TN-2946, National Advisory Committee for Aeronautics, Washington, 1953.

73. Pressey, D.C., "Temperature Stable Capacitance Pressure Gage," Journal of Scientific Instruments, January 1953.

74. Ragni, V.F., Hot Wire Angle-of-Attack Indicator. Report No. R-49-17, Curtiss-Wright Corporation, Columbus, Ohio, 23 May 1949.

75. Roberts, C.C. and O'Hara, W.W., "Techniques for Measuring and Controlling Vacuum," Product Engineering, September 1953.

76. Ruskin, R.E. and others, Development of the NRL Axial-Flow Vortex Thermometer. Report 4008, Naval Research Laboratory, Washington, September 1952.

77. Russell, Walter R. and Gracey, William, Wind-tunnel Investigation of a Shielded Total-pressure Tube at a Mach Number of 1.61. RM L53L23a, National Advisory Committee for Aeronautics, Washington, 10 March 1954.

78. Schaaf, S. A. and Mann, W. R., Pressure Distributions on Static Pressure Probes. HE-150-29, University of California, Berkeley, California, 24 September 1947.

79. Schubauer, G. B. and Klebanoff, P. S., Theory and Application of Hot-Wire Instruments in the Investigation of Turbulent Boundary Layers. ACR 5K27, National Advisory Committee for Aeronautics, Washington, March 1946.

80. Schwartz, Herman, Preliminary Report on Three Temperature Probes for Measuring Ambient Air Temperature in Clear Air and Clouds. WCT 54-94, Wright Air Development Center, Wright-Patterson Air Force Base, Ohio, September 1954.

81. Seamans, R. C., Jr., Greene, R. H., Jr., and Brainerd, H. B., Tracking Control. Report No. 6445-2, Massachusetts Institute of Technology, Boston, 15 January 1947.

82. Seeley, Leonard W., Flight Investigation of a 1-g Angle-of-Attack Position Error Calibration Technique. NOTS 681, U.S. Naval Ordnance Test Station, China Lake, California, 17 April 1953.

83. Segel, Leonard, Methods of Predicting the Angle of Attack Position Error for Flow in the Vicinity of Aircraft. Masters Thesis, University of Buffalo.

84. Shepard, Charles E., A Self-Excited Alternating-Current, Constant-Temperature Hot-Wire Anemometer. TN-3406, National Advisory Committee for Aeronautics, Washington, April 1955.

85. Spencer, Robert, Improvement, Spencer Angle of Attack System Wing Lift Instrumentation, Explanation and Mechanization. Technical Report No. 111, The Aerotec Corporation, Greenwich, Connecticut, December 1954.

86. Spencer, Robert, Instrumenting an Aircraft for Pitch-up and Tolerable Buffet. Technical Report No. 109, The Aerotec Corporation, Greenwich, Connecticut, August 1954.

87. Spencer, Robert, Spencer Wing Lift Instr[illegible]ation System: Mach Number and Altitude Considerations, S[illegible] Transonic and Supersonic. Technical Report No. 112, The Aerote[illegible] Corporation, Greenwich, Connecticut, March 1955.

88. Stine, Howard A. and Scherrer, Richard, Experimental Investigation of the Turbulent Boundary Layer Temperature Recovery Factor on Bodies of Revolution at Mach Number from 2.0 to 3.[illegible] [illegible]-2664, National Advisory Committee for Aeronautics, Washington, March 1952.

89. Study of Radome and Radar Antenna Installation Design Criteria, A. D-1276, McMillan Laboratory, Inc., Ipswich, Massachusetts, 1 June 1954.

90. Supersonic Wind Tunnel Tests of a NIKE Angle-of-Attack Indicator. Report No. SM-13948, Douglas Aircraft Company, Inc., Santa Monica, California, August 1951.

91. Symposium on Flight Data Measuring Equipment for Aircraft Fire Control Systems. Report No. IH-820-P1, Cornell Aeronautical Laboratory, Buffalo, New York, 1 September 1952.

92. Tchen Chan Mou, Heat Delivery in a Compressible Flow and Applications to Hot-Wire Anemometry. TN-2436, National Advisory Committee for Aeronautics, Washington, August 1951.

93. Test of Self-calibrating Directional Probe. Memo from F. R. Feldman to H. W. Bell, North American Aviation, Inc., Downey, California, 28 March 1951.

94. Thomas, G. B., Supersonic Wind Tunnel Tests of a NIKE Angle of Attack Indicator. Report No. SM-13735, Douglas Aircraft Company, Inc., Santa Monica, California, 17 May 1950.

95. Thompson, Jim Rogers, Bray, Richard S., and Cooper, George E., Flight Calibration of Four Airspeed Systems on a Swept-wing Airplane at Mach Numbers up to 1.04 by the Radar-phototheodolite Method. RM A50H24, National Advisory Committee for Aeronautics, Washington, 27 October 1950.

96. Von Dardel, G., "Combined Pirani and Ionization Gage Circuit, Journal of Scientific Instruments, April 1953.

97. Vortex Free Air Thermometer. Report No. IH-775-P-2, Cornell Aeronautical Laboratory, Inc., Buffalo, New York, April 1953.

98. Wall, Nancy, Chordwise Pressure Distributions on a 12 Foot-Span Wing of NACA-66 Series Airfoil Sections up to a Mach Number of 0.60. TN-1696, National Advisory Committee for Aeronautics, Washington, October 1948.

99. Walter, L. W. and Redman, E. J., Needle Static-pressure Probes Insensitive to Flow Inclination in Supersonic Air Streams. NAVORD Report 3694, U.S. Naval Ordnance Laboratory, White Oak, Maryland, 15 March 1954.

100. Werner, F.D. and others, Design and Performance Studies for Improved Multiple-Shielded Total Temperature Probes. Technical Report 53-194, Wright Air Development Center, Wright-Patterson Air Force Base, Ohio, April 1953.

101. Weske, John R., Methods of Measurement of High Air Velocities by the Hot-Wire Method. TN-880, National Advisory Committee for Aeronautics, Washington, February 1943.

102. Wimbrow, R. William, Experimental Investigation of Temperature Recovery Factors on Bodies of Revolution at Supersonic Speeds. TN-1975, National Advisory Committee for Aeronautics, Washington, October 1949.

103. Witte, N. F., A Study of Two Methods for Making In-flight Calibrations of Angle-of-attack Measuring Devices. U.S. Naval Ordnance Test Station, China Lake, California, 7 September 1951.

104. Young, D. W., "The Measurement of Angle-of-Attack and Angle-of-Yaw in Flight," Technical Data Digest, November 1950.

105. Zalovcik, J. A., Summary of Stall-Warning Devices. TN-2676, National Advisory Committee for Aeronautics, Washington, May 1952.

106. Zelinsky, Dan, Course of DZ in Pursuit of the Angle of Attack. Air Materiel Command, Wright-Patterson Air Force Base, Dayton, Ohio, 29 August 1945.

UNCLASSIFIED

UNCLASSIFIED